# The isotope geochemistry of zinc and copper

**Frédéric Moynier[1,2], Derek Vance[3], Toshiyuki Fujii[4], Paul Savage[5]**

*[1]Institut de Physique du Globe de Paris, Université Paris Diderot, Université Sorbonne Paris Cité, CNRS UMR 7154, 1 rue Jussieu, 75238 Paris Cedex 05*

*[2]Institut Universitaire de France, Paris, France*

*[3]ETH Zürich, Institute for Geochemistry and Petrology, Department of Earth Sciences, Clausiusstrasse 25, 8092 Zürich, Switzerland.*

*[4]Research Reactor Institute, Kyoto University, 2-1010 Asashiro Nishi, Kumatori, Sennan, Osaka 590-0494, Japan*

*[5]Department of Earth and Environmental Sciences, University of St Andrews, Irvine Building, Fife KY16 9AL, United Kingdom*

Corresponding author: *moynier@ipgp.fr*

## INTRODUCTION

Copper, a native metal found in ores, is the principal metal in bronze and brass. It is a reddish metal with a density of 8920 kg $m^{-3}$. All of copper's compounds tend to be brightly colored: for example, copper in hemocyanin imparts a blue color to blood of mollusks and crustaceans. Copper has three oxidation states, with electronic configurations of $Cu^0([Ar]3d^{10}4s^1)$, $Cu^+([Ar]3d^{10})$, and $Cu^{2+}([Ar]3d^9)$. $Cu^0$ does not react with aqueous

hydrochloric or sulfuric acids, but is soluble in concentrated nitric acid due to its lesser tendency to be oxidized. Cu(I) exists as the colorless cuprous ion, $Cu^{+}$. Cu(II) is found as the sky-blue cupric ion, $Cu^{2+}$. The $Cu^{+}$ ion is unstable, and tends to disproportionate to $Cu^{0}$ and $Cu^{2+}$. Nevertheless, Cu(I) forms compounds such as $Cu_2O$. Cu(I) bonds more readily to carbon than Cu(II), hence Cu(I) has an extensive chemistry with organic compounds.

In aqueous solutions, $Cu^{2+}$ ion occurs as an aquacomplex. There is no clearly predominant structure among the four-, five-, and six- fold coordinated Cu(II) species (Chaboy et al. 2006). Hydrated Cu(II) ion has been represented as the hexaaqua complex $Cu(H_2O)_6^{2+}$, which shows the Jahn-Teller distortion effect (Sherman 2001; Bersuker 2006), whereby the two Cu-O distances of the vertical axial bond ($Cu\text{-}O_{ax}$) are longer than four Cu-O distances in the equatorial plane ($Cu\text{-}O_{eq}$). The Jahn-Teller effect lowers the symmetry of $Cu(H_2O)_6^{2+}$ from octahedral $T_h$ to $D_{2h}$. The sixfold coordination of hydrated Cu(II) species is questioned by a finding of fivefold coordination (Pasquarello et al. 2001; Chaboy et al. 2006; Little et al. 2014b; Sherman et al. 2015). The bond distance related to $Cu(H_2O)_6^{2+}$ is considered to reflect a rapid switch between the square pyramid and trigonal bipyramid configurations (Pasquarello et al. 2001; de Almeida et al. 2009). The fivefold coordination is supported by computational (Amira et al. 2005) and spectroscopic (Benfatto et al. 2002) studies.

In aqueous media at elevated temperatures, Cu(I) is thermodynamically more stable than Cu(II). The structures of Cu(I) species are thought to be due to the splitting of degenerate $4p_{x,y,z}$ orbitals by a ligand field (Kau et al. 1987). Cu(I) complexes possess simple linear structures (Fulton et al. 2004) due to $4p_z$ and $4p_{x,y}$ orbitals. The splitting of $4p_{x,y}$ orbital and/or the formation of degenerate $4p_{y,z}$ orbitals give the Cu(I) species

47 threefold coordination structures (T-shaped or trigonal planar coordination). For the
48 fourfold tetrahedral coordination ($T_d$) structure, the $p_{x,y,z}$ orbitals may be close to
49 degenerate.

50 Zinc is an element of Group 2B, the last column of the *d* block. Zinc is not a
51 transition metal by definition because it has a *d* subshell that is only partially occupied.
52 Zinc has two oxidation states, with electronic configurations of $Zn^0([Ar]3d^{10}4s^2)$ and
53 $Zn^{2+}([Ar]3d^{10})$, where Zn(II) has $3d^{10}$ with two electrons per orbital. Zinc is sometimes
54 included with the transition metals because its properties are more similar to these than to
55 the post-transition metals, whose properties are determined by partially filled *p* subshells.
56 Fresh zinc has a shiny metallic luster, but it tarnishes easily. It is hard and brittle,
57 becomes malleable with increasing temperature, and melts at 419.53°C. Metallic zinc is
58 easily oxidized and hence it is used as a reducing agent. Reduction of acids like HCl to
59 $H_2$ by $Zn^0$ is well known.

60 In compounds or complex ions, Zn is present only as Zn(II). Hydrated $Zn^{2+}$ is
61 generally thought to be present as the octahedral $Zn(H_2O)_6^{2+}$, this being the most stable
62 structure (Mhin et al. 1992). Besides the marked preference for sixfold coordination, Zn(II)
63 can easily be fourfold or fivefold coordinated. The coordination number is attributable to
64 a balance between bonding energies and repulsions among the ligands.

65 Zinc and Cu are both moderately volatile elements, with 50% condensation
66 temperatures ($T_c$) of 726K and 1037K, respectively (Lodders 2003). It was long thought
67 that Zn behaved as a lithophile element during planetary (and especially, Earth's)
68 differentiation, hence there is negligible Zn in Earth's core (e.g. McDonough 2003). This

assumption was used to place broad bounds on the amount of S (which has a similar $T_c$ to Zn) in Earth's core (around 1.7wt% Dreibus and Palme 1996). However, more recent work indicates that Zn behaves as a moderately siderophile element, with potentially ~30% of terrestrial Zn stored in Earth's core (Siebert et al. 2011), significantly affecting the conclusions of Dreibus and Palme (1996). Zinc is the most abundant lithophile element with a $T_c$<750K, 100 times more abundant than the second-most abundant (Br, Tc=546K). Its high abundance relative to other moderately volatile elements (due to the relatively high binding energies per nucleon of its isotopes) makes Zn a good tracer of volatility in rocks and a major application of its isotopes has been related to understanding volatility processes.

Copper is a siderophile and highly chalcophile element (Siebert et al. 2011), with ~2/3 of the terrestrial Cu thought to be stored in Earth's core (Palme and O'Neill 2003). Copper is also moderately volatile, but is the most refractory of the chalcophile elements, meaning that Cu may be a good tracer of the role of sulphides during differentiation and igneous processes.

Zn is comprised of five natural stable isotopes, $^{64}$Zn (49.2%), $^{66}$Zn (27.8%), $^{67}$Zn (4.0%), $^{68}$Zn (18.4%) and $^{70}$Zn (0.6%) and Cu of two stable isotopes, $^{63}$Cu (69.2%), and $^{65}$Cu (30.8%) (Shields et al. 1964). Due to their relatively high first ionization potentials (9.4 eV for Zn and 7.7 eV for Cu), the measurement of Zn and Cu isotope ratios by Thermal-Ionization Mass-Spectrometry (TIMS) is very difficult. This explains the very limited amount of Zn and Cu isotopic data produced before the advent of Multiple-Collector Inductively-Coupled-Plasma Mass-Spectrometry (MC-ICP-MS). In addition, since Cu has only two stable isotopes it is not possible to use a double spike technique to

correct for instrumental bias on TIMS. Since the first commercialized MC-ICP-MS in the late 90s and the first 'high precision' Zn and Cu isotope ratio measurements (Maréchal et al. 1999), more than 500 papers have been published (source: ISI Web of Science) on various geochemical topics associated with Zn and Cu isotopes (e.g. oceanography, cosmochemistry, environmental sciences, medical sciences). With the exception of medical sciences, for which there is a dedicated chapter in this volume, here we review these varied applications and discuss the potential of these isotope systems for future studies.

## METHODS

Measurement of Zn and Cu isotope ratio was originally made using TIMS (Shields et al. 1964; Shields et al. 1965; Rosman 1972). As for any element with only two isotopes, it was not possible to properly assess the instrumental isotopic fractionation for Cu and the analytical uncertainty was therefore poor (no better than 2 ‰/amu; Shields et al. 1964; Shields et al. 1965). With five stable isotopes, for Zn it is possible to correct for instrumental bias and TIMS was originally used with double spike methods to measure Zn isotopic compositions. The earliest measurements, on the older generation of TIMS were associated with analytical precisions of around 1 ‰/amu (Rosman 1972; Loss et al. 1990), but modern generation TIMS can reach precisions of 0.1-0.2 ‰/amu (Ghidan and Loss 2011).

The vast majority of recent Cu and Zn isotopic data have been acquired by MC-ICP-MS, either by standard-sample bracketing (e.g. Maréchal et al. 1999; Mason et al.

115 2004ab; Weiss et al. 2005; Bermin et al. 2006; Viers et al. 2007; Balistrieri et al. 2008;
116 Peel et al. 2008; Vance et al. 2008; Savage et al. 2015a, b; Sossi et al. 2015) or by the
117 double spike method (e.g. Bermin et al. 2006; Arnold et al. 2010b; Conway and John 2015)
118 for Zn. The pioneering work of Maréchal et al. (1999) showed that instrumental mass bias
119 could be corrected by a combination of elemental doping (Cu for Zn, and Zn for Cu) and
120 standard bracketing, so that it was possible to obtain isotope ratios of both Cu and Zn with
121 precisions better than 0.1 ‰/amu on the VG Elemental Plasma 54 MC-ICP-MS.
122 Subsequent studies by Zhu et al. (2000; 2002) and Archer and Vance (2002; 2004) have
123 further tested this approach and together with Maréchal et al. (1999) provided the ground
124 work for modern Zn and Cu isotopic studies. An alternative method using Ni doping
125 (instead of Zn) for Cu isotope analyses has also been used (Larner et al. 2011).

126 More recently, double spike Zn isotopic measurements by MC-ICP-MS have also
127 been employed, providing consistent results with those obtained by standard bracketing
128 techniques. An advantage of the double spike technique is that it provides high precision
129 absolute elemental abundances together with the isotope ratios. The fact that the double
130 spike approach also accounts for mass discrimination during chemical separation means
131 that it has been a key methodology for the analysis of Zn in difficult matrixes such as
132 seawater (e.g. Bermin et al. 2006; Arnold et al. 2010b; Zhao et al. 2014; Conway and John
133 2015; Vance et al. In review). Using a similar approach, the absolute abundance of Zn
134 isotopes were determined by analyzing synthetic isotope mixtures (Tanimizu et al. 2002;
135 Ponzevera et al. 2006).

136 The precision of Zn and Cu isotopic measurements depends on the quality of the
137 chemical extraction (purity, low blank compared to the amount of Zn and Cu present in the

138 samples, high/quantitative yields) and on the correction of the instrumental bias. The high
139 purity of the final Zn fraction is needed to remove both isobaric interferences and non-
140 isobaric interference that are the cause of so-called 'matrix effects' (see Chaussidon et al.
141 20XX, this volume). As Zn and Cu isotopes can be fractionated during ion-exchange
142 chromatography (Maréchal and Albarède, 2002) the chemical procedure requires
143 quantitative yields, unless a double-spike is added pre-column chemistry.

144 The chemical purification of Cu and Zn is generally made by ion-exchange
145 chromatography in 6-10N HCl medium on either macro-porous resin such as AG-MP1 or
146 on regular bead resin such as AG1-X8 (e.g. Maréchal et al. 1999; Archer and Vance 2004;
147 Borrok et al. 2007; Conway and John 2015; Sossi et al. 2015). In order to obtain a very
148 pure elution of Cu, many workers (e.g. Savage et al. 2015b; Vance et al., 2016) repeat the
149 whole procedure. For Zn purification, an alternative method takes advantage of the strong
150 complexation of Zn with bromide, which allows for the use of more dilute acids
151 ($HBr/HNO_3$ media) on micro-columns (0.1 µl) of anion-exchange resin (AG1-X8; Luck et
152 al. 2005; Moynier et al. 2006; Moynier and Le Borgne 2015).

153 When analyzing Zn by MC-ICPMS, the potential nickel interference on mass 64 is
154 normally monitored and corrected for by analyzing the intensity of the $^{62}Ni$ beam.
155 Typically, $^{70}Zn$ is not measured (or at least, not reported) due to the low abundance of this
156 isotope, and the potential for overwhelming interference from $^{70}Ge$. In most instances, it is
157 not necessary to measure $^{70}Zn$ (even when using the double-spike method), as terrestrial
158 isotope variations are all mass-dependent. However, the introduction of higher resistance
159 amplifiers attached to Faraday detectors should allow the more accurate measurement of
160 $^{70}Zn$ in, for example, studies involving mass-independent Zn isotope variations. However,

161 so far the results have been inconclusive (Moynier et al. 2009a; Savage et al. 2014). For
162 Cu, neither masses 63 and 65 have direct elemental interferences, although there is
163 evidence that the formation of $^{23}Na^{40}Ar+$ and $^{25}Mg^{40}Ar+$ in the plasma can create
164 anomalous isotope ratios (Archer and Vance 2004; Larner et al. 2011; Savage et al. 2015b),
165 so that careful monitoring to ensure complete removal of both Na and Mg from each sample
166 aliquot is necessary to ensure accurate data.

167 The correction of instrumental mass bias by elemental doping (Cu for Zn and Zn
168 for Cu, or Ni for Cu) has been extensively discussed in Maréchal et al. (1999) and further
169 by Larner et al. (2011). The principle is that the instrumental bias can be expressed with an
170 exponential law, for example for the $^{66}Zn/^{64}Zn$ and $^{65}Cu/^{63}Cu$ ratios:

171 $$\left(\frac{^{66}Zn}{^{64}Zn}\right)_{Measured} = \left(\frac{^{66}Zn}{^{64}Zn}\right)_{True} \times \left(\frac{M_{66}}{M_{64}}\right)^{f_{Zn}} \quad (1)$$

172 $$\left(\frac{^{65}Cu}{^{63}Cu}\right)_{Measured} = \left(\frac{^{65}Cu}{^{63}Cu}\right)_{True} \times \left(\frac{M_{65}}{M_{63}}\right)^{f_{Cu}} \quad (2)$$

173

174 where $M_{63}$, $M_{64}$, $M_{65}$, $M_{66}$ are the atomic masses of $^{64}Zn$, $^{65}Cu$, $^{66}Zn$, $^{68}Zn$,
175 respectively. $f_{Zn}$ and $f_{Cu}$ are mass-independent fractionation factors that depend on the
176 element. Taking the example of Zn measurements, the elemental doping method consists
177 of adding an identical Cu elemental standard to all aliquots to be analysed, which can then
178 be used to determine the $f_{Zn}$. Because the ionization behavior of Cu and Zn is not the same,
179 $f_{Zn}$ cannot be assumed to be equal to $f_{Cu}$, and thus the relation between $f_{Cu}$ and $f_{Zn}$ is

estimated by taking the Napierian logarithm of equations (1) and (2) and ratioing the two equations:

$$\frac{ln\left(\frac{^{66}Zn}{^{64}Zn}\right)_{Measured} - ln\left(\frac{^{66}Zn}{^{64}Zn}\right)_{True}}{ln\left(\frac{^{65}Cu}{^{63}Cu}\right)_{Measured} - ln\left(\frac{^{65}Cu}{^{63}Cu}\right)_{True}} = \frac{f_{Zn}}{f_{Cu}} \frac{ln\left(\frac{M_{66}}{M_{64}}\right)}{ln\left(\frac{M_{65}}{M_{63}}\right)} \quad (3)$$

By plotting $ln\left(\frac{^{66}Zn}{^{64}Zn}\right)_{Measured}$ vs $ln\left(\frac{^{65}Cu}{^{63}Cu}\right)_{Measured}$ for the standard solution data generated during a session of analyses, the $\frac{f_{Zn}}{f_{Cu}}$ ratio can be estimated from the slope of this diagram (see for example Fig. 9 in Maréchal et al. 1999). The calculated $f_{Zn}$ can then be used to calculate $\left(\frac{^{66}Zn}{^{64}Zn}\right)_{true}$ (and vice-versa for Cu isotopic measurements), provided that there is enough drift in the mass bias during an analytical session. This correction is coupled with a standard bracketing method that consists of measuring a standard before and after each sample, whereby the same correction is applied to both the standard and sample ratios. Once all isotope ratios are corrected for mass discrimination, the data are usually reported using the delta notation:

$$\delta^{65}Cu = \left[\frac{\left(^{65}Cu/_{^{63}Cu}\right)_{sample}}{\left(^{65}Cu/_{^{63}Cu}\right)_{NIST-SRM-976}} - 1\right] \times 1000 \quad (4)$$

197

198 $$\delta\,^{x}Zn = \left[\frac{\left(^{x}Zn/_{64}Zn\right)_{sample}}{\left(^{x}Zn/_{64}Zn\right)_{JMC-Lyon}} - 1\right] \times 1000 \quad (5)$$

199

200 With x=66, 67, 68 or 70.

201 The double spike approach to mass discrimination was first described for Zn by
202 Bermin et al. (2006), and involves the addition of a mixture of a tracer solution of known
203 exotic isotopic composition to each sample (e.g. Dodson 1963; Rudge et al. 2009; John
204 2012). Equations that relate three measured and mass-bias corrected isotope ratios, for
205 $^{66}Zn/^{64}Zn$, $^{67}Zn/^{64}Zn$ and $^{68}Zn/^{64}Zn$ in terms of mixing, the exponential mass discrimination
206 law, and natural mass-dependent fractionation relative to a standard, are solved to obtain
207 the isotopic composition of the sample. The quality of data obtained with any double spike
208 depends on the spike isotopes used and the sample/spike ratio in the mixture created, which
209 control the magnification of analytical uncertainties propagated through the double spike
210 algebra; hence, optimal spike compositions and abundances need to be deduced, although
211 there is a range for both over which good isotopic data are obtainable. Other considerations
212 include the potential for isobaric interference. Thus, although the optimal Zn spike is a
213 mixture of $^{66}Zn$ and $^{70}Zn$, practical applications have used a $^{64}Zn$-$^{67}Zn$ spike (e.g. Bermin
214 et al. 2006; Conway et al. 2013). Bermin et al. (2006) showed that such a spike yields
215 precise and accurate sample isotopic compositions over about a factor 20 range in
216 sample/spike ratios in the mixture. Over a 2 year period, on a Neptune at ETH Zürich, the
217 $\delta^{66}Zn$ of IRMM-3702 standard gave +0.300 ±0.058‰ relative to JMC Lyon (2SD, n =

163). For comparison, standard-sample bracketing standard precisions are of a similar magnitude (i.e. long term 2SD quoted by Chen et al., 2013, is $\delta^{66}Zn \pm 0.04‰$) but this is on samples with relatively high Zn concentrations (~100ppm) and relies heavily on very stable instrument running conditions.

All of the Zn isotopic variations measured in terrestrial samples that have been analyzed to date follow a mass-dependent law, i.e., $\delta^{70}Zn/3 \approx \delta^{68}Zn/2 \approx \delta^{67}Zn/1.5 \approx \delta^{66}Zn$. By contrast, extra-terrestrial mass-independent isotopic effects on $^{66}Zn$ of over 1500ppm have been observed in refractory inclusions (Loss and Lugmair 1990; Völkening and Papanastassiou 1990) and, more recently, these isotope anomalies have been discovered in bulk primitive meteorites, albeit of a much smaller magnitude (20-70ppm Savage et al. 2014). The survival of these anomalies is perhaps surprising, given the volatile behavior of Zn during solar system condensation. These will be discussed further below.

Because it only has two isotopes, mass independence in Cu isotope variations measured in terrestrial samples cannot be discerned, although there is no reason to assume that such variations occur in this realm. For extra-terrestrial samples, Luck et al. (2003) showed that the Cu isotope variations correlate with $\Delta^{17}O$ anomalies in bulk primitive meteorites, which suggests that the variations measured between solar system materials may not be completely generated by 'mass-dependent' fractionation processes.

A number of different reference standards have been used for Cu and Zn isotopic measurements; NIST SRM 976 for Cu isotopes and the JMC 3-0749C (usually called JMC-Lyon) are the two standards used in the original work of Maréchal et al. (1999). Though neither standard is still commercially available they are still the most commonly cited as

240 references. Following Maréchal et al. (1999) other standards have been developed and used
241 in a routine manner in different laboratories . Data for those that have been measured by a
242 number of different laboratories are summarized in Table 1. Other standards relevant to
243 more specific areas of research have been detailed in Cloquet et al. (2008). We suggest, for
244 the sake of consistency, that future data should always be normalized with respect to NIST
245 SRM 976 for Cu and JMC Lyon for Zn. New reference standards for both Cu and Zn will
246 need to be developed soon, and for Zn a round-robin analysis programme of one such new
247 standard is under way (C. Archer, ETH Zürich, pers. comm.). When these new reference
248 standards come on line, we recommend maintaining the isotopic compositions of the
249 original references at zero, with a reference value for new standards set relative to that, as
250 recently proposed for Mo isotopes (Nägler et al. 2014), so that old data can be directly
251 compared with new.

252

253 **ZINC AND COPPER ISOTOPE FRACTIONATION FACTORS FROM *AB***
254 ***INITIO* METHODS**

255 A considerable amount of progress has been made in calculating isotope
256 fractionation factors between free metal ions and inorganic complexes in aqueous solution,
257 laying the basis for an understanding of surface terrestrial fluids. Almost all the Cu and Zn
258 in the oceans, in rivers and in soils is organically-complexed or sorbed to the surfaces of
259 oxyhydroxides and clays (see section on low temperature processes later in the chapter),
260 rather than being found as a free metal ion. There is therefore an urgent need to build on

261 the existing theoretical work to extend the calculations to species and processes that
262 represent those that are most important at the surface of the Earth.

263 The equilibrium constant of an isotopic exchange reaction can be theoretically
264 obtained as the Reduced Partition Function Ratio (RPFR or β) of isotopologues (e.g.
265 Schauble 2004). Here we will summarize the isotopic enrichment factors that have been
266 calculated for aqueous solutions and molecules relevant to Zn and Cu in biogeochemistry.
267 We also provide new results for certain molecules that were missing from the published
268 studies (see Tables 2, 3, 4) using the method described in Fujii et al. (2014).

269 The isotope enrichment factor is evaluated from the reduced partition function ratio
270 $(s/s')f$ (Bigeleisen and Mayer 1947), also denoted β, such that,

$$ln\frac{s}{s'}f = \sum\left[ln\,b(u_i') - ln\,b(u_i)\right] \quad (6)$$

271 where

$$ln\,b(u_i) = -ln\,u_i + \frac{u_i}{2} + ln\left(1 - e^{-u_i}\right) \quad (7)$$

272 and

$$u_i = \frac{h\nu_i}{kT} \quad (8)$$

273

274 In the latter expression, ν stands for vibrational frequency, *s* for the symmetry
275 number of the considered compound, *h* for Plank's constant, *k* for the Boltzmann constant,
276 and *T* for the absolute temperature. The subscript *i* denotes the *i*th normal mode of

277 molecular vibration, and primed variables refer to the light isotopologue. The isotope
278 enrichment factor due to molecular vibrations can be evaluated from the frequencies $\nu_i$
279 summed over all normal modes.

280 The ln β values of Cu(I) and Cu(II) species (Seo et al. 2007; Fujii et al. 2013;
281 Sherman 2013; Fujii et al. 2014; Telouk et al. 2015) are shown in Tables 2 and 3. The
282 inorganic aqueous Cu species are represented in Figure 1. At low pH, positive $\delta^{65}Cu$ is
283 found in copper sulfates and carbonates, relative to other inorganic species like hydrated
284 $Cu^{2+}$ and chlorides. At pH ~6, $^{65}Cu$ is enriched in $CuSO_4$ and $CuHCO_3^+$, while $^{63}Cu$ is
285 enriched in the other inorganic species like $Cu^{2+}$ and $CuCl^+$ (Fig. 1). With increasing pH,
286 $Cu(OH)_2$ and $CuCO_3$ become the prevalent species (Zirino and Yamamoto 1972). At high
287 pH, $\delta^{65}Cu$ is positive in Cu hydroxides and negative in carbonates. At a typical pH of
288 seawater (8.22; Macleod et al. 1994), isotope fractionation among inorganic species favors
289 $^{63}Cu$ in $CuCO_3$ and $^{65}Cu$ in $Cu(OH)_2$. However, Cu in soil solutions, rivers and seawater is
290 overwhelmingly complexed to organics (McBride 1981; Coale and Bruland 1988; Moffett
291 and Brand 1996; Shank et al. 2004; Grybos et al. 2007; Vance et al. 2008; Ryan et al. 2014),
292 and the above calculations for inorganic species are relevant only to the tiny inorganic pool
293 of Cu. Little et al. (2014b) and Sherman et al. (2015) show how heavy Cu in simple organic
294 complexes controls seawater Cu isotopes. Note that the interpretation strongly depends on
295 the speciation diagram applied (Fujii et al. 2013). Powell et al. (2007) uses small hydrolysis
296 constants, which depress the role of hydroxides in Cu isotope fractionation; isotope
297 fractionation may therefore not be seen in Cu(II) hydroxide, but Cu in $CuCO_3$ should
298 nevertheless remain isotopically light with respect to the remaining inorganic pool of Cu
299 in seawater, and much lighter than the dominant organically-complexed pool.

300 Since sulfide-bearing euxinic seawater systems are reducing, isotope fractionation
301 of Cu caused by the co-presence of Cu(I) becomes important (Fujii et al. 2013). The ln β
302 value of sulfides is 1-2‰ lower than Cu(II) carbonates, hydroxides, and hydrated $Cu^{2+}$.
303 This suggests that the dominant organically-complexed pool, as well as minor $Cu^{2+}$, Cu(II)
304 chlorides, carbonates, and hydroxides will all be isotopically heavier than sulfides. The
305 speciation of Cu(I) under hydrothermal conditions (Mountain and Seward 1999) indicates
306 that the prevailing species are CuCl, $CuCl_2^-$, CuHS, and $Cu(HS)_2^-$. Increasing complexation
307 of Cu(I) chlorides and sulfides results in decreasing ln β. The ln β values of Cu(II) chlorides
308 and sulfides at 573 K are 0.2-0.5‰ higher than those of corresponding Cu(I) species (Fujii
309 et al. 2013; Fujii et al. 2014). Under hydrothermal conditions, the $\delta^{65}$Cu value of Cu(I) may
310 be 0.2-0.5‰ lower than that of Cu(II) with a ±0.1‰ range of variation among Cu(I)
311 species.

312 As an application to plant uptake, $\delta^{65}$Cu for Cu phosphates, citrates, hydroxides,
313 and hydrated $Cu^{2+}$ ions was estimated as a function of pH (Fujii et al., 2014). At neutral
314 pH, the major Cu(II) species are phosphates and citrates, and a range of ~0.5‰ can be
315 expected for $\delta^{65}$Cu. This range overlaps with observations on higher plants (Weinstein et
316 al. 2011; Jouvin et al. 2012). A reduction of $Cu^{2+}$ to $Cu^+$ by a reductase within roots has
317 also been reported by Jouvin et al. (2012). Since the range of ln β values for Cu(I) species
318 is ~2‰ smaller than those of Cu(II) species at 298 K, a fractionation of -0.84 to -0.11‰
319 between roots and nutrient solutions (Jouvin et al. 2012) may be expected.

320 A variety of metabolic processes may induce Cu isotope fractionation. A positive
321 $\delta^{65}$Cu of 1.5‰ was found in both sheep kidney (Balter and Zazzo 2011) and mouse kidney

322 (Albarède et al. 2011), which may be interpreted in terms of isotope exchange reactions
323 among Cu(I) and Cu(II) species. Oxalic acid is a ubiquitous toxic organic acid in bodily
324 fluids. High oxalate contents in urine and plasma may be correlated with kidney damage.
325 Ascorbate is efficiently converted to oxalate when the coexisting copper concentration is
326 high (Hayakawa et al. 1973). The $\delta^{65}$Cu of the Cu species relative to the bulk solution as a
327 function of Eh and extent of oxalate formation has been estimated (Fujii et al. 2013); $\delta^{65}$Cu
328 of Cu ascorbate varies from –1.0 to +0.5‰ when Eh increases from –1 V to +1 V, but its
329 mole fraction remains very small, while the heavy isotope is enriched (+0.6 to +2.5‰) in
330 the Cu oxalate relative to total Cu. It is expected that degradation of ascorbate and excretion
331 of oxalate should leave isotopically heavy Cu in the kidney. With respect to food, which
332 has a $\delta^{65}$Cu value of about 0‰, if even trace amounts of oxalate form it should leave behind
333 copper with a $\delta^{65}$Cu of ~1.4‰ ($\delta^{65}$Cu at 0‰ extent of oxalate formation). This value is
334 very close to the $\delta^{65}$Cu (1.5‰) found in sheep (Balter and Zazzo 2011) and mice (Albarède
335 et al. 2011) kidneys.

336 Variations in Cu isotopes among $Cu^{2+}$-amino acid complexes have been estimated
337 (Fujii et al. 2014). The ln β of $Cu^{2+}$ complexes with O and N-donor amino acids is ~1‰ (at
338 the body temperature of 310 K typical for mammals) higher than those with S-donor amino
339 acids. In a same donor amino acid complex, $\delta^{65}$Cu of ~1‰ may be created via $Cu^{2+}/Cu^{+}$
340 redox processes in biological activity. This latter study also theoretically estimated the β
341 of Cu lactates. The extent of $^{65}$Cu preference over $^{63}$Cu in Cu lactates with respect to Cu
342 bound to cysteine is more than 1‰. From a study on the $^{65}Cu/^{63}Cu$ ratios in the serums of
343 cancer patients, a $\delta^{65}$Cu alarm threshold was found to be at -0.35‰. The decrease of $\delta^{65}$Cu

344 in the serum of cancer patients is assigned to the extensive oxidative chelation of copper
345 by cytosolic lactate (Telouk et al. 2015).

346 The ln β values of Zn(II) species (Fujii et al. 2010; Black et al. 2011; Fujii et al.
347 2011; Fujii and Albarède 2012; Fujii et al. 2014) are shown in Table 4 and some species
348 are represented in the Figure 2. It is known that Zn sulfate and carbonate create larger ln β.
349 The fivefold and sixfold coordination of Zn in carbonate complexes, for which carbonates
350 are treated as monovalent and divalent ligands, results in large ln β (Fujii et al. 2011; Fujii
351 et al. 2014). At circumneutral pH the dominant inorganic species of free $Zn^{2+}$ shows small
352 isotope fractionation relative to the total inorganic pool. Zinc sulfate is enriched in $^{66}Zn$,
353 whereas Zn chlorides are enriched in $^{64}Zn$ with a $\Delta^{66}Zn$ ~0.5‰ being expected between Zn
354 sulfate and chloride. With increasing pH, $Zn(OH)_2$ and $ZnCO_3$ become the dominant
355 species. Small amounts of free $Zn^{2+}$ and $ZnCl^+$ still exist at pH = 8.2. In seawater, a
356 fractionation $\Delta^{66}Zn$ of ~1‰ is expected between Zn carbonate and chloride. Zinc
357 hydroxides and sulfates do not play an important role for Zn isotope fractionation for pH
358 ≥ 8.2. It is again noted, however, that the free and inorganically-complexed pool of both
359 Cu and Zn in soil solutions, rivers and seawater is very minor (in seawater, on the of order
360 2%; McBride 1981; Coale and Bruland 1988; Moffett and Brand 1996; Shank et al. 2004;
361 Grybos et al. 2007; Vance et al. 2008; Ryan et al. 2014) and most is organically complexed.
362 As such, the above discussion is only relevant to the minor free metal and inorganically-
363 complexed pool.

364 The role of sulfides is central to a broad range of geological scenarios. The status
365 of sulfur in ancient oceans in particular is still an outstanding issue (Canfield 1998).

366 Hydrothermal vent solutions discharging either at mid-ocean ridges (Edmond et al. 1979)
367 or along subduction zones (Mott et al. 2004) comprise additional environments dominated
368 by sulfides. Fujii et al. (2011) evaluated the isotope fractionation among the different Zn
369 sulfide species present in geological fluids between 298 and 573 K (Fig. 2). At the high
370 $P_{CO2}$ conditions of hydrothermal solutions, Zn precipitated as sulfides is isotopically nearly
371 unfractionated with respect to a low-pH parent fluid. In contrast, negative $\delta^{66}$Zn, down to
372 at least -0.6‰, can be expected in sulfides precipitated from solutions with pH > 9. Zinc
373 isotopes in sulfides and rocks therefore represent a potential indicator of mid to high pH in
374 ancient hydrothermal fluids (Pons et al. 2011).

375 Citric acid also plays an important role in the transport of trace metals in the soil-
376 plant system. Citrate is released from the roots of vascular plants and acts as a biological
377 chelating agent for the uptake of metals from soil. Isotope fractionation induced by higher
378 plants has been found for Zn (Weiss et al. 2005; Moynier et al. 2009b). In a pioneering
379 study of isotope fractionation of Zn in the soil-plant system, Weiss et al. (2005) found that
380 Zn was isotopically lighter in the shoots relative to the roots, with a $\delta^{66}$Zn difference of -
381 0.13 to -0.26‰. The origin of this isotope fractionation may be isotopic exchange between
382 Zn(II) phosphates in roots and citrates (or malates) in plants (Fujii and Albarède 2012).

383 The ln β values for optimized structures of $Zn^{2+}$-amino acid complexes have been
384 calculated (Fujii et al. 2014). Heavy isotopes tend to bind to O-donor ligands, whereas light
385 isotopes are positively fractionated by S-donor ligands (Balter et al. 2013; Moynier et al.
386 2013a). This is clearly seen in complexes with identical coordination number (four and
387 six). Isotope fractionation correlated with N-donor ligands may be intermediate between

O-donor and S-donor systems or even stronger than with O-donor ligands. Besides the donor type, coordination number is important, implying that four-fold complexation gives larger ln β values relative to complexes with six-fold coordination. The ln β of $Zn(His)^{2+}$ complexes is 0.2 to 0.6‰ larger than that of $Zn(Cys)^{2+}$. This matches the observation that organs rich in proteins with histidine residues show larger $\delta^{66}Zn$ than organs in which proteins rich in cysteine residues dominate (Moynier et al. 2013a).

## ZINC AND COPPER IN EXTRA-TERRESTRIAL SAMPLES AND IGNEOUS ROCKS

***Chondritic Reference Frame and meteorites.*** Luck et al. (2003; 2005) were the first to measure Cu and Zn isotopes in a selection of carbonaceous and ordinary chondrites by MC-ICP-MS. The carbonaceous chondrite data show resolvable isotopic variation for both Zn and Cu isotopes between the different groups (e.g. CI, CV, CO, CM…) with the latter system showing the largest variability ($0.16<\delta^{66}Zn<0.52$ and $-1.44<\delta^{65}Cu<-0.09$, Fig. 3 and 4). For both systems, each carbonaceous group has a distinct isotope composition (Fig. 3 and 5). There is also a broad positive co-variation between the Cu and Zn isotope compositions of the carbonaceous chondrites, with the CI chondrites defining the heaviest compositions in both systems. The most robust average composition for the CI chondrites has been obtained from the average composition of 6 large chips of the Orgueil meteorite as well as samples from Ivuna and Alais and is $\delta^{65}Cu = 0.05\pm0.16$‰ and $\delta^{66}Zn = 0.46\pm0.08$‰ (Barrat et al. 2012).

For the ordinary chondrites, Zn isotopes define the larger range ($-1.30<\delta^{66}Zn<0.76$, Fig. 4), compared to Cu ($-0.51<\delta^{65}Cu<0.10$, Fig. 3), although the difference between groups (H, L, LL) is much clearer in the Cu system, whereas the variations in Zn isotopes in ordinary chondrites seem to be controlled by degree of parent body metamorphism, as well as subsequent secondary alteration on the Earth's surface (i.e., 'falls' are much less variable than 'finds').

Luck et al. (2003) showed that the $\delta^{65}Cu$ composition of carbonaceous and ordinary chondrites varies systematically with their mass-independent $\Delta^{17}O$ value ($\delta^{18}O-0.52*\delta^{17}O$, Fig. 3) and $^{58}Ni/^{65}Cu$ ratio, although the two groups fall on distinct trends. They interpreted this phenomenon as revealing the presence of at least two, and potentially three, distinct Cu isotope reservoirs in the early solar system, which subsequently mixed via nebular processing to create the distinct chondritic bodies. They further suggested, based on the relationship with $^{58}Ni/^{65}Cu$ ratio, that the range of Cu isotope compositions was potentially defined early in solar system history by the heterogeneous distribution of a phase enriched in the short-lived radionuclide $^{63}Ni$, which decays to $^{63}Cu$.

Luck et al. (2005) discovered a negative correlation between $\delta^{66}Zn$ and Mg/Zn in carbonaceous chondrites and un-equilibrated ordinary chondrite falls (Fig. 5). This was taken as robust evidence against evaporation as the origin of the variability of Zn abundance between chondrites groups (with the exception of EL6, see later), and rather suggested that the variation in the volatile element content of chondrite parent bodies was fixed by nebular processes. This argument was later developed by Albarède (2009) to suggest that the volatile element abundance in chondrites was inherited from nebular

conditions during accretion, and that the Earth must have accreted "dry" and acquired its volatile elements via later impact events.

Enstatite chondrites are the most reduced type of chondrites and the only group that shares similar isotopic anomaly patterns with Earth for most elements (e.g. O, Cr, Ni, Ti; Moynier and Fegley 2015). For Cu isotopes, the high (EH) and low (EL) iron groups have identical average compositions ($\delta^{65}Cu \approx -0.25‰$; Savage et al. 2015b), falling in the center of the chondritic range, although the more volatile depleted EL define a larger range (Fig. 3). Enstatite chondrites of types EH and EL3 (low thermal metamorphic grade) have a similar Zn isotopic composition ($0.15‰<\delta^{66}Zn<0.31‰$, Moynier et al. 2011) to that of carbonaceous chondrites, unequilibrated ordinary chondrites and current estimates of BSE (Fig. 4A). On the other hand, those EL chondrites which experienced strong thermal metamorphic alteration (EL6) are highly enriched in the heavier isotopes ($\delta^{66}Zn$ up to 7.35‰, Fig. 4B) and are highly depleted in Zn and other moderately volatile elements. The enrichment in the heavier isotopes of Zn is evidence that the origin of the volatile element depletion between EL3 and EL6 chondrites was due to volatilization during thermal metamorphism (Moynier et al. 2011). Why such large enrichments in heavy Zn are not reflected by the Cu isotope composition of EL6 chondrites is puzzling; however, it should be noted that the amount of Cu loss between EH and EL6 is much less significant than the amount of Zn loss; also there are no EL3 Cu isotopic measurements – it could be that EL3 chondrites have a lighter Cu isotope composition than EH, and that the similarity between EH and EL6 is merely coincidence. This question remains unanswered.

Ureilites are ultramafic achondrites which are widely considered as mantle restites. Ureilites with different shock degrees and volatile element abundances show a positive correlation between $\delta^{66}Zn$ (with values up to 1 ‰) and 1/Zn, whereby samples with the lowest Zn content have the heaviest Zn isotopic compositions (Moynier et al. 2010b). This was taken as evidence that, as with EL6 meteorites and terrestrial tektites (see later), the variations in the abundance of Zn (isotopes) between ureilite samples is controlled by evaporation processes. In addition, the more depleted samples also exhibited a higher shock state, suggesting an impact may have been responsible for the heating event.

The HED (howardites, eucrite, diogenites) meteorites, presumably derived from the asteroid 4-Vesta, have highly variable $\delta^{66}Zn$ (-2 to +1.7‰, Paniello et al. 2012b). On the other hand, unbrecciated eucrites ($1.6<\delta^{66}Zn< 6.22$‰, n=4) and diogenites ($0.94‰<\delta^{66}Zn< 1.6$‰, n=3) are all isotopically heavy and are all more depleted in Zn (and other moderately volatile elements) than brecciated HED suggesting that some volatile loss by evaporation occurred during the formation of the Vestan crust.

Iron meteorites are mostly composed of Fe and Ni and are enriched in siderophile elements compared to chondrites. The so-called magmatic groups (or fractionally crystallized iron groups) are thought to represent the cores of disrupted asteroids while the silicate-bearing groups have a more complex history, and may have formed as pools of impact-produced melt near the base of a regolith on a chondritic parent body (Wasson and Wang 1986). Luck et al. (2005) found that the IIIAB magmatic iron meteorites show very limited isotopic variations of both Cu and Zn, while silicate-bearing iron meteorites from group IA and IIICD are enriched in the heavier isotopes of Zn by up to 3.7‰ (although

474 their Cu isotopes are mostly unfractionated). Bridgestock et al. (2014) have expanded the
475 set of Zn isotopic data in the silicate bearing IA irons and in the IIAB and IIIAB groups
476 with high precision Zn concentration determined by isotope dilution. They found that, in
477 general, all iron meteorites are isotopically heavy in Zn relative to terrestrial/carbonaceous
478 chondrites, and that the $\delta^{66}$Zn is negatively correlated with 1/Zn for each individual group.
479 They also showed that chromites are Zn-rich and isotopically light ($\delta^{66}$Zn~0) and proposed
480 that the correlation observed between $\delta^{66}$Zn and 1/Zn correspond to the segregation of
481 chromite from metal. Chen et al. (2013a) and Bishop et al. (2012) measured the Cu and Zn
482 isotope compositions of a large set of irons, including Zn-poor iron meteorite groups such
483 as IVA and IVB, and did not find any particular enrichments in the heavier isotopes relative
484 to other iron meteorite groups, suggesting that the low volatile element contents recorded
485 in these meteorites is not related to evaporation during the parent body history. Bishop et
486 al. (2012) found that, as observed in chondrites by Luck et al. (2003), $\delta^{65}$Cu correlates with
487 $\Delta^{17}$O for silicate bearing iron meteorites. Such a correlation between mass-dependent and
488 non-mass dependent isotopic fractionation must reflect mixing between at least two solar
489 nebula components (see above); hence, the variations in the Cu isotopic composition of the
490 silicate-bearing iron meteorites originates from nebular processes rather than from
491 planetary differentiation effects. Bishop et al. (2012) further proposed that the same may
492 be true for magmatic iron meteorites (which do not contain silicates and so for which it is
493 not possible to determine the $\Delta^{17}$O) and that Cu isotopes could be used to determine genetic
494 connections between meteorite groups. Chen et al. (2016) measured the Cu isotope
495 composition of the IVB (magmatic) iron meteorites and found a very large range of
496 variation (-5.84 ‰ < $\delta^{65}$Cu < -0.24 ‰ ). The IVB irons are the most volatile depleted iron

meteorites, with Cu concentration depletions several orders of magnitude larger than other iron meteorites groups and Ni/Cu ratios of ~$10^5$. Chen et al. (2016) show that the Cu isotope variations are controlled by neutron capture due to galactic cosmic ray irradiation by a reaction on $^{62}$Ni to form $^{63}$Ni, which decays to $^{63}$Cu ($t_{1/2} \approx 100$ yrs).

Williams and Archer (2011) reported the Cu isotopic composition of phase separates (metal, troilite and silicate) from a variety of iron meteorites and coupled these with Fe isotope composition of the same phases. They found a large range of Cu isotope variations among metals and troilites (~ 10‰ variations) and also within the calculated metal-troilite fractionation factor (≤~5‰ variations) suggesting a kinetic control on the isotopic fractionation between the different phases. However, the most equilibrated samples display the smallest metal/troilite fractionation factor of ~0.5‰, with the metal phase being enriched in the heavier Cu isotope.

***Mass-independent Zn anomalies in extra-terrestrial material.*** In terms of nucleosynthesis, Zn is classed as an iron peak (IP) element, along with Ca, Ti, Cr, Ni and of course, Fe. These elements have the highest nuclear binding energies per nucleon, and the 'iron-(abundance)-peak' is defined by the heaviest nuclides for which nuclear fusion becomes is energetically unfavourable during element synthesis ($^{56}$Ni, which decays to $^{56}$Fe). As such, IP elements are only formed in the cores of massive stars or by explosive nucleosynthesis, where formation of some of the nuclides is dominated by nuclear statistical (quasi)equilibrium during explosive nucleosynthesis (NSE/QSE; see Wallerstein et al., 1997, for a review). The measurement of so-called isotope anomalies (identification of isotope reservoirs that do not fall on the terrestrial fractionation line) of the iron peak elements in extra-terrestrial materials have afforded many important insights into the stellar

520 sources of material into the solar system, early solar system processes, and the building
521 blocks of the terrestrial planets (e.g. Birck 2004; Moynier and Fegley 2015).

522 Of the IP element isotope systems, Zn isotope anomalies are, arguably, the least
523 well constrained with (at the time of writing), less than 10 studies available in the literature.
524 The initial work (using TIMS, Loss and Lugmair 1990; Völkening and Papanastassiou
525 1990) focused on the analysis of refractory inclusions from primitive meteorites (those
526 phases thought to be the first to condense from a cooling nebula gas). Previously measured
527 Ca, Ni and Cr anomalies in these materials (see Birck 2004 and refs therein) were modelled
528 by Hartmann et al. (1985) in terms of nuclear statistical equilibrium, which also predicted
529 relatively large $^{66}$Zn excesses. Although Loss and Lugmair (1990) and Volkening and
530 Pappanastassiou (1990) measured resolvable $^{66}$Zn anomalies, these were much smaller
531 than those predicted by the models, and this was explained as a result of the higher volatility
532 of Zn compared to the other IP elements; i.e. by the time Zn began to condense, mixing in
533 the solar nebula had diluted most anomalous Zn. Nevertheless, the presence of anomalous
534 Zn in refractory inclusions is extremely puzzling, because Zn should not condense at all
535 during their formation, and so all Zn in these inclusions must have been introduced by
536 secondary processes. This implies that Zn isotope anomalies survived the hot initial stage
537 of the solar system, potentially as a distinct sulphide phase, but this is a long standing and
538 poorly understood issue (e.g. Chou et al. 1976).

539 TIMS measurements could not resolve any Zn anomalies at the bulk meteorite
540 scale, and this was apparently confirmed by the first MC-ICP-MS measurements, which
541 showed that bulk chondrites plotted within error of the terrestrial mass fractionation line in
542 $\delta^{66}$Zn vs. $\delta^{68}$Zn space (Luck et al. 2005) – seemingly confirming that Zn condensed too

543 late for resolvable anomalies to be detected at this scale. The requirement of such large
544 $^{66}$Zn excesses to accompany other neutron rich IP anomalies, particularly $^{48}$Ca, was also
545 relaxed with the advancement of nucleosynthesis models into so-called quasi-equilibrium
546 (e.g., Meyer et al. 1998). Nevertheless, the first paper to specifically investigate Zn isotope
547 anomalies on the bulk meteorite scale was Moynier et al. (2009a), which utilized MC-
548 ICPMS. The advantages of MC-ICPMS over TIMS, regarding the detection of Zn
549 anomalies, are the much better precision attainable, the ability to accurately measure $^{67}$Zn,
550 which always suffered from an unidentified interference on TIMS and, finally, the ability
551 to switch individual amplifier resistances to increase the dynamic range of the instrument.
552 Moynier et al. (2009a) used a smaller resistance amplifier on the $^{64}$Zn detector to allow for
553 higher concentration samples to be analysed, with the specific aim of investigating
554 potential $^{70}$Zn heterogeneity in bulk solar system materials – important as this can constrain
555 the distribution of $^{60}$Fe (a short-lived radionuclide) in the solar nebula. At the precisions
556 attained in their study (±100 ppm), no resolvable $^{66}$Zn, $^{67}$Zn or $^{70}$Zn anomaly patterns were
557 measured (when normalized to $^{68}$Zn/$^{64}$Zn), which indicated relatively homogeneous
558 distribution of Zn isotopes, and also $^{60}$Fe; however, there were some hints in their anomaly
559 patterns that, with further improvements in precision, anomalies in $^{66}$Zn or $^{67}$Zn may be
560 present and measureable.

561 With techniques modified from Moynier et al. (2009a) and with analytical precision
562 at the ±10ppm level, Savage et al. (2014) showed for the first time that carbonaceous
563 chondrites do have resolvable $^{66}$Zn and $^{68}$Zn excesses (when normalized to $^{67}$Zn/$^{64}$Zn), and,
564 also that enstatite and potentially ordinary chondrites have smaller $^{66}$Zn deficits; this is
565 consistent with the sense of $^{48}$Ca, $^{50}$Ti, $^{54}$Cr and $^{62}$Ni anomalies measured in the same

samples (Trinquier et al. 2009, Steele et al., 2012, Dauphas et al. 2014; Moynier and Fegley 2015; Schiller et al. 2015). The complementary excesses and deficits exhibited by the carbonaceous and enstatite/ordinary chondrites, the more volatile nature of Zn, and the correlations between Zn and other iron-peak anomalies adds further credence to the 'unmixing' hypothesis of solar nebula evolution, where specific phases were remobilized via thermal processing in a previous well-mixed nebula cloud (e.g. Trinquier et al. 2009; Schiller et al. 2015). Sequential leaching experiments show that the Zn anomalies are not limited to one phase, although this is most likely due to post-formation remobilization of Zn. One important insight from this dataset is that Earth is not similar to enstatite chondrites, in terms of Zn isotope budget, adding to a slowly growing group of isotope systems (O, Ti, Mo) which bring in to question the 'enstatite chondrite' Earth model (e.g. Moynier and Fegley 2015). Now that Zn isotope anomalies have been discovered in bulk primitive meteorites, there is potential to discover such anomalies in other solar system materials, and the new insights from this system could be hugely important for our understanding of our solar system.

***Bulk Silicate Earth composition.*** The estimation of the isotopic composition of the bulk silicate Earth is not trivial since both Zn and Cu are fractionated during partial melting of the mantle, hence during differentiation processes their isotopes may be fractionated also. In addition, as both Zn and Cu are trace elements, metasomatism or low-temperature alteration could overwhelm any primitive signal that a rock once held. Therefore, in order to estimate the Cu and Zn isotopic compositions of the bulk silicate Earth (BSE) it is necessary to 1) choose pristine samples; 2) constrain the extent to which igneous

588 differentiation processes fractionate the isotopes, and; 3) analyze as wide a variety of
589 mantle derived samples as possible.

590 The first modern Cu and Zn isotope estimates of BSE were based on the average
591 composition of MORB samples taken from three ocean basins: $\delta^{65}Cu = 0‰$ and $\delta^{66}Zn =$
592 0.25‰ (Ben Othman et al. 2006). The reason that no precision is given is that these data
593 are given in a conference abstract; nevertheless, for the following decade, these estimates
594 were the accepted values (the abstract was never written up and no further systematic
595 studies were performed).

596 It is only recently that further investigations into this area have been made. Since
597 Cu is highly incompatible and strongly chalcophile, its behavior during mantle melting is
598 controlled by the fusion of sulfides (Lee et al. 2012); for partial melting degrees <25%,
599 residual sulfides may be retained in the source and could potentially create isotopic
600 fractionation. In order to test the possible effect of partial melting on the isotopic
601 composition of Cu, Savage et al. (2015b) measured komatiites (ultra-mafic lavas formed
602 by >25% partial melting; $\delta^{65}Cu = 0.06\pm0.06‰$, 2sd, n=14) and compared these to fertile
603 orogenic lherzolites (mantle samples that have undergone the least melt depletion:
604 $\delta^{65}Cu=0.07\pm0.09‰$, 2sd, n=16: Ben Othman et al. 2006; Ikehata and Hirata 2013), as well
605 as a representative selection of both mid-ocean ridge and ocean island basalts. All groups
606 have identical Cu isotope compositions (Fig. 6) which suggests that during mantle melting
607 there is limited Cu isotope fractionation expressed in the melt. Savage et al. (2015a)
608 therefore used all this data to propose a $\delta^{65}Cu=0.07\pm0.10‰$ (2sd) for the BSE.
609 Furthermore, these authors measured the Cu isotope compositions of two magmatic

610 differentiation sequences, from Kilauea Iki, Hawaii, and Hekla, Iceland, systems. Both
611 suites define a large range of $SiO_2$ and MgO contents and evolved from a cogenetic source
612 with limited contaminations by crustal materials. The samples from Kilauea Iki showed no
613 variation away from BSE with increasing degree of differentiation, as would be expected
614 given the lack of sulfide fractionation in this system. In comparison, the samples from
615 Hekla show more variability, which seems to be related to the removal of sulfides in the
616 magma chamber. However, these variations are limited (range of compositions from Hekla
617 $-0.08‰<\delta^{65}Cu<0.20‰$) and, crucially, the basalts from Hekla are identical to BSE. This
618 indicates that significant igneous differentiation generates only limited Cu isotope
619 fractionation, further confirmed by the similarity of I-type granite ($\delta^{65}Cu=0.03\pm0.15‰$,
620 2sd: Li et al. 2009) to BSE.

621 Liu et al. (2015) reached similar conclusions to Savage et al. (2015b) by comparing
622 a large set of both unmetasomatised cratonic and orogenic peridotites with MORB, and
623 OIB and proposed a $\delta^{65}Cu=0.06\pm0.20‰$ (2sd) for the BSE. Their data for metasomatised
624 peridotites were much more variable, demonstrating the susceptibility of Cu-depleted rocks
625 to secondary isotope fractionation; this was also seen in large negative Cu isotope
626 excursions in Kilbourne Hole peridotites which correlate with LREE enrichment, and with
627 large positive komatiite Cu isotope enrichments which only occur in those samples whose
628 Cu contents do not plot on olivine control lines (Savage et al. 2015a). This suggests that
629 Cu isotopes could be further utilized as a tracer of recycled materials in the mantle and, for
630 instance, island arc material; indeed, Liu et al. (2015) provide a large set of arc basalt data
631 whose range is much larger than that defined by both MORB and OIB (Fig. 6).

632 Compared to the Cu isotope system, fewer studies have attempted to address the
633 behavior of Zn isotopes during igneous processes. Chen et al. (2013a) evaluated the extent
634 to which Zn isotopes are fractionated during igneous processes by the same set of samples
635 as Savage et al. (2015a) for Cu isotopes, those of Kilauea Iki, USA, and Hekla Volcano,
636 Iceland. Both sets of samples show ~0.1 per mille isotopic variation but only the $\delta^{66}$Zn of
637 the Kilauea Iki samples vary systematically, correlating with the degree of differentiation
638 (MgO contents) with the most evolved samples enriched in the heavier isotopes (see Fig.
639 7). These isotopic variations are interpreted as the result of crystallization of isotopically
640 light olivines, and Ti-oxides at the very end of the differentiation sequence (Chen et al.
641 2013b). Chen et al. (2013b) combined the data from mafic rocks from Herzog et al. (2009),
642 and their own data to determine the $\delta^{66}$Zn of the BSE to be 0.28 ± 0.08‰. More recently,
643 Sossi et al. (In review) have shown that ultramafic rocks comprising unmetasomatised
644 peridotites from the Balmuccia massif and komatiites with ages varying from 3.5 to 2.7Ga
645 are all isotopically lighter than basalts and complement the $\delta^{66}$Zn vs MgO trend defined by
646 Chen et al. (2013b). Sossi et al. (In review) used the average of these ultramafic samples
647 to determine the most up to date $\delta^{66}$Zn composition of the BSE to be 0.15 ± 0.05‰. Telus
648 et al. (2012) showed that most granites are not isotopically fractionated in Zn with regards
649 to the BSE value, but pegmatites and some granites are isotopically heavy (up to ~0.9‰).
650 Telus et al. (2012) interpreted these heavy isotopic compositions in terms of fluid
651 exsolution and suggest that Zn isotopes can be used to trace fluid exsolution in rocks.

652 ***Isotopic fractionation during core formation.*** Given that both Zn and Cu can partition in
653 measureable quantities into the metal phase during metal-silicate equilibration, there is the
654 potential that both isotope systems could reveal insights into the physiochemical conditions

655 of Earth's differentiation into a planet with a metallic core and silicate mantle. However,
656 for both Zn and Cu, their isotope partitioning behavior is only now being investigated via
657 experimental studies – but there is huge potential for further work.

658 In the case of Zn, Bridgestock et al. (2014) showed that there appears to be no
659 isotope effect associated with metal silicate equilibration. This indicates that, even if there
660 is measureable Zn in Earth's core, partitioning into this reservoir would not leave its
661 isotopic fingerprints on Earth's mantle. This is consistent with the similarity of the BSE
662 composition with those of carbonaceous, unequilibrated ordinary and EH chondrites (see
663 above).

664 The case of Cu is more complicated. A series of metal-silicate experiments
665 performed by Savage et al. (2015b) indicated that the heavier Cu isotope prefers to enter
666 the metal phase. This would suggest (given that 2/3 of Earth's Cu is in the core) that bulk
667 Earth is isotopically heavier than the value estimated for BSE (see above). The problem is
668 that there are no primitive meteorites thus far measured which match this isotopically heavy
669 composition (in fact, the Cu isotope composition of BSE is still heavier than most
670 chondrites; Fig. 3). Assuming that the bulk Earth is chondritic, i.e., the bulk Earth has a
671 lighter Cu isotope composition than its mantle, this could imply a number of possibilities:

672 1) Cu is also a moderately volatile element, depleted in Earth's mantle relative to
673 chondrites. It could be that impact-driven volatilization created this depletion,
674 which would preferentially lead to the loss of light Cu, leaving a heavy residue.
675 However, as Zn and to a lesser extent Cu isotopes in chondrites have shown,

676 Earth's volatile depletion was more likely caused by nebula processes (see
677 above).
678 2) Earth's mantle Cu isotope composition is not in equilibrium with its core: it
679 could be that late addition of Cu to the Earth, during the final stages (i.e. the
680 giant impact) or post-core formation (i.e. the late veneer) may have set the BSE
681 composition. In the case of the late veneer, there is not enough mass delivered
682 by this process to account for all the Cu in the mantle today. In the case of the
683 giant impactor, this is dependent on the composition of the impactor – even if
684 it was CI-like (e.g. Schonbachler et al. 2010), the disruption created by this
685 event would still have led to phase equilibration in the following magma ocean.
686 3) Earth contains a hidden, isotopically light Cu reservoir. Savage et al. (2015b)
687 performed sulfide-silicate Cu isotope fractionation experiments, and found that,
688 in this instance, the sulfide phase preferentially takes the lighter isotope of Cu;
689 hence, rather than 2/3 of Cu being held in the core, this reservoir may be split
690 into an isotopically heavy metal and isotopically light sulfide (relative to BSE).
691 One possibile sulfide reservoir is that of a 'Hadean Matte' (O'Neill 1991; Lee
692 et al. 2007), an Fe-O-S phase that remains as the final liquid after the
693 crystallization of a magma ocean. Modelling this in terms of [Cu] and $\delta^{65}$Cu
694 suggests that, if such a reservoir formed and eventually was admixed into the
695 core (it would sink through the mantle due to its higher density), it could add
696 up to ~0.8wt.% S to the core (Savage et al. 2015b).

697 Although there are caveats associated with each of the above models, Cu isotopes could be
698 a powerful tool in tracing the fate of sulfides in various igneous and planetary processes,

699 but the framework to understand this fractionation is still required, and more experimental
700 work is required.

701 ***Isotopic fractionation by evaporation on Earth.*** While the Zn and Cu isotopic database
702 for terrestrial igneous rocks is very limited, tektites are extremely fractionated (Moynier et
703 al. 2009c). Tektites are terrestrial natural glasses produced during a hypervelocity impact
704 of an extraterrestrial projectile onto the Earth's surface, and are extremely depleted in
705 volatile elements, e.g., they are among the driest terrestrial samples (<0.02% of water).
706 Moynier et al. (2009c) found that tektites are extremely enriched in the heavier isotopes of
707 Zn, up to 2.5 ‰ and attributed this enrichment to kinetic isotopic fractionation during
708 evaporation. Copper can be even more fractionated than Zn, with $\delta^{65}$Cu up to 12.5 ‰ found
709 in some European tektite samples (Rodovka et al. In review). The difference of behavior
710 between Cu and Zn has been explained by isotopic fractionation in a diffusion-limited
711 regime, where the magnitude of the isotopic fractionation is regulated by the competition
712 between the evaporative flux and the diffusive flux at the diffusion boundary layer
713 (Moynier et al. 2010a). Copper diffuses much faster than Zn (due to the difference in ionic
714 charge in silicates of $Zn^{2+}$ vs. $Cu^{+}$), hence the larger isotopic fractionation in Cu than in Zn
715 in tektites is due to the significant difference in their respective chemical diffusivity.

716 ***The Moon.*** The isotopically heavy lunar regolith (2.2‰<$\delta^{66}$Zn < 6.4‰ and 2.6‰<$\delta^{65}$Cu
717 <4.5‰) reflects billions of years of evaporation due to solar wind sputtering and
718 micrometeorite impact gardening (Moynier et al. 2006; Herzog et al. 2009). On the other
719 hand, the low-Ti ($\delta^{66}$Zn = 1.31 ± 0.13‰) and high-Ti basalts ($\delta^{66}$Zn = 1.39 ± 0.39) have a
720 more limited isotopic variations and are systematically ~1 ‰ heavier than the BSE for Zn

721 (Paniello et al. 2012a; Day and Moynier 2014; Kato et al. 2015). The only data available
722 for Cu isotopes ($\delta^{65}$Cu =0.5±0.1‰, Herzog et al. 2009) suggests that there is a similar
723 enrichment in the heavy Cu isotope in lunar? rocks, but this will need further investigation
724 in the future. Since the isotopically heaviest carbonaceous chondrite group (CI) has a $\delta^{66}$Zn
725 = 0.46‰ and $\delta^{65}$Cu = 0.05‰ (Luck et al. 2003, 2005; Barrat et al. 2012), mixing with
726 chondrites does not explain the Zn or Cu isotopic composition of the lunar basalts. In
727 addition, lunar plutonic rocks (alkali and magnesian suite samples) are isotopically heavier
728 than the mare basalts ($\delta^{66}$Zn up to 6.27‰) suggesting that the volatile loss could have
729 occurred in two stages: during the proto-lunar disk stage, where a fraction of lunar volatiles
730 accreted onto Earth, and from degassing of a differentiating lunar magma ocean, implying
731 the possibility of isolated, volatile-rich regions in the Moon's interior (Kato et al. 2015).

732 **ZINC AND COPPER IN LOW TEMPERATURE GEOCHEMISTRY**

733 Since the pioneering work of Maréchal et al. (1999; 2000), and Francis Albarède's
734 chapter on Cu and Zn isotopes in the first RiMG volume on non-traditional stable isotopes
735 (Albarède 2004), a considerable amount of effort has gone into understanding and applying
736 isotope variations of these two elements in samples from Earth's surface. As with the
737 development of any relatively new isotope system, documentation of stable isotope
738 variations in nature has been coupled with experimental and theoretical studies aimed at
739 characterizing isotopic fractionations associated with key surface Earth processes. Copper-
740 Zn stable isotope geochemistry of the surface Earth environment has been part of reviews
741 by Cloquet et al. (2008) and Wiederhold (2015). An emerging new interest lies in the
742 application of Zn and Cu isotopes to the study of biological pathways and changes in

743 metabolism associated with diseases. These applications are here treated in chapter X
744 (Albarède et al. 20XX, this volume).

745 The data obtained to date for important surface Earth reservoirs are summarized in
746 Figure 8. One of the first order features of Cu-Zn isotope geochemistry that this
747 compilation confirms is the contrast between the relative homogeneity of samples whose
748 isotopic characteristics are determined by high temperature processes, versus the
749 variability in materials formed and equilibrated at low temperatures. Thus, igneous rocks
750 (excluding ultramafic rocks) show a very tight distribution, with $\delta^{66}Zn = 0.30\pm0.07‰$ (n =
751 77, 1SD) and $\delta^{65}Cu = 0.08\pm0.17‰$ (n = 287) which overlaps with the BSE estimate
752 presented earlier in this chapter (note that these averages were taken using all igneous rock
753 data available in the literature, without screening for the possibility of secondary
754 alteration/metasomatism – hence they are slightly different, and have poorer precisions, to
755 those defined in the section above). Another first-order feature of the data in Figure 8 is
756 that sediments that have undergone physical, but minimal chemical, processing through the
757 fluid envelopes of the surface Earth (i.e. clastic sediments from rivers, lakes, oceans, as
758 well as aerosols/dust), have average Cu and Zn isotope signatures that are identical to high
759 temperature igneous rocks, and are not much more variable. In contrast, environmental
760 samples that *have* seen such biogeochemical processing record a roughly 2.5‰ range in
761 Cu and Zn isotopes, or about 30-40 times the analytical precision. Ore minerals that formed
762 at high temperatures exhibit a range of roughly 1‰ that is also more or less centred on the
763 peak in igneous rocks (Fig. 8, black bars at bottom). In contrast, the isotope compositions
764 of minerals from the supergene environment, containing Cu that has undergone (possibly
765 multiple) oxidation and reduction cycles, exhibit huge (~20‰) variability (e.g. Maréchal

et al. 1999; Larson et al. 2003; Mason et al. 2005; Mathur et al. 2005; Markl et al. 2006; Asael et al. 2007; Mathur et al. 2009; Mathur et al. 2010).

In the following sections we first review the experimental constraints on the size and sign of isotope fractionations of Cu and Zn associated with key surface, low temperature, processes. Secondly, we discuss the origin of, and geochemical constraints available from, Cu and Zn isotope variability in "natural" samples – i.e. those not significantly impacted by human activities. This large subject is separated into sub-sections on (1) the weathering-soil-plant system, and (2) the oceans, their inputs, outputs and internal cycling. In this section we also briefly outline the very few studies that have sought to apply Cu-Zn isotopes in Earth history, and outline the prospects for the future of such a pursuit. Isotopic variations, and their expression in environmental samples, superimposed by human activity on this natural biogeochemical cycling represent a somewhat distinct topic, and are treated in a third section. For convenience, and since ore minerals often represent the starting material from which pollution of the Anthropocene environment derives, the very large variability seen in ore minerals is also dealt with in this third section.

## Experimental constraints on fractionation mechanisms

A survey of the literature reveals four general isotope fractionation mechanisms causing the roughly 2.5‰ variation in both Cu and Zn isotopes in environmental samples, as well as the much greater degree of variability in supergene Cu ore minerals:

1. Equilibrium isotope distributions between Cu in different oxidations states;

7872. Equilibrium isotope distribution between dissolved aqueous species;

7883. Equilibrium and kinetic effects caused by interactions between solids – abiotic as well as
789 living cells - and aqueous solutions (sorption, precipitation);

7904. Kinetic and equilibrium effects related to uptake into the cells of living microbes and higher
791 plants.

792 The sign and magnitude of these fractionations are summarized in Figure 9 and are
793 discussed in turn below. Though the separate processes bulleted above makes discussion
794 more convenient, distinction between these fractionation mechanisms is not often sharp.
795 To some extent this lack of clarity represents some confusion in the literature. Thus, for
796 example, all metals sorb to the external surfaces of microbial cells, and to some extent the
797 roots of higher plants. This is a somewhat distinct phenomenon from uptake into the cells
798 for metabolic use in enzymes and proteins. When metal uptake is studied in
799 microbiological or hydroponic plant growth experiments, the vast majority of the metals in
800 solution in the media are bound to an added organic complexant, such as EDTA. This
801 leaves only a small pool of free metal ion, which is often regarded as the pool that is
802 available for uptake. The isotopic composition of the metal taken up can be lighter than the
803 bulk experiment, for example where uptake is transport (diffusion)-limited (e.g. John et al.
804 2007b), or it can be heavier, for example for some plant species that actively bind external
805 metals using phytosiderophores (e.g. Arnold et al. 2010a).

806 On the other hand, in experiments where organic complexants have not been added,
807 the free metal ion pool is often many orders of magnitude more concentrated. In this case
808 the metals sorb to external surfaces. Though sometimes described as “uptake” in the

809 literature, there is almost certainly no metabolic function of the metals in this case. Such
810 sorption often involves binding to deprotonating functional groups such as carboxyls and
811 amines, so that the fractionation factors measured in these experiments are more relevant
812 to categories 2 and 3 above than 4. On the other hand, there is sometimes genuine
813 uncertainty over whether a pool of metals associated with a cellular experimental product
814 is intra-cellular or sorbed on external surfaces. Some researchers have been able to
815 distinguish between these two mechanisms using experiments with living (active metabolic
816 uptake) versus dead (passive adsorption) cells, or by removing the extra-cellular pool using
817 a desorptive wash prior to analysis (e.g. John et al. 2007b; Navarette et al. 2011). Finally,
818 Cu uptake into microbial cells has been interpreted as involving reduction of external
819 Cu(II) to internal Cu(I) – i.e. a component of 1 above (e.g. Zhu et al. 2002; Navarette et al.
820 2011; Jouvin et al. 2012; Ryan et al. 2013).

821 ***Changes in oxidation state.*** Zinc does not undergo changes in oxidation state at Earth
822 surface conditions. Thus, although a substantial isotope fractionation has been
823 characterized in an electroplating experiment involving reduction of aqueous Zn (II) to Zn
824 metal (Kavner et al. 2008), this is unlikely to be relevant to natural systems. For copper,
825 on the other hand, the transition between Cu(I) and Cu(II) happens at redox conditions
826 relevant to the Earth's surface, and Cu occurs in both reduced and oxidized forms in Earth
827 materials. Further, it is clear that the redox transition involves large isotope fractionations.
828 This fractionation was first characterized by Zhu et al. (2002) in experiments that found
829 $\Delta^{65}Cu_{Cu(II)-Cu(I)} = 4‰$ for the reduction of aqueous Cu(II) to a Cu(I) iodide precipitate at
830 20°C (here and throughout $\Delta^{65}Cu_{x-y} = \delta^{65}Cu(\text{phase x}) - \delta^{65}Cu(\text{phase y})$). Ehrlich et al. (2004)
831 followed this up with experiments involving the precipitation of Cu(I)S (covellite) from an

aqueous Cu(II) solution and found $\Delta^{65}Cu_{Cu(II)aq\text{-}Cu(I)S} = 3.06\pm0.14‰$ at 20°C. Furthermore, and importantly, they contrasted this large fractionation with the small one ($\Delta^{65}Cu_{Cu(II)aq\text{-}Cu(II)(OH)2} = 0.27\pm0.02‰$) for Cu(II) hydroxide precipitation from a $Cu(II)_{aq}$ solution. This finding, as well as that by Maréchal and Sheppard (2002) of small (0.2-0.4‰) isotopic differences between Cu(II) in solution versus malachite, strongly suggests that it is the change in oxidation state, and not the phase change, that causes the large isotopic shift seen in these and other redox experiments. These results were further confirmed by Mathur et al. (2005), who found that Cu (I) in chalcocite ($Cu_2S$) and chalcopyrite ($CuFeS_2$) was 1.3 and 2.74‰ lighter than aqueous Cu(II) in abiotic batch oxidative leach experiments. In analogous experiments inoculated with *Thiobacillus ferrooxidans* the heavy oxidized Cu was located in amorphous Cu-Fe oxide minerals surrounding bacterial cells.

Zhu et al. (2002) found that Cu incorporated into proteins expressed in bacteria and yeast cells was 1.0-2.1‰ lighter than in the parent solutions and media, and used these findings to suggest that the biogenic uptake of light Cu also involved reduction. Likewise, Navarette et al. (2011) interpret Cu isotope variations in media from which live bacterial cells remove Cu as due to cellular uptake (as opposed to sorption, which induces a different fractionation in their experiments, as observed in dead cells). This is associated with preferential uptake of the light isotope – by up to 4.4‰ - and was also interpreted to involved reduction of Cu(II). As noted in this study, if this reduction occurs within the cell, the changes seen in the media require that there is also efflux of heavy Cu from the cells, allowing equilibration of the two Cu pools. As discussed later in this section, uptake of isotopically light Cu by bacteria and higher plants probably also involves reduction by a

854 reductase protein (e.g. Navarette et al. 2011; Weinstein et al. 2011; Jouvin et al. 2012; Ryan
855 et al. 2013).

856 ***Organic complexation.*** Copper forms very strong inner sphere complexes
857 (conditional stability constants up to $10^{25}$) with functional groups in organic matter
858 (McBride 1981; Grybos et al. 2007; Ryan et al. 2014). Virtually all Cu in the operationally-
859 defined dissolved phase (that fraction passing through a 0.45μm filter) of rivers and the
860 oceans is bound in these organic complexes (e.g. McBride 1981; Coale and Bruland 1988;
861 Moffett and Brand 1996; Shank et al. 2004; Grybos et al. 2007; Vance et al. 2008; Ryan et
862 al. 2014), such that inorganically-complexed and free $Cu^{2+}$ ion concentrations are 2-5
863 orders of magnitude lower than total dissolved Cu. Similarly, up to 98% of the "dissolved"
864 Zn in many natural waters is also complexed to organic ligands, though with stability
865 constants that are of order $10^{9}$-$10^{11}$ (e.g. Wells et al. 1998; Bruland 1999; John et al. 2007b).
866 Grybos et al. (2007) suggest that two important processes compete to control transition
867 element behavior in soils: binding to organic complexes, both in condensed organic matter
868 and in an aqueous phase, versus sorption to the surfaces of secondary minerals such as
869 clays and Fe-Mn oxyhydroxides. The last decade of research on Cu-Zn isotopes has
870 revealed that this competition is almost certainly key for isotope distributions, not only in
871 soils but also between the dissolved and particulate phases in rivers and the oceans (e.g.
872 Vance et al. 2008; Bigalke et al. 2010a; b; Bigalke et al. 2011; Little et al. 2014b; Vance et
873 al. 2016). In quantifying the isotopic fractionations between an (often) aqueous
874 organically-complexed pool and the sorbed pool, the universal approach has thus far been
875 to measure the isotopic separation between each of these and a dissolved free metal ion
876 ($Cu^{2+}$, $Zn^{2+}$) pool. Each of these, therefore, are here dealt with separately.

877 Ban et al. (2002) were the first to quantify the isotopic impact of this important
878 process, finding $\Delta^{66}Zn_{EDTAZn\text{-}Zn2+} \sim 0.2‰$ (here and throughout $\Delta^{66}Zn_{x\text{-}y} = \delta^{66}Zn_{(phase\ x)}$-
879 $\delta^{66}Zn_{(phase\ y)}$). Jouvin et al. (2009) used Donnan membranes to separate free Zn from that
880 complexed to humic acid. These authors found no fractionation at pH ≤5.4, but $\Delta^{66}Zn_{Humic\text{-}}$
881 $_{Zn2+} = +0.24\pm0.06‰$ at pH 6.1-7.2. The variable fractionation as a function of pH was
882 interpreted in terms of the partitioning of the bound Zn between high affinity (HA, bound
883 to phenols) and low affinity (LA, bound to carboxylate groups) sites, and the fact that, at
884 equilibrium, isotopically heavy Zn is partitioned into the strongly-bound species. Zinc is
885 increasingly bound to the HA sites at higher pH (50:50 LA and HA at pH around 6.1-6.2).
886 Based on calculated mass balance between the species, Jouvin et al. (2009) proposed a
887 fractionation factor, $\alpha_{HAS\text{-}Zn2+}$, of 1.0004. Bigalke et al. (2010a) performed the same
888 experiment for Cu at pH 2-7. In the case of Cu there is no apparent isotopic difference
889 between LA and HA sites, and only 11-35% of the bound Cu is in HA sites. For both,
890 $\Delta^{65}Cu_{Humic\text{-}Cu2+} = +0.26\pm0.11‰$. More recently, Ryan et al. (2014) measured the Cu isotope
891 fractionation between free Cu and a range of soluble organic ligands. They see a "strong"
892 positive correlation between the isotopic fractionation and the value of the stability
893 constant for each complex. Thus for natural riverine fulvic acid (log K = 8) $\Delta^{65}Cu_{complex\text{-}free}$
894 $= +0.14\pm0.11‰$, whereas for desferrioxamine B (DFOB logK = 24.7) $\Delta^{65}Cu_{complex\text{-}free} =$
895 $+0.84\pm0.30‰$.

896 ***Sorption to abiotic substrates.*** As with the fractionations associated with organic
897 complexation outlined above, isotopic effects associated with sorption have also been
898 measured experimentally relative to a dissolved free metal ion pool. Pokrovsky et al. (2005)
899 measured Zn isotope fractionations upon sorption from simple aqueous solutions of low

900 ionic strength (0.01M), where Zn is speciated as a hexaquocomplex, and where the sorption
901 equilibrium can often be envisaged as (omitting the solvating waters in the aqueous
902 species):

903 $$>MeOH^0 + Zn^{2+} = MeO\text{-}Zn^+ + H^+$$

904 They found a small preference for the light isotopes of Zn (by about ~0.18-0.23‰) on
905 goethite and birnessite ($\delta$-$MnO_2$) surfaces, and for the heavy isotopes (by about ~0.11-
906 0.14‰) on pyrolusite ($\beta$-$MnO_2$) and aluminium oxides. Zinc sorbed to hematite exhibited
907 the largest isotopic separation from dissolved free Zn, with $\Delta^{66}Zn_{sorbed\text{-}free} = +0.61$‰ when
908 sorption starts at pH 5.5, but decreasing to zero at higher pH as sorption increases. Not all
909 the results of this pioneering study have been reproduced. Indeed in all subsequent studies,
910 sorbed Zn has been found to be universally heavy relative to the aqueous free metal ion
911 pool. Bryan et al. (2015) discuss possible reasons for these discrepancies, including the
912 possibility of kinetic effects in short duration experiments. Moreover, theoretical
913 considerations (e.g. Schauble 2004) suggest that the lower co-ordination of the metal
914 sorbed on these surfaces (e.g. Peacock and Sherman 2004; Balistrieri et al. 2008; Juillot et
915 al. 2008) should prefer the heavy isotope.

916 Balistrieri et al. (2008) find heavy Cu and Zn sorbed onto ferrihydrite, in a study
917 incorporating both natural data from streams draining a metal sulphide deposit and
918 experimental results. The experiments were also done with low ionic strength solutions
919 (0.008M). The sorption experiments only lasted 2-3 hours, but in this case the sorption of
920 heavy isotopes as well as a close-to-linear relationship between the fraction of dissolved
921 metal and isotopic composition rule out a kinetic effect. Again, however, only the aqueous

922 phase was measured so that the mass balance was not confirmed. This study also mixed
923 water draining a mine (acidic and metal-rich) with water from the river (uncontaminated
924 and alkaline) it drains into. Overall, aqueous Cu and Zn concentrations decrease as pH
925 increases and as they are sorbed onto ferrihydrite, and the aqueous phase becomes light.
926 The $\Delta_{sorbed\text{-}solution}$ values are +0.73±0.08‰ for Cu and +0.52±0.04‰ for Zn. Despite
927 potential variation in aqueous speciation with pH, these sorption experiments are well
928 modeled by a single process, which they suggest to be a change in co-ordination and bond
929 length – octahedral co-ordination in solution with Me-O bond distances of 2.0-2.4Å, versus
930 tetrahedral-co-ordination on ferrihydrite and other Fe oxides and bond lengths of 1.8-2Å.
931 Pokrovsky et al. (2008) corroborate the finding of sorption of heavy Cu, finding $\Delta^{65}Cu_{sorbed\text{-}}$
932 $_{solution}$ = 0.8±0.2‰ for goethite and1.0±0.2‰ for gibbsite.

933 Juillot et al. (2008) confirmed this result for Zn sorption to ferrihydrite ($\Delta^{66}Zn_{sorbed\text{-}}$
934 $_{solution}$ = +0.53‰). These authors also obtained $\Delta^{66}Zn_{sorbed\text{-}solution}$ for goethite = +0.29‰. In
935 these experiments ionic strength was kept at 0.1M using $KNO_3$ and some solids were
936 measured to close the mass balance. Moreover, time-dependent experiments found light
937 Zn taken up onto ferrihydrite in the first hour, before the observations settled down to a
938 constant heavy value at about 18 hours, possibly explaining the light value found in the
939 Pokrovsky et al. (2005) study. These authors also interpret their results in terms of changes
940 in co-ordination and bond-length. The smaller fractionation for goethite is ascribed to the
941 fact that bond-lengths are shorter on the surface relative to solution, even though Zn is
942 octahedrally co-ordinated on goethite, versus tetrahedral co-ordination on ferrihydrite.
943

944 Recently, Bryan et al. (2015) conducted a much more extensive study of Zn isotopic
945 fractionation during sorption to poorly crystalline Mn oxyhydroxide, which dominates the
946 sorption of many metals, including Zn, in the marine environment (e.g. Koschinsky and
947 Hein 2003; Wasylenki et al. 2011; Little et al. 2014b). Isotopic fractionations were
948 monitored as a function of equilibration time, ionic strength of the solution, speciation of
949 inorganic zinc in the aqueous phase, and degree of loading of the Mn oxide surface. The
950 Zn isotopic composition of both solid and dissolved phase were measured, allowing an
951 assessment of overall experimental mass balance as well as of the relative importance of
952 kinetic versus equilibrium fractionation. For low ionic strengths there is a small kinetic
953 effect ($\Delta^{66}Zn_{sorbed\text{-}dissolved} \sim -0.2‰$) for experimental durations up to 48 hours, but for
954 equilibration times greater than 100 hours fractionations are within uncertainty of zero
955 ($\Delta^{66}Zn_{sorbed\text{-}dissolved} = +0.05\pm0.08‰$). For high ionic strength solutions heavy isotopes are
956 always preferentially adsorbed, but there is a strong dependence on surface loading, with
957 $\Delta^{66}Zn_{sorbed\text{-}solution} = +2.74‰$ for low surface loadings (8%), reducing to +0.16‰ for high.
958 The authors interpret this variation in terms of a change in co-ordination from tetrahedral
959 to octahedral as surface loading increases from tetrahedral for Mn oxide with Zn/Mn =
960 0.008 to octahedral at Zn/Mn = 0.128 (Manceau et al. 2002). The difference in behavior
961 at different ionic strengths is partially attributed to the fact that in the low ionic strength
962 experiments the surface loadings were also high (Zn/Mn ~ 0.2). There may also be an effect
963 of speciation. The authors suggest that it is free $Zn^{2+}$ that is sorbed. The isotopic
964 composition of free Zn is predicted to change as ionic strength and the proportions of
965 inorganic carbonate and chloride complexes of Zn, with different equilibrium
966 fractionations relative to free Zn (Fujii et al. 2010, 2014; Black et al. 2011), change. For

967 Zn sorption to kaolinite (Guinoiseau et al., 2016), qualitatively similar variation in $\Delta_{\text{sorbed-free aqueous ion}}$ (Fig. 9) has been interpreted as a shift from outer sphere complexation of Zn in
968
969 basal exchange sites at low pH, when edge sites are protonated, to inner sphere
970 complexation on edge sites, and larger fractionations, at higher pH and ionic strength.

971

972 ***Sorption/binding to biological suurfaces.*** Both elements under consideration here
973 are essential nutrients for plants and animals, but they are toxic at high concentrations in
974 both the terrestrial and marine realm (e.g. Anderson and Morel 1978; Flemming and
975 Trevors 1989; Marschner 1995; Moffett and Brand 1996; Sold and Behra 2000; Peers and
976 Price 2006; Broadley et al. 2007; Yruela 2009; Sinoir et al. 2012; Bruland et al. 2014).
977 Thus, there are important interactions with the cells of living matter that induce significant
978 isotope fractionations. As noted earlier a careful distinction must be made, one that is not
979 always made in the literature (though see John et al. 2007b; Navarette et al. 2011), between
980 metals that are sorbed or bound to the surfaces of microbial cells and plant roots, and those
981 taken up for metabolic utilization. In terms of basic chemical and isotopic mechanisms, the
982 former process is more akin to the binding to the functional groups of both organic matter
983 and inorganic surfaces discussed in previous sections, and usually favours the heavy
984 isotopes. The latter may favour either the light isotope, if governed by a transport-limited,
985 kinetic, process (e.g. John et al. 2007b) or if it involves reduction as may be the case for
986 Cu (e.g. Zhu et al. 2002; Navarette et al. 2011), or the heavy, if it occurs through active
987 uptake by phytosiderophores (e.g. Arnold et al. 2010a).

Gélabert et al. (2004; 2006) conducted experiments that characterized the nature of interactions between marine and freshwater diatoms and aqueous Zn, including isotope fractionation. The aqueous phase (the medium) in these experiments had inorganic Zn concentrations of 0.3-20 μM. With no organic complexant stabilizing Zn in solution, the process studied is sorption, not "uptake". Zinc sorption was strongly controlled by organic layers covering the silica frustule, specifically by carboxylate and silanol groups, with the amount of Zn sorbed to an organic-free silica skeleton being factor five less than cell with organic surface layers. They find $\Delta^{66}Zn_{diatomcell\text{-}medium}$ = +0.1‰ to +0.5‰ in the presence or absence of organic layers. Coutaud et al. (2014) conducted experiments that characterized fractionation upon uptake and release by and from a "phototrophic biofilm" (an aggregate of micro-organisms embedded in a exopolysaccharide matrix) and see adsorption of heavy isotopes to a much greater degree than this – by up to 1.2±0.4‰ relative to solution. Some of these fractionations for sorption to cells are very similar to those measured for those outlined earlier for complexation of Zn to organic functional groups, which may be the dominant binding process (Gélabert et al. 2004; Gelabert et al. 2006). They are also often similar to those found for externally-bound Zn in culturing experiments by John et al. (2007b) that were primarily targeted at documenting fractionation upon uptake into the cells themselves.

Three additional studies have been aimed at quantifying and understanding the sorption of Cu and Zn onto cells, but differ in their interpretation of the exact driver of the fractionations observed, specifically whether it was sorption or biological uptake. Pokrovsky et al. (2008), in experiments with Cu sorption onto abiotic metal surfaces and onto bacterial and diatom cells at low ionic strength (0.01-0.1M), see virtually no

1011 fractionation upon sorption to bacterial cells at circumneutral pH (5.1-6.1, $\Delta^{65}Cu$ = mostly
1012 0±0.3‰). They see light Cu sorbed onto the cells of soil bacteria at pH 1.8-3.3 (by up to
1013 1.8‰). The rationale given for the sorption of light Cu in this case relates to an outer-
1014 sphere monodentate complex likely to form between Cu and phosphoryl groups – with
1015 apparently longer bond distances - on bacterial surfaces at low pH.

1016 Navarette et al. (2011), on the other hand, contrast two sets of Cu uptake
1017 experiments with live versus dead cells of *E. coli* and *B. subtilis*. When the cells are alive
1018 the solution gets much heavier as it loses Cu to the cells, with $\Delta^{65}Cu_{cells\text{-}solution}$ as low as -
1019 2.6‰ and -4‰ at different pH values. On the other hand, when cells were dead, the solution
1020 was lighter, and only by about 0.4‰. As with the small fractionations of Zn in the Gélabert
1021 et al. (2004; 2006) experiments, it is likely that the latter process is analogous to the
1022 complexation of Cu to organic functional groups outlined earlier (e.g. Bigalke et al. 2010c;
1023 Ryan et al. 2014). The uptake of light Cu by live cells, on the other hand, is interpreted in
1024 terms of active intra-cellular complexation. Navarette et al. (2011) confirm this finding in
1025 experiments where the aqueous Cu is stabilised by organic complexants so that it is not
1026 sorbed. They again document large separation factors, with $\Delta^{65}Cu_{cells\text{-}solution}$ = -1.2 to -
1027 4.4‰, depending on species and the nature of bacterial consortia used in each experiment.
1028 The authors suggest that the light uptake may be due either to a kinetic fractionation –
1029 irreversible incorporation – or to an equilibrium reduction to Cu(I) within the cell. If the
1030 latter is important there has to be communication with the outside of the cell to allow the
1031 efflux of the oxidized Cu back to the solution. The theme of a paper by Kafantaris and
1032 Borrok (2014) is similar, in this case applied to Zn, in that their objective was to try to
1033 understand the relative importance of surface complexation versus intracellular

1034 incorporation. For experiments with high Zn/bacterial cells ratios, Zn sorption varies with
1035 increasing pH in a very similar way to abiotic experiments, presumably due to increased
1036 deprotonation of cell surface organic functional groups and consequent binding of Zn. Zinc
1037 isotopic data are best fitted by an equilibrium model with a separation factor $\Delta^{66}Zn_{cells-solution}$ +0.46‰. In contrast, this study found heavy Zn in solutions at low Zn/bacterial cells
1039 ratios, with $\Delta^{66}Zn_{cells-solution}$ = -2.5‰. This is interpreted in terms of the complexation of
1040 Zn in the dissolved phase by organic exudates, generating two pools of Zn, a complexed
1041 (heavy) and a free (light) pool, with the light free Zn pool sorbing onto cell surfaces. This
1042 would, however, require an isotope separation factor between organically-complexed and
1043 free Zn of 2-3‰, an order of magnitude greater than that found in experiments to date (Ban
1044 et al. 2002; Jouvin et al. 2009). On the other hand, these authors also used an electrolyte
1045 wash to remove extra-cellular Zn in an attempt to quantify intra-cellular inventories and
1046 isotopic composition, and also found Zn isotopes in cells to be slightly, to very, heavy
1047 relative to the aqueous phase. It should be noted, however, that these experiments were
1048 conducted at Zn concentrations 3-4 orders of magnitude greater than found in nature,
1049 perhaps at levels where Zn is toxic. Moreover, precipitates containing high levels of Zn on
1050 cell surfaces, probably not removed by their wash, is likely at these high concentrations.

1051

1052 ***Metabolic uptake by algae and higher plants.*** Primary production by
1053 photosynthesis on Earth is roughly equally split between higher plants on land and algae
1054 in the oceans (Field et al. 1998). As noted earlier, Cu and Zn are both essential
1055 micronutrients for photosynthesizing organisms and are indeed required for enzymes and

1056 proteins in all organisms, but are also both toxic to plants and algae at very high
1057 concentrations. There have been a relatively small number of studies characterizing
1058 fractionation of Cu and Zn isotopes during uptake by plants – as opposed to absorption or
1059 binding to external surfaces as discussed in the previous section.

1060 John et al. (2007b) report culturing experiments with the diatom *Thalassiosira*
1061 *oceanica* across a range of free Zn ion concentrations, controlled in their media by the
1062 addition of complexant EDTA, representative of coastal and open ocean waters. In order
1063 to document fractionation during uptake, such culturing studies must remove externally
1064 adsorbed Zn by washing prior to analysis, and John et al. (2007b) find that the externally-
1065 sorbed Zn isolated in this way has an isotopic composition that is 0.1-0.5‰ heavier than
1066 the medium, consistent with other studies where binding of Zn to diatom external surfaces
1067 has been specifically targeted (Gelabert et al. 2006). In contrast, Zn in washed cells
1068 (targeting the internalized cellular Zn pool) is isotopically lighter than the medium. John et
1069 al. (2007b) document a range in fractionations, from $\Delta^{66}Zn_{diatom\text{-}medium}$ = -0.2‰ at low
1070 medium free Zn concentrations to -0.8‰ at high, with a step-like transition at free Zn
1071 concentrations that are in the range for natural seawater, at around $10^{-10}$M. The authors
1072 ascribe these two different fractionations to two different Zn uptake systems – high and
1073 low affinity. These two systems are well-documented in previous culturing studies (e.g.
1074 Sunda and Huntsman 1992), with the high affinity pathway up-regulated when available
1075 Zn is low but saturated at high seawater/medium Zn concentrations. The low affinity
1076 pathway likely involves diffusive transport across the cell membrane, thus favouring the
1077 light isotope. John and Conway (2014) document the same magnitude of fractionation upon
1078 uptake into a different kind of phytoplankton – the marine flagellate chlorophyte

1079 *Dunaliella tertiolecta*. The $\Delta^{66}Zn_{cells\text{-}medium}$ = -0.76±0.02‰ obtained is the same as for the
1080 low affinity uptake system in the diatom experiments, consistent with the high free Zn
1081 concentrations in their medium.

1082 There have been more studies focusing on fractionations of Cu and Zn isotopes
1083 upon uptake into higher plants. Taken as a whole, these studies have documented a number
1084 of important features of plant uptake systems for Cu and Zn: (1) all plants have a bulk Cu
1085 isotope composition that is lighter than the external pool (c.f. bacterial uptake of Cu in
1086 Navarette et al. (2011), discussed earlier), leading to the suggestion that Cu reduction upon
1087 uptake is an important process; (2) bulk plant Zn isotopic compositions are both lighter and
1088 heavier than the external bioavailable pool, perhaps depending on whether free Zn or a
1089 complex is taken up; (3) all plants preferentially transfer the lighter isotopes of Zn upwards
1090 into stems and leaves, whereas early studies document preferential upward translocation of
1091 both light and heavy Cu isotopes.

1092 Before discussing the details of experimental isotopic studies for Cu and Zn in
1093 higher plants, it is useful to briefly set the context in terms of plant uptake systems and the
1094 constraints that have come from the better studied Fe isotopic system (see Russel et al.
1095 2003 for useful summaries; Jouvin et al. 2012). For Fe, two fundamentally different uptake
1096 strategies lead to different isotope fractionations (e.g. Guelke and Von Blanckenburg
1097 2007). Iron acquisition by Strategy I (non-graminaceous) plants involves the uptake of a
1098 free metal ion and requires a reduction step that favours uptake of isotopically light Fe.
1099 Analogously uptake of free Cu via transporters such as COPT1 has been described (e.g.
1100 Sancenon et al. 2004; Jouvin et al. 2012), and would also require reduction of soil Cu (II)
1101 to Cu (I) by a reductase enzyme. For Zn there is no oxidation state change involved. As

1102 with the diatom studies outlined above, Strategy I uptake of Zn may involve both a low
1103 and high affinity uptake system (see Jouvin et al. 2012). Low affinity uptake, active at
1104 external bioavailable Zn concentrations in excess of perhaps $10^{-7}$M (e.g. Wang et al. 2009;
1105 Jouvin et al. 2012), involves diffusive transport via ion channels and electrogenic pumps,
1106 favouring the light isotope. High affinity Strategy I uptake involves zinc-iron-permease
1107 (ZIP) proteins that bind free Zn from the external pool at the cell membrane, probably
1108 favouring the heavy isotope, and facilitate its uptake and transmembrane transport. In
1109 contrast, Strategy II uptake (graminaceous plants), under metal-deficient conditions, can
1110 actively complex soil Fe (III) to a phytosiderophore derived from their root – with no
1111 reduction step and a small positive isotope fractionation for Fe (e.g. Guelke and Von
1112 Blanckenburg 2007; Moynier et al. 2013b). Uptake of Zn and Cu in "phytosiderophores",
1113 organic complexes that will favour the heavy isotope as discussed in earlier, have been
1114 discussed in the isotopic literature as outlined below.

1115 The pioneering study of Weiss et al. (2005) showed that the roots of tomato, rice
1116 and lettuce were all slightly enriched in the heavy isotopes of Zn relative to the bulk nutrient
1117 solution in which they were grown – by 0.1-0.2‰. In contrast, the shoots, housing 75-85%
1118 of the Zn inventory of the plant, were isotopically light relative to the same nutrient solution
1119 – by 0.25-0.5‰, so that the bulk plants contain light Zn relative to the external pool. The
1120 simplest explanation of this observation requires the uptake of isotopically light Zn,
1121 through ion channels or electrogenic pumps, coupled to the preferential upward transfer of
1122 even lighter Zn, leaving the residual root pool heavy. Fujii and Albarède (2012) re-
1123 interpreted these observations using *ab initio* calculations and suggested that the
1124 fractionation is controlled by the difference in Zn speciation between the root system

1125 (isotopically heavy Zn-phosphates) and the upper parts, rich in isotopically light citrates
1126 and malates. It is noteworthy that the predicted isotopic signal of Strategy I behavior is
1127 found in a Strategy II plant like rice. In a follow up study, however, Arnold et al. (2010a)
1128 demonstrate that rice grown in soil rather than hydroponically is isotopically *heavy* relative
1129 to the soil, particularly under Zn deficiency. They attribute this to uptake of Zn bound to a
1130 "Zn-phytosiderophore". On the other hand, Tang et al. (2012) also observe Zn in plants
1131 that is up to ~0.6‰ heavier than in soils, but reject the phytosiderophore hypothesis
1132 because the species concerned do not release them. Instead, they favour uptake of heavy
1133 isotopes by ZIPs. The upwards transfer of light Zn has been confirmed by later studies (e.g.
1134 Moynier et al. 2009b; Caldelas et al. 2011; Jouvin et al. 2012; Tang et al. 2012).

1135 This earlier work on Zn uptake by plants has been followed up by a series of more
1136 targeted studies aimed at more detailed investigation of the mechanisms by which plants
1137 take up Zn and its isotopes, especially with regard to speciation and including Zn uptake
1138 by zinc hyperaccumulators from contaminated soils (Aucour et al., 2011, 2015; Houben et
1139 al., 2014; Couder et al., 2015).

1140 Weinstein et al. (2011) first measured the isotopes of Cu in plants, documenting
1141 light isotopes in every part of Strategy II plants – by 0.3-0.8‰ - relative to the soils in
1142 which they were grown. They also document significant transfer of light Cu upwards from
1143 the roots, or from the initial stock of Cu in lentils grown from seed without further Cu
1144 addition. In all cases, the topmost and youngest leaves contain the lightest Cu. These
1145 findings were confirmed by Jouvin et al. (2012). Though the latter study found a difference
1146 between Strategy I ($\Delta^{65}Cu_{plant\text{-}nutrient\ solution}$ = -0.84 to -0.47‰) and Strategy II ($\Delta^{65}Cu_{plant\text{-}}$
1147 $_{nutrient\ solution}$ = -0.48 to -0.11‰), all of them took up the light isotope, suggesting that

reduction of Cu (II) is an important factor in the uptake of Cu by all plants whether the Cu is complexed or not. Like the previous two studies, Ryan et al. (2013) observe much lighter Cu in plants than the soils in which they were grown, and a very clear difference between Strategy I ($\Delta^{65}Cu_{\text{whole plant-nutrient solution}}$ = -1.02±0.37‰) and Strategy II ($\Delta^{65}Cu_{\text{whole plant-nutrient solution}}$ = -0.15±0.11‰) plants. However, in contrast to the previous two studies, their Strategy II plants have a fairly constant isotopic composition in different parts of the plant while for Strategy I the heavier isotope preferentially moves upwards (shoots 0.87-1.35‰ heavier, leaves 0.53-0.98‰ heavier). These authors rationalize their observations in terms of the upward transfer of Cu in organic complexes like nicotinamine, which would indeed preferentially transport the heavy isotope (Ryan et al. 2014), if translocation upwards was not close to quantitative.

**Cu-Zn isotopes in the weathering-soil-plant system**

Soils represent the interface between the solid Earth and its fluid envelope, the place where chemical weathering of primary minerals and precipitation of secondary minerals begin, the substrate for plant growth, and the locus for the initial partitioning of elements between solid material and the aqueous phase that drains into groundwater, rivers and, eventually, the oceans. In addition, transfer of chemical elements between the atmosphere and soils occurs through the ablation, transport and deposition of dust. As such, soils are sites of complex processes that involve Cu and Zn transfer and isotopic fractionation via all of the mechanisms detailed in the previous section. For ease of discussion here we separate these processes as follows: (1) isotopic effects associated with leaching and dissolution of primary minerals; (2) the partitioning of Cu and Zn and their isotopes between a dissolved pool, often complexed to soluble organics, and a pool sorbed to

1171 secondary minerals; (3) overprinting of weathering processes via the addition of
1172 atmospheric aerosol to soils; (4) uptake into plants and associated isotope fractionations in
1173 the upper organic-rich levels of soils. Anthropogenic addition of Cu and Zn to soils is a
1174 fifth important process but is dealt with in the section on the Anthropocene later in this
1175 chapter.

1176 ***Weathering release of Cu and Zn from primary minerals.*** To our knowledge there
1177 are only two studies that have characterized Cu-Zn isotope compositions upon release from
1178 primary minerals to an experimental leachate designed to simulate the weathering process.
1179 Fernandez and Borrok (2009) measured isotopic compositions of fluids released during
1180 oxidative leaching experiments on rocks containing sulphides (pyrite, chalcopyrite, galena,
1181 sphalerite). Copper released is 2‰ heavier than the starting rocks at pH 2 and 5. Zinc
1182 released is both heavier and lighter than the primary sulphide, depending on the precise
1183 rock/mineral being leached, but only by order 0.2‰. For Cu the release of heavy isotopes
1184 is almost certainly related to an oxidation state change, from Cu(I) in the sulphides to Cu(II)
1185 in the leachates. Weiss et al. (2014) conducted experiments on leaching of biotite granite
1186 using 0.5M HCl and oxalic acid. Zinc mobilized into the aqueous phase in the first hour
1187 was as light as -1.2‰ relative to starting material, with 30-40% of the initial rock Zn pool
1188 released. The Zn in solution then moved back towards the initial rock, but never got beyond
1189 0.1 -0.3‰ lighter after 168 hours (with 45-75% of the original starting Zn mobilised). The
1190 early, very negative, fractionations are interpreted as being kinetic.

1191 ***Cu-Zn isotopes of soils and the impact of sorption and aqueous complexation.***
1192 Though experimental studies are a useful template for the interpretation of field data, real
1193 weathering of rocks in soils is more complex for two main reasons. Firstly, Cu and Zn are

not necessarily located in sulphide minerals such as in the Fernandez and Borrok (2009) experimental leaching study. Where this *is* the case the results obtained from field studies are consistent with the experiments. Thus Mathur et al. (2012) studied Cu isotopes in soils and soil waters developed on black shales in Pennsylvania USA, where a very large proportion of the Cu is located in pyrite. Loss or gain of an element of interest (*i*) during the soil development process is often expressed in terms of a tau ($\tau$) value (Chadwick et al. 1990), which normalizes the concentration (C) of the element in a particular soil horizon (*h*) to both that in the parent material (*p*) and to the concentration of an immobile element (*j*, often Nb, Zr or Ti):

$$\tau_{i/j} = \frac{(C_i/C_j)_h}{(C_i/C_j)_p} - 1$$

Tau values greater than zero denote addition of the element of interest relative to the immobile element, and values less than zero loss. Unfortunately, not all studies of Cu and Zn isotopes in soils report tau values (Viers et al. 2007; Mathur et al. 2012; Liu et al. 2014; Vance et al. 2016), but they are essential for identifying net loss or gain of an element given changes in mass that occur during soil development. Tau values for the Mathur et al. (2012) soils are about -0.5, implying loss of 50% of the original Cu in the rock, while $\delta^{65}$Cu is about 0.5-1‰ lighter than the original Cu. In contrast, soil pore waters are all enriched in the heavy isotope, by 0.7-1.7‰. The authors attribute these findings to the preferential

1214 mobilization of heavy isotopes due to the oxidative leaching of pyrite, consistent with an
1215 abundance of experimental data, including those of Fernandez and Borrok (2009).

1216 Secondly soil solutions, and the interactions between this aqueous phase and the
1217 residual solids in the soil, are more complex than those in the experimental studies
1218 described above. Mathur et al. (2012) discuss other possible interpretations of their Cu
1219 isotopic data, such as organic complexation in solution with a preference for the heavy
1220 isotope, but dismiss their relevance to that particular setting given the dominance of pyrite
1221 as a reservoir for Cu in the parent rock. However, in many soil settings it is the equilibrium
1222 partitioning of both Cu and Zn and their isotopes between dissolved organic complexes in
1223 an aqueous phase versus sorption to residual secondary minerals in the soil that appears to
1224 dominate trace metal distributions (e.g. Grybos et al. 2007), and the isotopic patterns seen
1225 for both Cu-Zn (Bigalke et al. 2010b; Bigalke et al. 2011; Vance et al. 2016) and other
1226 metals (e.g. Wiederhold et al. 2007).

1227 No soil has yet been studied where conditions are reducing enough for the large
1228 isotope fractionations between Cu(I) and Cu(II) to be relevant. However, environmentally-
1229 relevant redox conditions *do* control the availability of Fe-Mn oxyhydroxides phases as a
1230 substrate for sorption. Figure 10a,b documents the isotopic impact of this control in soils
1231 distributed across three sites on the island of Maui, Hawaii, that have seen different annual
1232 rainfall amounts and in which there is a transition from well-drained conditions that retain
1233 Fe oxides to waterlogged conditions that do not (Vance et al. 2016). If Fe oxides are
1234 retained in the soils, depletion of Cu and Zn is accompanied by preferential loss of the
1235 heavy isotopes of Cu and slight preferential loss of the heavy isotopes of Zn. When Fe
1236 oxides disappear the remaining Cu and Zn is almost completely stripped from the soil and

1237 residual isotopic compositions move towards heavy values. Patterns consistent with those
1238 seen in Hawaii are also observed by Bigalke et al. (2010c; 2011). The most likely
1239 interpretation is that heavy Cu is mobilized into aqueous organic complexes, while the
1240 oxides in the soil preferentially sorb the light isotopes. As noted earlier, both soluble
1241 organic complexes and sorption show a preference for heavy isotopes relative to free Cu
1242 ion in aqueous solution, so that this interpretation requires that the preference of the organic
1243 complexes for heavy Cu is greater than that of sorption. This in turn, would require the
1244 dissolved complexes to bind Cu at least as strongly as the strongest organic ligands in the
1245 experiments of Ryan et al. (2014), but there is evidence from the partitioning of Cu isotopes
1246 between the aqueous and particulate phases in rivers (Vance et al. 2008 , discussed below)
1247 that this is indeed the case. The data for Zn in Figure 10a,b document a much more subtle
1248 isotopic effect in free-draining soils, mirroring more subtle differences between the
1249 dissolved and particulate load of rivers (e.g. Chen et al. 2008; Chen et al. 2009; Little et al.
1250 2014a, also discussion below), and consistent with the fact that the isotopic effects of
1251 aqueous complexation versus sorption to mineral surfaces may cancel each other out.
1252 Figure 10a,b also show such an effect when Cu and Zn are almost completely stripped
1253 away in water-logged conditions. As the Fe oxyhydroxides are removed, the isotopic
1254 composition tends towards heavier values, perhaps reflecting the retention of a very small
1255 residual pool on aluminium hydroxides or on condensed organic matter or the addition of
1256 dust (see below).

1257 ***Addition of atmospheric aerosol to soils.*** There have been few studies of the impact of
1258 atmospheric aerosol deposition on soils, and all but one of these concern anthropogenic
1259 aerosol deposition (discussed in a later section). Deposition of natural aerosol dust from

1260 the atmosphere has the potential to confound and overprint weathering signals. Here we
1261 illustrate the impact of such a process again using data from the relatively un-polluted
1262 Hawaiian Islands from Vance et al. (2016). The geochemical impact of the deposition of
1263 Asian desert-derived dust on Hawaiian soils is well-documented for many elements (e.g.
1264 Kurtz et al. 2001; Vance et al. 2016 and references therein). Its impact on Cu and Zn
1265 isotopes is illustrated in Figure 10c,d. Tau data for very young (300 years) soils from the
1266 island of Hawaii further help to define the weathering depletion trend illustrated in Figure
1267 10a,b (thick solid black arrow). However, soils with ages in the range 20-150 kyr show
1268 deviations from this tau pattern that fall on arrays that are consistent with the addition of
1269 Asian dust (thick dashed arrows). The potential impact of this on Cu isotopes is illustrated
1270 by the dashed arrows in Figure 10d, but the precise trajectory on this plot depends on the
1271 relative concentrations of Cu in the dust versus those in the soil when the dust was added.
1272 In general, it might be expected that dust addition would tend to buffer soil Cu and Zn
1273 isotopes back to about 0‰ and +0.3‰ respectively, the average Cu and Zn isotope
1274 compositions in natural atmospheric aerosol (c.f. Fig. 8). However, Weiss et al. (2007)
1275 document a heavier Zn isotopic composition for background (un-contaminated) dust
1276 deposition in Finland, $\delta^{66}Zn$ = +0.9‰, while Dong et al. (2013) found variations of up to
1277 0.5‰ in $\delta^{65}Cu$ among the different size fractions of Asian dust, with some samples of the
1278 >63µm fraction giving isotopic values = 0.4-0.5‰. The fact that natural atmospheric
1279 aerosol may be isotopically heavier than the lithogenic values for Cu and Zn isotopes may
1280 indicate either a significant contribution from a non-lithogenic source or isotope
1281 fractionation during atmospheric processing.

1282 ***The impact of plants on soil Cu and Zn isotopes.*** The surface organic-rich layers of soils
1283 are often enriched in the light isotopes of both Cu and Zn (e.g. Weiss et al., 2007; Bigalke
1284 et al., 2010a, 2011; Liu et al., 2014; Vance et al., 2016). Though an interpretation in terms
1285 of addition from the atmosphere has been discussed (e.g. Bigalke et al. 2010b; Bigalke et
1286 al. 2011), another likely process relates to the concentration of the light isotopes in these
1287 surface layers by plant growth and decay. Viers et al. (2007) was the first study to highlight
1288 the potential importance of plant cycling for Zn, while Bigalke et al. (2010b; 2011)
1289 conclude that light Cu in the upper organic layers of soils is likely attributable to decaying
1290 plant material. Likewise, Liu et al. (2014) point to light Cu and high TOC in the upper
1291 layers of soils from Hainan, China, as evidence for plant activity. However, in these
1292 particular soils Cu is uniformly depleted in the upper relative to deeper soil horizons,
1293 whereas the other soils where isotopically light Cu and Zn in the upper organic horizons
1294 has been attributed to plants are definitely (Vance et al. 2016) or probably (Bigalke et al.
1295 2010b; Bigalke et al. 2011) enriched relative to those underneath. Thus the Liu et al. (2014)
1296 data may be more consistent with the loss of heavy Cu by mobilization in aqueous organic
1297 complexes, as for the Hawaiian soils discussed above. Schulz et al. (2010) observed the
1298 effect of "biolifting" on the distribution and isotopic composition of Fe in soils from Santa
1299 Cruz, California. Biolifting is the process by which plant roots and symbiotic fungi
1300 (mycorrhizae) transport an element from deep in the regolith to the shallow soil. Vance et
1301 al. (2016) observed increasing $\tau_{Cu}$ and $\tau_{Zn}$ coupled to increasing $\tau_{P}$ with soil age in the
1302 uppermost horizons of Scottish soils, but decreases at depth, suggesting movement of Cu
1303 and Zn upwards with increasing soil development (eg. Fig. 10e). As with the experimental
1304 studies of plants discussed earlier, these authors document significantly lighter Zn in plant

material than in soils, suggesting that biolifting and fractionation by vegetation can also explain some aspects of soil $\delta^{66}Zn$ and $\delta^{65}Cu$ (e.g. Fig. 10f) for the surface layers of these soils. In contrast, Viers et al. (2015) find little variation in soil Zn isotope compositions related to plant activity in Siberian permafrost soils, which they attribute to the homogenizing impact of seasonal freezing front migration. Plants developed on these latter soils exhibit Zn isotope compositions both lighter and heavier than the bulk soil, possibly due to climate-driven changes in speciation of the plant-available pool.

***Summary.*** Figure 11 presents Cu-Zn isotopes in soils in the form of integrated tau values and isotopic compositions for whole soil profiles (where tau data are also available: Viers et al. 2007; Mathur et al. 2012; Liu et al. 2014; Vance et al. 2016), in order to make a summary assessment of the degree of loss and isotopic fractionation that occur in this setting. Such an assessment is important for the significance of weathering and other pedogenic processs in global biogeochemical budgets, and sets the scene for the discussion of one of the main inputs to the oceans, rivers, in the next section. It is already relatively clear from this still small dataset that soils lose heavy Cu during the weathering process, whether it is because of oxidation of sulphides (e.g. Mathur et al. 2012) or through retention of light Cu isotopes on residual Fe-Mn oxides coupled to the mobilization of heavy Cu in aqueous organic complexes (Bigalke et al. 2010b; Bigalke et al. 2011; Vance et al. 2016). In contrast, the isotopic impact of chemical weathering on Zn is much more subdued, with the majority of soils retaining very slightly heavy Zn. It should be noted that the real impact of weathering removal on its own would be more pronounced than these data suggest, given that nearly all these soils will have seen the addition of some dust, buffering the isotopic

composition closer to the parent rock than would otherwise be the case. The main point of presenting the summary in Figure 11 is that it predicts that the complementary aqueous reservoir to the residual solids in soils, the dissolved phase of rivers, should be significantly heavier than the average continental crust for Cu, and not very different from the latter for Zn. It will be seen in the next section that this prediction is borne out for estimates of the Cu and Zn isotope composition of the dissolved riverine flux to the oceans obtained from measurements of the dissolved pool in large and small, relatively unpolluted, rivers (Vance et al. 2008; Little et al. 2014a).

**The oceans: inputs, outputs and internal cycling of Cu and Zn isotopes**

The oceanic dissolved pool and authigenic metals extracted from it to be delivered to sediments represent the ultimate fate of Cu and Zn mobilized on the continents via weathering and erosion, discussed in the previous section. Measurements of the Cu and Zn isotope composition of the dissolved pool of the oceans is extremely challenging due to the low abundances of both metals in seawater (concentrations of order $10^{-10}$-$10^{-9}$M). This presents difficulties related to clean sampling and analysis, in addition to the problem of obtaining large ion currents for the precise measurement of isotope ratios. The challenge is to achieve efficient, low blank, chemical extraction and purification of Cu and Zn from large volumes (of order 0.1-10 litres) of seawater, containing up to 8 orders of magnitude more interfering ions such as Mg and Na. The availability of the double spike approach for Zn eliminates concerns over isotope fractionation artefacts during the chemical extraction process, but this approach is not available for Cu. The isotope geochemistry of seawater started with the pioneering work of Bermin et al. (2006) and Vance et al. (2008), but has gained momentum recently and is likely to grow in importance over the next decade for

two principal reasons. The first is the inception of the GEOTRACE programme (www.geotraces.org), an international collaboration involving many chemical oceanographers worldwide that is now providing large, cleanly-collected, seawater samples for a huge body of work aimed at reaching a quantitative understanding of trace elements and their isotopes in seawater. The second is the development of a key new methodology, using Nobias chelate PA-1 resin (e.g. Conway and John 2014; Takano et al. 2014; Conway and John 2015; Vance et al. In review). This new approach is capable of producing a very clean transition metal fraction from seawater, that can then be taken on to the usual anion column for the purification of separate Cu and Zn (as well as Fe, Cd, Mo) fractions.

The data currently available from these endeavours is summarized in Figure 12 and 13. Two principal scientific themes have emerged both from this early work on the dissolved pool of the oceans themselves, as well as from Cu-Zn isotopic characterization of the inputs and outputs: (1) the overall mass balance of Cu and Zn cycling through the oceans as a whole; (2) the cycling of Cu and Zn within the oceans, by biological uptake and regeneration, and through interaction with the surfaces of both biological and abiotic particulates, often termed "scavenging". We discuss each of these in turn below. The work done so far on Cu and Zn isotopes in rivers, atmospheric aerosols, hydrothermal systems, as well as the chemical sediments that represent the outputs from the dissolved pool, are all tied up with the first of these topics and are discussed as part of it.

***The overall oceanic budget of Cu and Zn in the oceans.*** The dissolved pool of the oceans is conventionally regarded as being in steady state with regard to inputs and outputs. Though there are both isotopic and elemental records and models for long residence time

1374 elements such as Sr and Mg that suggest the contrary (e.g. Vance et al. 2009; Coggon et al.
1375 2010; Pogge von Strandmann et al. 2014), long-term records of Cu and Zn isotopes in the
1376 oceans (Little et al. 2014a) demonstrate a temporal constancy that makes this a useful
1377 starting point here.

1378 Vance et al. (2008) and Little et al. (2014a) have characterized the isotopic
1379 composition of the dissolved pool of rivers for Cu and Zn isotopes, including relatively
1380 unpolluted large and small catchments such as the Amazon and the Kalix (Arctic Circle,
1381 Sweden). A key finding for Cu is that the dissolved pool of rivers is isotopically heavier
1382 than the continental crust as sampled in high temperature igneous rocks and clastic
1383 sediments (Fig. 8), with a discharge- and [Cu]-weighted average $\delta^{65}$Cu of about +0.7‰.
1384 This result is common to a number of transition metals, including Mo (Archer and Vance
1385 2008) and Ni (Cameron and Vance 2014), which are also all characterized by weak positive
1386 relationships between isotope composition and reciprocal metal concentration. In the case
1387 of Cu, at least one small river carries a particulate load with $\delta^{65}$Cu = -0.4 to -0.6‰, and the
1388 two pools balance to suggest an estimated total load that is about the same as the rocks
1389 being weathered. Vance et al. (2008) attributed this difference between the dissolved and
1390 particulate load to a roughly 1.2±0.4‰ equilibrium isotopic fractionation between heavy
1391 Cu in dissolved aqueous organic complexes and light Cu in particulate material. Though
1392 this suggestion is qualitatively consistent with the fact that the small number of soil systems
1393 so far analysed seem to lose heavy Cu (Fig. 11), and with the experimental finding that
1394 organic complexes preferentially sequester the heavy isotope of Cu (Fig. 10: Bigalke et al.
1395 2010a; Ryan et al. 2014), the fractionation seen between the dissolved and particulate
1396 phases in rivers is much larger. Little et al. (2014a) found that Zn isotopes in a subset of

1397 the same large and small rivers is less variable, and that the discharge- and [Zn]-weighted
1398 riverine flux to the oceans, at about +0.33‰, is very close to the continental crust (Fig. 8).
1399 This finding is also completely consistent with the very subtle isotopic variations seen in
1400 soils (Fig. 11), and with the fact that there is likely to be minimal isotopic difference
1401 between dissolved aqueous organic complexes of Zn and that sorbed to surfaces (Fig. 9
1402 and references in the caption).

1403 Other work on rivers has concentrated on rather small catchments, often with a
1404 focus on modification of riverine processes due to human activities such as smelting and
1405 agriculture (see Anthropocene section). However Ilina et al. (2013), in a study of pristine
1406 rivers in subarctic watersheds (NW Russia), also found heavy Cu in the dissolved load
1407 ($\delta^{65}Cu$ = +0.46±0.05‰), and used ultrafiltration to demonstrate that this isotopic
1408 composition characterizes the riverine load down to <1kDa, even though 40-60% of the
1409 Cu in the rivers they studied is colloidal. Szynkiewicz and Borrok (2015) document a much
1410 wider range of Zn isotope compositions ($\delta^{66}Zn$ = -0.57 to +0.41‰) than in the global
1411 survey of Little et al. (2014a) in streams of the Rio Grande catchment (USA), which they
1412 attribute to preferential removal of the light isotope from the dissolved load by adsorption
1413 onto particulates. Though part of a study of a river estuary that is at least partially
1414 anthropogenically-disturbed, particulate and dissolved Cu isotopes in the Gironde estuary
1415 show $\Delta^{65}Cu_{particulates\text{-}dissolved}$ around +0.4‰ for Cu (Petit et al. 2013). Finally, Chen et al.
1416 (2008; 2009), though also in a study primarily aimed at using Zn isotopes to study pollution
1417 sources in the River Seine, France, observe rather subtle isotopic differences between the
1418 particulate and dissolved load.

1419 Little et al. (2014a) in an assessment of the overall oceanic mass balance of Cu and
1420 Zn isotopes, present and summarise further data on the size and isotopic composition of
1421 the likely inputs. This paper suggests that the dissolved riverine load is dominant for both,
1422 but uncertainties remain. It is conventionally assumed that the metal load of hydrothermal
1423 fluids is precipitated and scavenged very close to mid-ocean ridges, and Little et al. (2014a)
1424 conclude that the flux that gets past this trap is likely to be very small indeed. However,
1425 the recent finding that substantial amounts of iron are transported 1000s of km from
1426 hydrothermal systems across the deep Pacific (Resing et al. 2015) may prompt a re-
1427 assessment of that conclusion. We know very little about the isotopic composition of end-
1428 member hydrothermal fluids, though the [Zn]-weighted $\delta^{66}$Zn in the only study so far (John
1429 et al. 2008) is very close to basalts, the continental crust and rivers, at around +0.25‰.
1430 Similarly the [Zn]-weighted average $\delta^{66}$Zn of thermal springs and fumaroles from one
1431 Caribbean volcano is +0.34‰ (Chen et al. 2014b). Dust, transported through the
1432 atmosphere from the continents, was estimated to represent only about 10% of the total
1433 input for both Cu and Zn in Little et al. (2014a), whereas Takano et al. (2014) estimate this
1434 source to be slightly larger than rivers for Cu. Much of this discussion depends on two
1435 inter-related uncertainties. Firstly, the Takano et al. (2014) dust estimate is derived from
1436 the Cu concentration of rainwater over Japan, taken to characterize the wet deposition flux
1437 of dust Cu to the Earth's surface. However, this rain is likely to be anthropogenically
1438 contaminated. Though the residence time of Cu in the oceans is not well-constrained it is
1439 certainly of order $10^3$-$10^4$ years, so that it seems unlikely that 100-200 years of this flux is
1440 relevant to the whole ocean budget at all. A second uncertainty relates to the size of the
1441 dust flux to the oceans itself, and in particular solubility of Cu in that dust. Little et al.

1442 (2014a) use a solubility of 27%, likely relevant for mineral dust (Desbouefs et al. 2005),
1443 but anthropogenic aerosol may contain a more soluble pool of metals, possibly explaining
1444 the high Cu concentrations in Japanese rain.

1445 These uncertainties are important, because the available data for sources and sinks
1446 point to missing budget terms (Little et al. 2014a). The isotopic composition of the input
1447 to the oceanic dissolved pool for Zn is fairly well-constrained despite large uncertainties
1448 on the amount of *total* Zn, simply because the isotopic composition of average rivers, dust
1449 and hydrothermal systems are all around +0.25 to +0.33 (Fig. 8). This is significantly
1450 lighter than the deep ocean dissolved pool and requires at least one sink from the oceans
1451 that is isotopically light. For Cu, the input shown on Figure 13 is that from Little et al.
1452 (2014a). If dust is much more important than suggested in that paper, and more like 60%
1453 of the total input as in Takano et al. (2014), and with an average $\delta^{65}$Cu in dust of +0.04‰
1454 (Fig. 8) then the total input would be substantially lighter than the dissolved pool of the
1455 oceans, so that at least one isotopically *heavy* sink is required.

1456 The current level of knowledge on the isotopic composition of these sinks is
1457 summarized in Figure 8 and Figure 12 and 13. For Zn, all the sinks in the open oxic ocean
1458 are heavy. One that is likely to be quantitatively important, and the one that we know most
1459 about (Little et al. 2014ab; Bryan et al. 2015), is that which occurs via scavenging of Zn to
1460 particulate Fe-Mn oxides and delivery with them to sediment. This sink, as recorded in Fe-
1461 Mn crusts, has an isotope composition = +0.94±0.14‰ (Marechal et al. 2000; Little et al.
1462 2014a, see also metalliferous sediments in Dekov et al. 2010), about 0.5‰ heavier than the
1463 deep oceans. This is qualitatively consistent with (1) the finding of Little et al. (2014b) that
1464 Zn and Cu are both very clearly associated with Mn oxide in these samples and (2) that of

1465 Bryan et al. (2015) that Zn sorbed to Mn oxide is heavier than a dissolved pool. However,
1466 Zn/Mn ratios in crusts suggest low surface loading, for which Bryan et al. (2015) document
1467 an isotopic fractionation upon sorption from a high ionic strength solution in which Zn is
1468 inorganically-speciated of as great as +2.7‰. The solution to this quantitative discrepancy
1469 put forward by Little et al. (2014b) and Sherman et al. (2015) – see schematic in Figure 14
1470 - is that, in the dissolved pool, the free metal Zn ion that is likely to be sorbed is actually
1471 much lighter than the total dissolved pool because of the fact that most of the oceanic
1472 dissolved pool of Zn is organically-complexed, which would be heavier than the free ion
1473 (Fig. 10 Jouvin et al. 2009).

1474 Organic complexation is likely to be even more important, quantitatively and
1475 isotopically, for Cu. Fe-Mn crusts are isotopically lighter than the oceanic dissolved pool
1476 by about 0.2‰ (Fig. 13 Little et al. 2014a). No experiments have yet characterized isotope
1477 fractionation of Cu upon sorption to Mn oxide surfaces, but experiments for other oxides
1478 have universally documented sorption of the heavy isotopes from an aqueous phase
1479 containing free Cu(II) (Fig. 10 Balistrieri et al. 2008; Pokrovsky et al. 2008; Navarette et
1480 al. 2011). As pointed out by Little et al. (2014b) and Sherman et al. (2015), sorption of the
1481 heavy isotope would be consistent with the change in co-ordination state of Cu (e.g.
1482 Schauble 2004) from V in solution to dominantly III-IV on birnessite ($\delta$-$MnO_2$). But this
1483 is inconsistent in sign, never mind magnitude, with the observation of light Cu in natural
1484 Fe-Mn crusts. However, Cu again, in all aqueous solutions at the surface of the Earth is
1485 ubiquitously complexed to organics (e.g. Coale and Bruland 1988), so that this conundrum
1486 probably has a solution similar to the Zn problem. In other words, the free ion that is sorbed
1487 is likely to be lighter than the total, as also shown schematically in Figure 14.

Returning to the whole ocean mass balance, at the level of knowledge discussed above there is clearly a substantial budgetary problem for Zn isotopes if the oceans are in steady state. The open ocean outputs are heavier than the dissolved pool while the inputs are light, implying that the oceans should be moving to lighter isotopic compositions through time, which is not seen in records (e.g. Little et al. 2014a). The solution to this problem is likely to lie in a sink for Zn into organic-rich sediments. Very recently, Little et al. (2016) have shown that sediments deposited beneath upwelling continental margins, rich in organic carbon due to high photic zone productivity, carry substantial authigenic Zn enrichments and that this Zn is isotopically light. Light Zn isotopes in organic-rich sediment could either be delivered there via uptake of light Zn into phytoplankton in the photic zone, sinking and preservation of the organic matter (e.g. John et al. 2007b; Peel et al. 2009). An alternative is suggested by the data of Vance et al. (In review) for the sulphidic Black Sea. In this setting Zn behaves very like Mo: sulphidisation leads to removal of Zn as particle reactive sulphide species that are isotopically light – by 0.6-0.7‰ (consistent with ab initio calculations: Fujii et al. 2011, see earlier in this chapter) – pushing the residual dissolved pool very heavy (Fig. 8). Pore waters within organic-rich sediments also become sulphidic just beneath the sediment-water interface, due to reduction of pore water sulphate when respiration depletes oxygen and other oxidants (e.g. Froelich et al. 1979). In the Black Sea this process is near-quantitative so that authigenic Zn in sediments is the same as the open ocean dissolved pool, but a non-quantitative version of the same process within the sediments of upwelling continental margins could close the oceanic Zn isotope budget.

1510 As noted earlier, what we currently know about the Cu isotope budget also requires
1511 an as yet unidentified sink, in this case isotopically heavy. But we know too little about the
1512 oceanic Cu isotope budget to say much more at this stage.

1513 ***Cycling of Cu and Zn isotopes within the oceans.*** The discussion in the previous
1514 section emphasized the homogeneity of Cu and Zn isotope compositions in the deep ocean
1515 (Figs. 12, 13), but there is clearly a great deal of variability *within* the oceanic dissolved
1516 pool, in the top 1000m and particularly for Zn, where the roughly 2‰ range is greater than
1517 any other Earth reservoir (Fig. 8). One of the most impressive features of ocean chemistry
1518 is the massive drawdown of Zn in the surface ocean, with concentrations there that are
1519 sometimes as low as 0.03 nM, more than 2 orders of magnitude lower than the highest
1520 concentrations in the deep ocean (Fig. 12 and references therein). For Cu, the surface-deep
1521 contrast is smaller, at a maximum of about factor 10 (Fig. 13 and references therein). Thus
1522 it is no surprise, if this drawdown is associated with even a small isotope fractionation, that
1523 there is substantial variability in the small residual dissolved pool of the upper ocean. The
1524 reasons for isotopic variability have focused on two explanations of both the surface ocean
1525 drawdown and the isotopic variation: (1) a kinetic fractionation leading to preferential
1526 uptake of the light isotope into phytoplankton cells in the photic zone; (2) reversible and
1527 non-reversible scavenging of Cu and Zn in both the surface and deep ocean.

1528 For Cu, scavenging is the process that is often regarded as dominant. Though Cu is
1529 an important component of enzymes and proteins in phytoplankton (e.g. Peers and Price
1530 2006), it is not limiting to phytoplankton growth and at high concentrations it is toxic (e.g.
1531 Moffett and Brand 1996). Indeed, the organic ligands that bind Cu in the dissolved phase
1532 of the oceans (and at least to some degree elsewhere on Earth) are probably exuded by

1533 phytoplankton to reduce the concentrations of free $Cu^{2+}$ ion beneath the threshold for
1534 toxicity at around $10^{-12}$M – some 3 orders of magnitude beneath *total* oceanic Cu
1535 concentrations (e.g. Moffett and Brand 1996). This dichotomy between the requirement for
1536 small amounts of Cu by phytoplankton, coupled to toxicity at high concentrations, has led
1537 to Cu being dubbed the "Goldilocks element" of ocean biogeochemistry (e.g. Thomson
1538 and Ellwood 2014). The approximately linear increase in Cu concentrations with depth
1539 (Fig. 13) is reminiscent of that attributed to reversible scavenging for some other oceanic
1540 metals (e.g. Bacon and Anderson 1982), and Little et al. (2013) demonstrated that depth
1541 profiles of Cu concentrations are very well modeled by such a process. In support of this,
1542 Takano et al. (2014) interpret a good positive relationship between Cu isotope composition
1543 and oxygen availability in the deep ocean in terms of preferential scavenging of the light
1544 isotope to Fe-Mn oxides, a suggestion that is consistent with what we know of the isotope
1545 composition of Cu in Fe-Mn crusts (Little et al. 2014a). Thompson and Ellwood (2014)
1546 concur with Vance et al. (2008) and Little et al. (2014a,b) in highlighting the importance
1547 of organic ligands in this process: without them, if Cu existed as a free metal ion in
1548 seawater, it seems almost certain that sorption would remove the heavy isotope (Balistrieri
1549 et al. 2008; Pokrovsky et al. 2008; Little et al. 2014b; Sherman et al. 2015).

1550 Little et al. (2013) showed that, in contrast to Cu, Zn concentrations are not at all
1551 well modeled by a reversible scavenging process and conclude that biogeochemical
1552 cycling, uptake into phytoplankton at the surface and regeneration by respiration at depth,
1553 must be the key process. If this is the case, and if Zn uptake into phytoplankton is associated
1554 with a kinetic isotope fractionation that favours uptake of the light isotope (Fig. 10 John et
1555 al. 2007b; John and Conway 2014), then the expectation is that drawdown of Zn in the

surface ocean should be associated with residual heavy isotopic compositions in the dissolved pool of the upper ocean. An initial examination of Figure 12 seems to imply, if anything, the opposite. John and Conway (2014) suggest that scavenging must play at least some role. These authors conducted a cell degradation experiment in an attempt to simulate regeneration of organic material by respiration, and found that the Zn released was 0.27±0.11‰ lighter than the cell inventory. They suggest that this is due to the preferential re-adsorption of the heavy isotopes onto residual organic particles, implying a $\Delta^{66}Zn_{adsorbed-dissolved}$ = +0.58‰. However, these experiments contained very high aqueous Zn concentrations and no ligand to complex it, very different from the real ocean where a large portion of the Zn in the dissolved pool is complexed to organic ligands.

We suggest that the main control on oceanic Zn distributions remains to be unequivocally established but that biological uptake and regeneration, with whatever isotope fractionation it is associated with, will turn out to be the key process. In making this suggestion, which will require further work to substantiate, we suggest that the following observations from the data we currently have are going to be key. First, the main oceanic region in which Zn is taken up into cells and exported to the deep is the Southern Ocean. Diatoms dominate the ecology in this region and their cells contain an order of magnitude more Zn than average oceanic phytoplankton (Twining and Baines 2013). Given that diatoms dominate the export of carbon to the deep ocean (e.g. Armbrust 2009), they must completely dominate the export of Zn. Second, the Zn isotopic data for the Southern Ocean (Fig. 12 Zhao et al. 2014) show no isotopic shift in the surface across a 2 order of magnitude drop in Zn concentration away from the locus of upwelling and as diatoms take it up, suggesting the massive uptake of Zn by diatoms in this region causes

1579 no isotope fractionation. Third, when the depth profiles in Figure 12 are examined in more
1580 detail it is clear that the surface-most point is isotopically heaviest, and the isotopically
1581 light Zn that is clearly seen in this figure occupies depths beneath the surface, at 50-200m
1582 (e.g. Zhao et al. 2014). All of these observations are most consistent with very shallow
1583 upper ocean recycling of Zn by non-diatom phytoplankton and associated with small
1584 isotope fractionations, superimposed on a quantitatively much more important deep export
1585 that is controlled by diatoms in the Southern Ocean but that imparts no isotopic variability.

1586 ***Applications to Earth history.*** There have been a small number of applications of
1587 Zn isotopes in the study of the oceans through Earth history (Pichat et al. 2003; Kunzmann
1588 et al. 2013; Pons et al. 2013). Though these have been hampered by a limited understanding
1589 of the modern cycle, there is now great potential for such applications given that this
1590 understanding has now reached quite an advanced stage through the datasets described in
1591 this review. A bridge between attempts to understand the modern cycle and the recent and
1592 deep past is provided by the study of the systematics of Zn isotopes in the biological
1593 components of core-top sediments, as in Andersen et al. (2011) and Hendry and Andersen
1594 (2013). Two studies have sought to harness Zn isotopes in marine carbonate as a monitor
1595 of photic zone primary productivity on both kyr timescales in the Quaternary, targeted at
1596 understanding upwelling supply of Zn to the photic zone as controlled by climate (Pichat
1597 et al. 2003), and on the much longer timescales represented by the recovery from Snowball
1598 Earth glaciations, focused on tracking the recovery of the biosphere through the
1599 hypothesized burial of isotopically light photosynthesized Zn. Pons et al. (2013), by
1600 contrast, link secular changes in Zn isotopes in Banded Iron Formations (BIFS) to
1601 relationships between the geochemical cycle of phosphate and isotopic fractionation of Zn

1602 isotopes, a phenomenon for which, in all the studies of the modern cycle summarized
1603 earlier, evidence has yet to emerge. The burial of light Zn with organic carbon (Little et al.,
1604 2016) and the likely control of this burial by sequestration of the light isotope into sulphide
1605 in pore waters suggested by the Black Sea data of Vance et al. (In review) together suggest
1606 that the future of successful applications of paleo-Zn isotopes probably lies in the
1607 investigation of the links between the biosphere and redox in the ancient oceans. Similarly,
1608 a very recent study of Cu isotopes in black shales from across the Great Oxidation Event
1609 at 2.7-2.1 Ga (Chi Fru et al., 2016) presents a viable interpretation in terms of removal of
1610 the light isotope of Cu into Fe formations before 2.2 Ga and the lack of this removal
1611 thereafter. It is not clear, however, whether this interpretation is unique, given what we still
1612 have to learn about the controls on other outputs of Cu from the modern ocean, such as to
1613 organic-rich sediments and in the sulphidic environments that likely dominated the oceans
1614 after the demise of BIFS. Finally, Pons et al. (2011) found that Zn isotopes in 3.8 Ga
1615 serpentinites from Isua are depleted in heavy isotopes compared to the BSE ($\delta^{66}$Zn down
1616 to -0.5‰), while serpentinites from modern ophiolites and mid-ocean ridges are
1617 isotopically similar to the BSE, at around +0.3‰. Theoretical calculations (Fujii et al.
1618 2011) show that the incorporation of isotopically light Zn in serpentinites requires that the
1619 serpentinisation reactions occurred at high-pH, with a fluid rich in carbonate at medium
1620 temperature (100-300 °C). In addition, Pons et al. (2011) point out that these are the
1621 conditions that are found in modern mud volcano environments such as the Mariana's
1622 forearc, where the serpentinites are also isotopically light ($\delta^{66}$Zn down to -0.3‰). Pons et
1623 al. (2011) further suggest that Zn isotopes could be used as a pH proxy for ancient
1624 hydrothermal fluids.

## Cu and Zn isotopes in the Anthropocene

A significant effort has gone into the identification and quantification of human disturbance of the natural Earth surface cycles of Cu and Zn, including via their stable isotopes (see recent review in Fekiacova et al., 2015). Approximately 25% of the Zn and 30% of the Cu released annually to the atmosphere derives directly from human activities such as agriculture, manufacturing and waste management (Rauch and Pacyna, 2009). Absolute anthropogenic emissions of Zn are close to double those of Cu (Rauch and Pacyna, 2009) and most of the isotopic work on environmental tracing of these emissions has focused on Zn. Virtually all the estimated Cu emitted to the atmosphere annually is thought to derive from non-ferrous metal production (70%) and fossil fuel combustion. For Zn about 70% is also from non-ferrous metal production, 16% from fossil fuel combustion, with 4-5% each via steel and cement production and waste disposal. In terms of riverine transport, Chen et al. (2014a) estimate that excess anthropogenic Cu and Zn in the Seine at Paris represent 15-20% of the total at low water, with little excess over continental crustal concentrations at high water stage.

***Zn and Cu isotopes in ore bodies and industrial products.*** An important starting point is the variability in, and processes responsible for, Cu and Zn isotopes in the mineral ores processed during the smelting that is responsible for about 70% of the emissions to the atmosphere. Though we briefly outline this topic here, it should be emphasized that industrial products and emissions – in the end and at least of Zn – do not reflect the massive variability seen in mineral ores (Fig. 8), implying homogenization of these isotope compositions during processing.

1647 Larson et al. (2003) first documented the large Cu isotope variations in ore minerals
1648 in the weathering/supergene environment ($\delta^{65}$Cu = - 3 to +2.5‰), while also noting that
1649 variability in primary high-temperature minerals was more subdued. These twin results
1650 have been confirmed by subsequent studies (Graham et al. 2004; Mason et al. 2005; Markl
1651 et al. 2006; Asael et al. 2007; Asael et al. 2009; Mathur et al. 2009; Mathur et al. 2010):
1652 primary ore minerals predominantly in the 0±0.5‰ range, while the range of Cu isotope
1653 compositions for the supergene environment has broadened to -16.5 to +10‰. As first
1654 noted by Larson et al. (2003) and confirmed subsequently, redox-induced fractionations
1655 almost certainly control the huge variability seen in the supergene environment, where
1656 oxidative leaching of high-temperature reduced Cu minerals in the vadose zone is followed
1657 by precipitation of reduced minerals beneath the water table (Larson et al. 2003; Ehrlich et
1658 al. 2004; Mathur et al. 2005). As noted by Sherman (2013), however, the variability in the
1659 natural minerals is much greater than the fractionation factors measured in experiments, so
1660 that multiple cycles of oxidation and reduction, or Rayleigh fractionation or open system
1661 behavior, or all three, must be in operation. Though redox processes are certainly dominant,
1662 Markl et al. (2006) also suggest there may be a component to fractionation controlled by
1663 phase changes between fluid and solid mineral. Asael et al. (2009) further suggest that the
1664 nature of the ligand-bonding in solution is also important, confirmed by Sherman et al.
1665 (2013) and Fujii et al. (2013) using *ab-initio* calculations to show that aqueous Cu
1666 complexes have a $\delta^{65}$Cu range of 1.3‰ (see earlier in this chapter).

1667 There have been fewer studies of Zn isotope variation in ore minerals and, without
1668 redox chemistry, the variability is more subdued. Mason et al. (2005) document a range in
1669 $\delta^{66}$Zn of 0.63‰ in a volcanic-hosted massive sulphide ore deposit, attributed to a Zn

1670 isotopic difference between co-existing sphalerite and chalcopyrite as well as Rayleigh
1671 fractionation during precipitation from a hydrothermal fluid. Wilkinson et al. (2005) and
1672 Gagnevin et al. (2012) also explain variability in Zn isotopic data for sphalerite from the
1673 Irish ore fields (-0.17 to +1.33‰) as due to a kinetic fractionation and Rayleigh
1674 fractionation during progressive precipitation from fluids percolating up from the
1675 basement.

1676 To our knowledge, the isotope composition of the final industrial products of these
1677 metals has only been measured for Zn. The main result of this study (John et al. 2007a)
1678 was that the variability seen in a small number of industrial products, which are mostly -
1679 0.4 to +0.2‰, was much less than in the raw ore minerals. In addition, the average $\delta^{66}$Zn
1680 of the products measured is identical – at +0.19±11‰ (2SD, n =14) - to the average for ore
1681 minerals in the Wilkinson et al. (2005) and Mason et al. (2005) studies – at +0.15‰. Sivry
1682 et al. (2008) note that the extraction yields for Zn processing are higher than 95%, so that
1683 a similarity between the final product and average initial ore is perhaps not surprising.

1684 ***Dispersal of anthropogenic Cu and Zn via the atmosphere.*** A number of studies
1685 have sought to use Zn isotopes (but only one to use Cu: Thapalia et al. 2010) to trace
1686 emissions of Zn to the atmosphere in the urban environment (e.g. waste combustors) and
1687 in the vicinity of mining and smelting activities through the analysis of lichens and
1688 anthropogenic aerosols (Cloquet et al. 2006; Dolgopolova et al. 2006; Gioia et al. 2008;
1689 Mattielli et al. 2009), ombrotrophic peat cores (Weiss et al. 2007), and in soils or sediments
1690 from rivers and lakes (Sivry et al. 2008; Sonke et al. 2008; Juillot et al. 2011; Aebischer et
1691 al. 2015). Though source signatures are not always easily partitioned into natural and
1692 anthropogenic (e.g. Cloquet et al. 2006), and though post-depositional processes can induce

substantial isotope variability that obscures initial source signatures (e.g. Weiss et al. 2007; Juillot et al. 2011, though c.f. Sonke et al. 2008), a systematic feature *has* often emerged from studies of smelting activities (see recent review in Yin et al., 2016). Generally, the slag residues, or tailings, are typically enriched in the heavy isotopes of Zn, while the fine dust and aerosol emitted from smelter chimney stacks tends to be isotopically light (Dolgopolova et al. 2006; Sivry et al. 2008; Sonke et al. 2008; Juillot et al. 2011). In contrast, Ochoa Gonzalez and Weiss (2015) find that heavy isotopes are emitted to the atmosphere during coal combustion while the light isotopes are retained in bottom ashes, an observation that may allow the fingerprinting of sources of Zn pollution from different activities.

Mattielli et al. (2009) provide the most extensive discussion of the causes and consequences of isotopic fractionation during the processing of Zn ores. These authors document a change in the size and Zn isotopic composition of aerosols away from the main chimney, with $\delta^{66}$Zn = +0.01 to +0.19‰ at ≤1km, and -0.52 to -0.02‰ at 2-5 km. They attribute the light Zn in aerosols to the high temperatures in the smelter (up to 1300K), leading to fractionation during volatilization/condensation (see above section on Isotopic fractionation by evaporation on Earth). Their main chimney dust samples have the lightest $\delta^{66}$Zn, at -0.67±0.10‰. In contrast Sivry et al. (2008) document Zn in tailings at a smelter with $\delta^{66}$Zn = +0.18 to +1.49‰, a signal also seen in polluted downstream sediments (+0.83 to +1.38‰). Similarly, Juillot et al. (2011) measure $\delta^{66}$Zn = +0.81±0.20‰ for slags at a French smelter and see a shift towards this isotope signature in heavily contaminated top soils within 500m of the smelter. Consistent with this, Thapalia et al. (2010) document a step towards lighter Zn isotopes in lake sediment ~ 100km from a smelter after it became

1716 active. This is perhaps the only study of a Cu isotope archive of anthropogenic activity,
1717 showing a subtle shift to heavier Cu isotopes ($\delta^{65}$Cu from +0.77±0.05 to +0.94±0.10‰)
1718 due to human activity.

1719 ***Processes affecting Cu and Zn isotopes in polluted rivers.*** A small number of
1720 studies have been undertaken of Cu and Zn isotopes in two classes of polluted rivers: (1)
1721 rivers that are clearly affected by mining, including acid mine drainage and (2) rivers in
1722 areas that have been intensely developed for agriculture and industrial activities more
1723 generally. Borrok et al. (2008) studied dissolved Cu and Zn and their isotopes in small
1724 streams located in 6 historical mining areas in the US and Europe. It should be noted that
1725 the Cu and Zn concentrations in these mining-impacted streams, not unexpectedly, are up
1726 to 4 orders of magnitude greater than those in the relatively unpolluted rivers studied in
1727 Vance et al. (2008) and Little et al. (2014a). The $\delta^{66}$Zn data covers the range +0.02 to
1728 +0.46‰ and exhibits a diel cycle that may be related to uptake by microorganisms. The
1729 range of $\delta^{65}$Cu is -0.7 to +1.4‰, similar to that in non-mining-impacted rivers. Kimball et
1730 al. (2009) document Cu in acid mine drainage that has $\delta^{65}$Cu about 1.5‰ heavier than the
1731 primary minerals, attributing this fractionation to oxidation of reduced Cu(I) in the
1732 minerals. More recently, Wanty et al. (2013, 2015) have documented Zn isotope
1733 fractionations associated with biomediated precipitation of hydrozincite in streams
1734 draining mining areas.

1735 Chen et al. (2008; 2009) present an array of data for the dissolved and particulate
1736 phase of the River Seine, including time-series data in Paris as well as contaminated waters
1737 draining roofs and waste water treatment plants. Dissolved Zn concentrations in the Seine

increase continuously downstream from 1 to 74 nM, while $\delta^{66}Zn$ decreases from a high in the headwaters of Aube tributary (0.58‰) to +0.09‰ at the estuary. The decreasing $\delta^{66}Zn$ values as anthropogenic Zn is added downstream, particularly in Paris, is consistent with generally light Zn isotope compositions in roadway and roof runoff, and plant-treated and waste water (-0.06±0.05‰). Fertilizers showed heavier Zn isotope values at +0.19 to +0.42‰, leading these authors to suggest that fertilizer Zn is strongly retained in soil. Data for suspended particulate matter presented a similar picture: $\delta^{66}Zn$ decreases from +0.3 to 0.08‰ downstream, associated with a 4-fold increase in concentration. Time-series samples in Paris show an inverse relationship between enrichment factor and isotopes. Chen et al. (2009) interpret the results as due to more or less conservative mixing of silicate and anthropogenic particles, ruling out sorption as an important process generating isotopic variability.

**Acknowledgments:** FM acknowledges funding from the European Research Council under the H2020 framework program/ERC grant agreement #637503 (Pristine), as well as the financial support of the UnivEarthS Labex program at Sorbonne Paris Cité (ANR-10-LABX-0023 and ANR-11-IDEX-0005-02), and the ANR through a chaire d'excellence Sorbonne Paris Cité. FM would like to thank Francis Albarède, James Day, Emily Pringle, Paolo Sossi and Damien Guinoiseau for discussions. Three anonymous reviewers and editor Fang-Zhen Teng greatly improved the text.

## REFERENCES


Aebischer, S, Cloquet, C, Carignan, J, Maurice, C, Pienitz, R (2015) Disruption of the geochemical metal cycle during mining: multiple isotope studies of lake sediments dfrom Schefferville, subarctic Québec. Chem. Geol. 412: 167-178

Albarède F (2004) The stable isotope geochemistry of copper and zinc. *In*: Rev Mineral Geochem. Vol 55. Johnson CM, Beard BL, Albarède F, (eds). Mineralogical Society of America, p 409-427

Albarède F (2009) Volatile accretion history of the terrestrial planets and dynamic implications. Nature 461:1227-1233, doi:Doi 10.1038/Nature08477

Albarède F, Telouk P, Lamboux A, Jaouen K, Balter V (2011) Isotopic evidence of unaccounted for Fe and Cu erythropoietic pathways. Metallomics 3:926-933, doi:Doi 10.1039/C1mt00025j

Albarède F, Balter V, Jaouen K, Lamboux A (2011) Applications of the stable isotopes of metals to physiology. The 38th Meeting of the Federation of Analytical Chemistry and Spectroscopy Societies (FACSS), Reno (abstract).

Albarède et al. (20XX, this volume) Emerging applications of non-traditional isotopes in biomedical research Rev. Mineral. Geochem. XX:xxxx

Amira S, Spångberg D, Hermansson K (2005) Distorted five-fold coordination of $Cu^{2+}$(aq) from a Car-Parrinello molecular dynamics simulation. Phys Chem Chem Phys 7:2874-2880

Andersen MB, Vance D, Archer C, Anderson RF, Ellwood MJ, Allen CS (2011) The Zn abundance and isotopic composition of diatom frustules, a proxy for Zn availability in ocean surface seawater. Earth Planet Sci Lett 301:137-145, doi:10.1016/j.epsl.2010.10.032

Anderson D, Morel F (1978) Copper sensitivity of Gonyaulax tamarensis. Limnol Oceanogr 23:283–295

Archer C, Vance D (2002) Mass discrimination correction in multiple collector plasma source mass-spectrometry: an example using Cu and Zn isotopes. J Anal At Spectrom, 64:356-365

Archer C, Vance D (2004) Mass discrimination correction in multiple-collector plasma source mass spectrometry: an example using Cu and Zn isotopes. J Anal At Spectrom 19:656-665, doi:Doi 10.1039/B315853e

Archer C, Vance D (2008) The isotopic signature of the global riverine molybdenum flux and anoxia in the ancient oceans. Nature Geoscience 1:597-600

Armbrust EA (2009) The life of diatoms in the world's oceans. Nature 459:185-192

Arnold T, Kirk GJD, Wissuwa M, Frei M, Zhao FJ, Mason TFD, Weiss DJ (2010a) Evidence for the mechanisms of zinc uptake by rice using isotope fractionation. Plant Cell Environ 33:370-381, doi:Doi 10.1111/J.1365-3040.2009.02085.X

Arnold T, Schonbachler M, Rehkamper M, Dong SF, Zhao FJ, Kirk GJD, Coles BJ, Weiss DJ (2010b) Measurement of zinc stable isotope ratios in biogeochemical matrices by double-spike MC-ICPMS and determination of the isotope ratio pool available for plants from soil. Anal Bio Chem 398:3115-3125, doi:Doi 10.1007/S00216-010-4231-5

Asael D, Matthews A, Bar-Matthews M, Halicz L (2007) Copper isotope fractionation in sedimentary copper mineralization (Timna Valley, israel). Chem Geol 243:238-254

Asael D, Matthews A, Oszczepalski S, Bar-Matthews M, Halicz L (2009) Fluid speciation controls of low temperature copper isotope fractionation applied to the Kupferschiefer and Timna ore deposits. Chem Geol 262:147-158

1805 Aucour, AM, Pichat, S, Macnair, MR, Oger, P (2011) Fractionation of stable isotope zinc
1806 isotopes in the zinc hyperaccumulator *Arabidopsis halleri* and nonaccumulator
1807 *Arabidopsis petrasea*. Environ Sci Technol 45: 9212-9217
1808 Aucour, AM, Bedell, J-P, Queyron, M, Magnin, V, Testemale, D, Sarret, G (2015)
1809 Dynamics of Zn in an urban wetland soil-plant system: coupling isotopic and EXAFS
1810 approaches. Geochim Cosmochim Acta 160: 66-69
1811 Bacon MP, Anderson RF (1982) Distribution of thorium isotopes between dissolved and
1812 particulate forms in the deep sea. J Geophys Res 87:2045-2056
1813 Balistrieri LS, Borrok DM, Wanty RB, Ridley WI (2008) Fractionation of Cu and Zn
1814 isotopes during adsorption onto amorphous Fe(III) oxyhydroxide: Experimental mixing of
1815 acid rock drainage and ambient river water. Geochim Cosmochim Acta 72:311-328,
1816 doi:DOI 10.1016/j.gca.2007.11.013
1817 Balter V, Zazzo A (2011) An animal model (sheep) for Fe, Cu, and Zn isotopes cycling in
1818 the body. Mineralogical Magazine 75:476
1819 Balter V, Lamboux A, Zazzo A, Telouk P, Leverrier Y, Marvel J, Moloney AP, Monahan
1820 FJ, Schmidt O, Albarède F (2013) Contrasting Cu, Fe, and Zn isotopic patterns in organs
1821 and body fluids of mice and sheep, with emphasis on cellular fractionation. Metallomics
1822 5:1470-1482, doi:10.1039/c3mt00151b
1823 Ban Y, Aida M, Nomura M, Fujii Y (2002) Zinc isotope separation by ligand-exchange
1824 chromatography using cation exchange resin. J Ion Exch 14:46-52
1825 Barrat JA, Zanda B, Moynier F, Bollinger C, Liorzou C, Bayon G (2012) Geochemistry of
1826 CI chondrites: Major and trace elements, and Cu and Zn Isotopes O. Geochim Cosmochim
1827 Acta 83:79-92
1828 Ben Othman D, Luck JM, Bodinier JL, Arndt NT, Albarède F (2006) Cu-Zn isotopic
1829 variations in the Earth's mantle. Geochim Cosmochim Acta 70:46
1830 Benfatto M, D'Angelo P, Della Longa S, Pavel NV (2002) Evidence of distorted fivefold
1831 coordination of the $Cu^{2+}$ aqua ion from an x-ray-absorption spectroscopy quantitative
1832 analysis. Phys Rev B 65:174205
1833 Bentahila Y, Ben Othman D, Luck J-M (2008) Strontium, lead and zinc isotopes in marine
1834 cores as tracers of sedimentary provenance: a case study around Taiwan orogeny. Chem
1835 Geol 62-82
1836 Bermin J, Vance D, Archer C, Statham PJ (2006) The determination of the isotopic
1837 composition of Cu and Zn in seawater. Chem Geol 226:280-297,
1838 doi:10.1016/j.chemgeo.2005.09.025
1839 Bersuker IB (2006) The Jahn-Teller effect;. Cambridge Univ. Press, New York
1840 Bigalke M, Weyer S, Wilcke W (2010a) Copper Isotope Fractionation during
1841 Complexation with Insolubilized Humic Acid. Environ Sci Technol 44:5496-5502, doi:Doi
1842 10.1021/Es1017653
1843 Bigalke M, Weyer S, Wilcke W (2010b) Stable Copper Isotopes: A Novel Tool to Trace
1844 Copper Behavior in Hydromorphic Soils. Soil Sci Soc Am J 74:60-73, doi:DOI
1845 10.2136/sssaj2008.0377
1846 Bigalke M, Weyer S, Kobza J, Wilcke W (2010c) Stable Cu and Zn isotope ratios as tracers
1847 of sources and transport of Cu and Zn in contaminated soil. Geochim Cosmochim Acta
1848 74:6801-6813, doi:DOI 10.1016/j.gca.2010.08.044
1849 Bigalke M, Weyer S, Wilcke W (2011) Stable Cu isotope fractionation in soils during oxic
1850 weathering and podzolization. Geochim Cosmochim Acta 75:3119-3134

1851 Bigeleisen J, Mayer MG (1947) Calculation of equilibrium constants for isotopic exchange
1852 reactions. J Chem Phys 15:261-267
1853 Birck JL (2004) An overview of isotopic anomalies in extraterrestrial materials and their
1854 nucleosynthetic heritage. *In*: Rev Mineral Geochem. Vol Rev. Mineral. 55. Johnson CM,
1855 Beard BL, Albarède F, (eds). Min. Soc. Amer., Washington, p 26-63
1856 Bishop MC, Moynier F, Weinstein C, Fraboulet JG, Wang K, Foriel J (2012) The Cu
1857 isotopic composition of iron meteorites. Meteoritics Planet Sci 47:268-276, doi:Doi
1858 10.1111/J.1945-5100.2011.01326.X
1859 Black J, Kavner A, Schauble E (2011) Calculation of equilibrium stable isotope partition
1860 function ratios for aqueous zinc complexes and metallic zinc. Geochim Cosmochim Acta
1861 75:769-783
1862 Borrok DM, Wanty RB, Ridley WI, Wolf R, Lamothe PJ, Adams M (2007) Separation of
1863 copper, iron, and zinc from complex aqueous solutions for isotopic measurement. Chem
1864 Geol 242:400-414, doi:10.1016/j.chemgeo.2007.04.004
1865 Borrok DM, Nimick DA, Wanty RB, Ridley WI (2008) Isotopic variations of dissolved
1866 copper and zinc in stream waters affected by historical mining. Geochim Cosmochim Acta
1867 72:329-344
1868 Bridgestock LS, Williams H, Rehkamper M*, et al.* (2014) Unlocking the zinc isotope
1869 systematics of iron meteorites. Earth Planet Sci Lett 400:153-164
1870 Broadley MR, White PJ, Hammond JP, Zelko I, Lux A (2007) Zinc in plants. New
1871 Phytologist 173:677-702
1872 Bruland KW (1999) Complexation of zinc by natural organic ligands in the central North
1873 Pacific. Limnol Oceanogr 34:269-285.
1874 Bruland KW, Middag R, Lohan MC (2014) Controls of trace metals in seawater. Treatise
1875 in Geochemistry 8:19-51
1876 Bryan AL, Dong S, Wilkes EB, Wasylenki LE (2015) Zinc isotope fractionation during
1877 adsorption onto Mn oxyhydroxide at low and high ionic strength. Geochim Cosmochim
1878 Acta 157:182-197
1879 Caldelas C, Dong SF, Araus JL, Weiss DJ (2011) Zinc isotopic fractionation in Phragmites
1880 australis in response to toxic levels of zinc. J Exp Bot 62:2169-2178, doi:Doi
1881 10.1093/Jxb/Erq414
1882 Cameron V, Vance D (2014) Heavy nickel isotopic composition of rivers and the oceans.
1883 Geochim Cosmochim Acta 129:195-211
1884 Canfield DE (1998) A new model for Proterozoic ocean chemistry. Nature 396:450-453.
1885 Chaboy J, Muñoz-Páez A, Merkling PJ, Sánchez Marcos E (2006) The hydration of $Cu^{2+}$:
1886 Can the Jahn-Teller effect be detected in liquid solution? J Chem Phys 124:064509
1887 Chadwick OA, Brimhall GH, Hendricks DM (1990) From a black box to a gray box - a
1888 mass balance interpretation of pedogenesis. Geomorphology 3:369-390
1889 Chaussidon et al. (20XX, this volume) In-situ analysis of non-traditional isotopes by
1890 SIMS and LA-MC-ICPMS Rev. Mineral. Geochem. XX:xxxx
1891 Chen H, Nguyem BM, Moynier F (2013a) Zinc isotopic composition of iron meteorites:
1892 Absence of isotopic anomalies and origin of the volatile element depletion. Meteorit Planet
1893 Sci 48:2441-2450
1894 Chen H, Savage P, Teng FZ, Helz RT, Moynier F (2013b) No zinc isotope fractionation
1895 during magmatic differentiation and the isotopic composition of the bulk Earth. Earth
1896 Planet Sci Lett 369:34-42

1897 Chen H, Moynier F, Humayun M, Bishop MC, Williams J (2016) Cosmogenic effects on
1898 Cu isotopes in IVB iron meteorites. Geochim Cosmochim Acta 182:145-154
1899 Chen J, Gaillardet J, Louvat P (2008) Zinc isotopes in the Seine River waters, France: a
1900 probe of anthropogenic contamination. Environ Sci Technol 43:6494-6501
1901 Chen J, Gaillardet J, Louvat P, Huon S (2009) Zn isotopes in the suspended load of the
1902 Seine River, France: isotopic variations and source determination. Geochim Cosmochim
1903 Acta 73:4060-4076
1904 Chen J, Gaillardet J, Bouchez J, Louvat P, Wang Y-N (2014a) Anthropophile elements in
1905 river sediments: overview from the Seine River, France. Geochem Geophys Geosyst
1906 15:4526-2546
1907 Chen J, Gaillardet J, Dessert C, Villemant B, Louvat P, Crispi O, Birck J-L, Wang Y-N
1908 (2014b) Zn isotope compositions of the thermal spring waters of La Soufrière volcano,
1909 Guadeloupe Island. Geochim Cosmochim Acta 127:67-82
1910 Chen S, Liu Y, Hu J, Zhang Z, Hou Z, Huang F, Yu H (2016) Zinc isotopic composition
1911 of NIST683 and whole rock reference materials. Geostandards and Geoanalytical
1912 Research. doi: 10.1111/j.1751-908X.2015.00377.x
1913 Chou C-L, Baedecker PA, Wasson JT (1976) Allende inclusions: volatile-element
1914 distribution and evidence for incomplete volatilization of presolar solids. Geochim
1915 Cosmochim Acta 40:85-94
1916 Chi Fru, E, Rodriguez, NP, Partin, CA, Lalonde, SV, Andersson, P, Weiss, DJ, El Albani,
1917 A, Rodushkin, I, Konhauser, KO (2016) Cu isotopes in marine black shales record the
1918 Great Oxidation Event. Proc Natl Acad Sci USA, in press, doi:10.1073/pnas.1523544113
1919 Cloquet C, Carignan J, Libourel G (2006) Isotopic composition of Zn and Pb atmospheric
1920 depositions in an urban/periurban area of northeastern France. Environ Sci Technol
1921 40:6594-6600
1922 Cloquet C, Carignan J, Lehmann MF, Vanhaecke F (2008) Variation in the isotopic
1923 composition of zinc in the natural environment and the use of zinc isotopes in
1924 biogeosciences: a review. Anal Bio Chem 390:451-463
1925 Coale KH, Bruland KW (1988) Copper complexation in the northeast Pacific. Limnol
1926 Oceanogr 33:1084-1101
1927 Coggon RM, Teagle DAH, Smith-Duque CE, Alt JC, Cooper MJ (2010) Reconstructing
1928 past seawater Mg/Ca and Sr/Ca from mid-ocean ridge flank calcium carbonate veins.
1929 Science 327:1114-1117
1930 Conway TM, Rosenberg AD, Adkins JF, John SG (2013) A new method for precise
1931 determination of iron, zinc and cadmium stable isotope ratios in seawater by double-spike
1932 mass spectrometry. Anal Chim Acta 793:44-52
1933 Conway TM, John SG (2014) The biogeochemical cycling of zinc and zinc isotopes in the
1934 North Atlantic Ocean. Glob Biogeochem Cycles 28:1111-1128
1935 Conway TM, John SG (2015) The cycling of iron, zinc and cadmium in the North East
1936 Pacific Ocean - Insights from stable isotopes. Geochim Cosmochim Acta 164:262-283,
1937 doi:10.1016/j.gca.2015.05.023
1938 Couder, E, Mattielli, N, Drouet, T, Smolders, E, Delvaux, B, Iserentant, A, Meeus, C,
1939 Maerschalk, C, Opfergelt, S, Houben, D (2015) Transpiration flow controls Zn transport
1940 in *Brassica napus* and *Lolium multiflorum* under toxic levels as evidenced from isotopic
1941 fractionation. Comptes Rendus Geoscience 347: 386-396

1942 Coutaud A, Mehuet M, Viers J, Rols J-L, Pokrovsky OS (2014) Zn isotope fractionation
1943 during interaction with phototrophic biofilm. Chem Geol 390:46-60
1944 Dauphas N, Chen JH, Zhang J, Papanastassiou DA, Davis AM, Travaglio C (2014)
1945 Calcium-48 isotopic anomalies in bulk chondrites and achondrites: Evidence for a uniform
1946 isotopic reservoir in the inner protoplanetary disk. Earth Planet Sci Lett 407:96-108,
1947 doi:10.1016/j.eps1.2014.09.015
1948 Day JM, Moynier F (2014) Evaporative fractionation of volatile stable isotopes and their
1949 bearing on the origin of the Moon. Philosophical transactions Series A, Mathematical,
1950 physical, and engineering sciences 372:20130259, doi:10.1098/rsta.2013.0259
1951 de Almeida KJ, Murugan NA, Rinkevicius Z, Hugosson HW, Vahtras O, Ågrena H, Cesar
1952 A (2009) Phys Chem Chem Phys 11:508-519
1953 Dekov, VM, Cuadros, J, Kamenov, GD, Weiss, D, Arnold, T, Basak, C, Rochette, P (2010)
1954 Metalliferous sediments from the H.M.S. Challenger voyage (1872-1876). Geochim
1955 Cosmochim Acta 74: 5019-5038
1956 Desbouefs KV, Sofikitis A, Losn R, Colin JL, Ausset P (2005) Dissolution and solubility
1957 of trace metals from natural and anthropogenic aerosol particulate matter. Chemosphere
1958 58:195-203
1959 Dodson MH (1963) A theoretical study of the use of internal standards for precise isotopic
1960 analysis by the surface ionization technique: Part I. General first-order algebraic solutions.
1961 J Sci Instrum 40:289–295
1962 Dolgopolova A, Weiss DJ, Seltmann R, Kober B, Mason TFD, Coles BJ, Stanley C (2006)
1963 Use of isotope ratios to assess sources of Pb and Zn dispersed in the environment during
1964 mining and ore processing within the Orlovka-Spokoinoe mining site (Russia). App
1965 Geochem 21:563-579, doi:10.1016/j.apgeochem.2005.12.014|ISSN 0883-2927
1966 Dong S, Weiss DJ, Strekopytov S, Kreissig K, Sun Y, Baker AR, Formenti P (2015)
1967 Stable isotope ratio measurements of Cu and Zn in mineral dust (bulk and size fractions)
1968 from the Taklimakan Desert and the Sahel and in aerosols from the eastern tropical North
1969 Atlantic Ocean. Talanta 114:103-109
1970 Dreibus G, Palme H (1996) Cosmochemical constraints on the sulfur content in the Earth's
1971 core. Geochim Cosmochim Acta 60:1125-1130
1972 Edmond JM, Measures C, Mangum B, Grant B, Sclater FR, Collier R, Hudson A, Gordon
1973 LI, Corliss JB (1979) On the formation of metal-rich deposits at ridge crests. Earth Planet
1974 Sci Lett 46:19-30
1975 Ehrlich S, Butler I, Halicz L, Rickard D, Oldroyd A, Matthews A (2004) Experimental
1976 study of copper isotope fractionation between aqueous Cu(II) and covellite, CuS. Chem
1977 Geol 209:259-269
1978 Fekiakova S, Cornu S, Pichat S (2015) Tracing contamination sources in soils with Cu and
1979 Zn isotope ratios. Science of the total environment 517:96-105
1980 Fernandez A, Borrok DM (2009) Fractionation of Cu, Fe and Zn isotopes during
1981 weathering of sulfide-rich rocks. Chem Geol 264:1-12
1982 Field CB, Behrenfeld MJ, Randerson JT, Falkowski P (1998) Primary production of the
1983 biosphere: integrating terrestrial and oceanic components. Science 281:237-240
1984 Flemming CA, Trevors JT (1989) Copper toxicity and chemistry in the environment – a
1985 review. Air Soil Pollut 44:143-158
1986 Froelich PN, Klinkahmmer GP, Bender ML, Luedtke NA, Heath GR, Cullen D, Dauphin
1987 P, Hammond D, Hartman B, Maynard V (1979) Early oxidation of organic matter in

1988 pelagic sediments of the eastern equatorial Atlantic: suboxic diagenesis. Geochim
1989 Cosmochim Acta 43:1075-1090
1990 Fujii T, Albarède F (2012) Ab Initio Calculation of the Zn Isotope Effect in Phosphates,
1991 Citrates, and Malates and Applications to Plants and Soil. Plos One 7, doi:ARTN
1992 e30726DOI 10.1371/journal.pone.0030726
1993 Fujii T, Moynier F, Telouk P, Abe M (2010) Experimental and Theoretical Investigation
1994 of Isotope Fractionation of Zinc between Aqua, Chloro, and Macrocyclic Complexes. J
1995 Phys Chem A 114:2543-2552, doi:Doi 10.1021/Jp908642f
1996 Fujii T, Moynier F, Pons ML, Albarède F (2011) The origin of Zn isotope fractionation in
1997 sulfides. Geochim Cosmochim Acta 75:7632-7643, doi:Doi 10.1016/J.Gca.2011.09.036
1998 Fujii T, Moynier F, Abe M, Nemoto K, Albarède F (2013) Copper isotope fractionation
1999 between aqueous compounds relevant to low temperature geochemistry and biology.
2000 Geochim Cosmochim Acta 110:29-44, doi:10.1016/j.gca.2013.02.007
2001 Fujii T, Moynier F, Blichert-Toft J, Albarède F (2014) Density functional theory estimation
2002 of isotope fractionation of Fe, Ni, Cu, and Zn among species relevant to geochemical and
2003 biological environments. Geochim Cosmochim Acta 140:553-576,
2004 doi:10.1016/j.gca.2014.05.051
2005 Fulton EA, Parslow JS, Smith ADM, Johnson CR (2004) Biogeochemical marine
2006 ecosystem models II: the effect of physiological detail on model performance. Ecol Model
2007 173:371-406, doi:Doi 10.1016/J.Ecolmodel.2003.09.024
2008 Gagnevin D, Boyce AJ, Barrie CD, Menuge JF, Blakemann RJ (2012) Zn, Fe and S isotope
2009 fractionation in a large hydrothermal system. Geochim Cosmochim Acta 88:183-198
2010 Gélabert A, Pokrovsky OS, Schott J, Boudou A, Fertet-Mazel A, Mielczarski J,
2011 Mielczarski E, Mesmer-Dudons N, Spalla O (2004) Study of diatoms/aqueous solution
2012 interface. I. Acid-base equilibria and spectroscopic observation of freshwater and marines
2013 species. Geochim Cosmochim Acta 68:4039-4058
2014 Gélabert A, Pokrovsky OS, Viers J, Schott J, Boudou A, Feurtet-Mazel A (2006)
2015 Interaction between zinc and freshwater and marine diatom species: Surface complexation
2016 and Zn isotope fractionation. Geochim Cosmochim Acta 70:839-857,
2017 doi:10.1016/j.gca.2005.10.026
2018 Gioia, S, Weiss, D, Coles, B, Arnold, T, Babinski, M (2008) Accurate and precise zinc
2019 isotope ratio measurements in urban aerosols. Anal Chem 80: 9776-9780
2020 Ghidan OY, Loss RD (2011) Isotope fractionation and concentration measurements of Zn
2021 in meteorites determined by the double spike, IDMS-TIMS techniques. Meteoritics Planet
2022 Sci 46:830-842, doi:Doi 10.1111/J.1945-5100.2011.01196.X
2023 Graham S, Pearson N, Jackson S, Griffin W, O'Reilly SY (2004) Tracing Cu and Fe from
2024 source to porphyry: in situ determination of Cu and Fe isotope ratios in sulfides from the
2025 Grasberg Cu-Au deposit. Chem Geol 207:147-169
2026 Grybos M, Davranche M, Gruau G, Petitjean P (2007) Is trace metal release in wetland
2027 soils controlled by organic mobility or Fe-oxyhydroxides reduction? J Colloid Interface
2028 Sci 324:490-501
2029 Guelke M, Von Blanckenburg F (2007) Fractionation of stable iron isotopes in higher
2030 plants. Environmental Science & Technology 41:1896-1901, doi:Doi 10.1021/Es062288j
2031 Hartmann D, Woosley SE, El Eid MF (1985) Nucleosynthesis in neutron-rich supernova
2032 ejecta. Astrophys J 297:837-845

2033 Guinoiseau, D, Gélabert, A, Moureau J, Louvat, P, Benedetti, MF (2016) Zn isotope
2034 fractionation during sorption onto kaolinite. Environ Sci Technol 50: 1844-1852
2035 Hayakawa K, Minami S, Nakamura S (1973) Kinetics of the oxidation of ascorbic acid by
2036 the copper(II) ion in an acetate buffer solution. Bull Chem Soc Jpn 46:2788.
2037 Hendry KR, Andersen MB (2013) The zinc isotopic composition of siliceous marine
2038 sponges: investigating nature's sediment traps. Chem Geol:33-41
2039 Herwartz D, Pack A, Friedrichs B, Bischoff A (2004) Identification of the giant impactor
2040 Theia in lunar rocks. Science 344:1146-1150
2041 Herzog GF, Moynier F, Albarède F, Berezhnoy AA (2009) Isotopic and elemental
2042 abundances of copper and zinc in lunar samples, Zagami, Pele's hairs, and a terrestrial
2043 basalt. Geochim Cosmochim Acta 73:5884-5904, doi:DOI 10.1016/j.gca.2009.05.067
2044 Houben D, Sonnet P, Tricot G, Matielli N, Couder E, Opfergelt S (2014) Impact of root-
2045 induced mobilization of zinc on stable Zn isotope variation in the soil-plant system.
2046 Environ Sci Technol 48:7866-73
2047 Ikehata K, Hirata T (2013) Evaluation of UV-fs-LA-MC-ICP-MS for Precise in situ
2048 Copper Isotopic Microanalysis of Cubanite. Anal Sci 29:1213-1217
2049 Ilina SM, Viers J, Lapitsky SA, Mialle S, Mavromatis V, Chmeleff J, Brunet P, Alekhin
2050 YV, Isnard H, Pokrovsky OS (2013) Stable (Cu, Mg) and radiogenic (Sr, Nd) isotope
2051 fractionation in colloids of boreal organic-rich waters. Chem Geol 434:63-75
2052 John SG, Park JG, Zhan ZT, Boyle EA (2007a) The isotopic composition of some common
2053 forms of anthropogenic zinc. Chem Geol 245:61-69
2054 John SG, Geis R, Saito M, Boyle EA (2007b) Zn isotope fractionation during high-affinity
2055 zinc transport by the marine diatom Thalassiosira oceanica. Limnol Oceanogr 52:2710-
2056 2714
2057 John SG, Rouxel OJ, Craddock PR, Engwall AM, Boyle EA (2008) Zinc stable isotopes in
2058 seafloor hydrothermal vent fluids and chimneys. Earth Planet Sci Lett 269:17-28
2059 John SG, Conway TM (2014) A role for scavenging in the marine biogeochemical cycling
2060 of zinc and zinc isotopes. Earth Planet Sci Lett 394:159-167
2061 Jouvin D, Louvat P, Juillot F, Marechal CN, Benedetti MF (2009) Zinc Isotopic
2062 Fractionation: Why Organic Matters. Environ Sci Technol 43:5747-5754,
2063 doi:10.1021/es803012e
2064 Jouvin D, Weiss D, Mason T, Bravin M, Louvat P, Zhao F, Ferec F, Hinsinger P, Benedetti
2065 M (2012) Stable Isotopes of Cu and Zn in Higher Plants: Evidence for Cu Reduction at the
2066 Root Surface and Two Conceptual Models for Isotopic Fractionation Processes. Environ
2067 Sci Technol 46:2652–2660
2068 Juillot F, Maréchal C, Ponthieu M, Cacaly S, Morin G, Benedetti M, Hazemann JL, Proux
2069 O, Guyot F (2008) Zn isotopic fractionation caused by sorption on goethite and 2-Lines
2070 ferrihydrite. Geochim Cosmochim Acta 72:4886-4900
2071 Juillot F, Marechal C, Morin G*, et al.* (2011) Contrasting isotopic signatures between
2072 anthropogenic and geogenic Zn and evidence for post-depositional fractionation processes
2073 in smelter-impacted soils from Northern France. Geochim Cosmochim Acta 75:2295-
2074 2308, doi:Doi 10.1016/J.Gca.2011.02.004
2075 Kafantaris F-C, Borrok DM (2014) Zinc isotope fractionation during surface adsorption
2076 and intracellular incorporation by bacteria. Chem Geol 366:42-51

2077 Kato C, Moynier F, Valdes MC, Dhaliwal JK, Day JM (2015) Extensive volatile loss
2078 during formation and differentiation of the Moon. Nature Com. 6:7617,
2079 doi:10.1038/ncomms8617
2080 Kau L-S, Spira-Solomon DJ, Penner-Hahn JE, Hodgson KO, Solomon EI (1987) X-ray
2081 absorption edge retermination of the oxidation state and coordination number of copper:
2082 Application to the type 3 site in Rhus vernicifera Laccase and its reaction with oxygen. J
2083 Am Chem Soc 109:6433-6442
2084 Kavner A, John SG, Sass S, Boyle EA (2008) Redox-driven stable isotope fractionation in
2085 transition metals: application to Zn electroplating. Geochim Cosmochim Acta 72:1731-
2086 1741
2087 Kimball BE, Mathur R, Dohnalkova AC, Wall AJ, Runkel RL, Brantley SL (2009) Copper
2088 isotope fractionatin in acid mine drainage. Geochim Cosmochim Acta 73:1247-1263
2089 Koschinsky A, Hein JR (2003) Acquisition of elements from seawater by ferromanganese
2090 crusts: Solid phase association and seawater speciation. Mar Geol 198:331-351
2091 Kunzmann N, Halverson GP, Sossi PA, Raub TD, Payne JL, Kirby J (2013) Zn isotope
2092 evidence for immediate resumption of primary productivity after snowball Earth. Geology
2093 41:27-30
2094 Kurtz AC, Derry LA, Chadwick OA (2001) Accretion of Asian dust to Hawaiian soils:
2095 Isotopic, elemental, and mineral mass balances. Geochim Cosmochim Acta 65:1971–1983
2096 Larner F, Rehkaemper M, Coles B, Kreissig K, Weiss D, Sampson B, Unsworth C,
2097 Strekopytov S (2011) A new separation procedure for Cu prior to stable isotope analysis
2098 by MC-ICP-MS. J Anal At Spectrom 26:1627-1632
2099 Larson PB, Maher K, Ramos FC, Chang Z, Gaspar M, Meinert LD (2003) Copper isotope
2100 ratios in magmatic and hydrothermal ore forming environments. Chem Geol 201:337-350
2101 Lee CTA, Yin Q-Z, Lenardic A, Agranier A, O'Neill C, Thiagarajan N (2007) Trace-
2102 element composition of Fe-rich residual liquids formed by fractional crystallization:
2103 implications for the Hadean magma ocean. Geochim Cosmochim Acta 71:3601-3615
2104 Lee CTA, Luffi P, Chin EJ, Bouchet R, Dasgupta R, Morton DM, Le Roux V, Yin Q-Z,
2105 Jin D (2012) Copper Systematics in Arc Magmas and Implications for Crust-Mantle
2106 Differentiation. Science 336:64-68, doi:10.1126/science.1217313
2107 Li W, Jackson S, Pearson NJ, Alard O, Chappell BW (2009) The Cu isotopic signature of
2108 granites from the Lachlan Fold Belt, SE Australia Chem Geol 258:38-49
2109 Little SH, Vance D, Siddall M, Gasson E (2013) A modelling assessment of the role of
2110 reversible scavenging in controlling oceanic dissolved Cu and Zn distributions. Glob
2111 Biogeochem Cycles 27:780-791
2112 Little SH, Vance D, Walker-Brown C, Landing WM (2014a) The oceanic mass balance of
2113 copper and zinc isotopes, investigated by analysis of their inputs, and outputs to
2114 ferromanganese oxide sediments. Geochim Cosmochim Acta 125:673-693,
2115 doi:10.1016/j.gca.2013.07.046
2116 Little SH, Sherman DM, Vance D, Hein JR (2014b) Molecular controls on Cu and Zn
2117 isotopic fractionation in Fe-Mn crusts. Earth Planet Sci Lett 396:213-222
2118 Little SH, Vance D, McManus J, Severmann S (2016) Critical role of continental margin
2119 sediments in the oceanic mass balance of Zn and Zn isotopes. Geology 44: 207-210.
2120 Liu S-A, Teng F-Z, Li S, Wei G-J, Ma J-L, Li D (2014) Copper and iron isotope
2121 fractionation during weathering and pedogenesis: insights from saprolite profiles. Geochim
2122 Cosmochim Acta 146:59-75

Liu S-A, Huang J, Liu J, Woerner G, Yang W, Tang Y-J, Chen Y, Tang L, Zheng J, Li S (2015) Copper isotopic composition of the silicate Earth. Earth Planet Sci Lett 427:95-103, doi:10.1016/j.epsl.2015.06.061

Lodders K (2003) Solar System abundances and condensation temperatures of the elements. Astrophys J 591:1220-1247

Loss RD, Lugmair GW (1990) Zinc isotope anomalies in Allende meteorite inclusions. Astroph J 360:L59-L62

Loss RD, Rosman KJR, Delaeter JR (1990) The Isotopic Composition of Zinc, Palladium, Silver, Cadmium, Tin, and Tellurium in Acid-Etched Residues of the Allende Meteorite. Geochim Cosmochim Acta 54:3525-3536

Luck JM, Othman DB, Barrat JA, Albarède F (2003) Coupled $^{63}$Cu and $^{16}$O excesses in chondrites. Geochim Cosmochim Acta 67:143-151

Luck JM, Othman DB, Albarède F (2005) Zn and Cu isotopic variations in chondrites and iron meteorites: Early solar nebula reservoirs and parent-body processes. Geochim Cosmochim Acta 69:5351-5363

Macleod G, Mcneown C, Hall AJ, Russel MJ (1994) Hydrothermal and oceanic pH conditions of possible relevance to the origin of life. Biosphere 24:19-41

Manceau A, Lanson B, Drits VA (2002) Structure of heavy metal sorbed birnessite. Part III: results from powder and polarized extended X-ray absorption fine structure spectroscopy. Geochim Cosmochim Acta 66:2639-2663

Maréchal C, Télouk P, Albarède F (1999) Precise analysis of copper and zinc isotopic compositions by plasma-source mass spectrometry. Chem Geol 156:251-273Maréchal CN, Douchet C, Nicolas E, Albarède F (2000) The abundance of zinc isotopes as a marine biogeochemical tracer. Geochem, Geophys, Geosyst 1:1999GC-000029

Maréchal C, Albarède F (2002) Ion-exchange fractionation of copper and zinc isotopes. Geochim Cosmochim Acta 66:1499–1509

Maréchal CN, Sheppard SMF (2002) Isotopic fractionation of Cu and Zn between chloride and nitrate solutions and malachite or smithsonite at 30° and 50°C (abstr.). Geochim Cosmochim Acta 66:A84

Markl G, Lahaye Y, Schwinn G (2006) Copper isotopes as monitors of redox processes in hydrothermal mineralization. Geochim Cosmochim Acta 70:4215-4228

Marschner H (1995) Mineral nutrition of higher plants. 2nd edition. Academic Press, London.

Mason TFD, Weiss DJ, Horstwood M, Parrish RR, Russell SS, Mullane E, Coles BJ (2004a) High-precision Cu and Zn isotope analysis by plasma source mass spectrometry. Part 1. Spectral interferences and their correction. J Anal At Spectrom 19:209-217

Mason TFD, Weiss DJ, Horstwood M, Parrish RR, Russell SS, Mullane E, Coles BJ (2004b) High-precision Cu and Zn isotope analysis by plasma source mass spectrometry. Part 2. Correcting for mass discrimination effects. J Anal At Spectrom 19:218-226

Mason TFD, Weiss DJ, Chapman JB, Wilkinson JJ, Tessalina SG, Spiro B, Horstwood MSA, Spratt J, Coles BJ (2005) Zn and Cu isotopic variability in the Alexandrinka volcanic-hosted massive sulphide (VHMS) ore deposit, Urals, Russia. Chem Geol 221:170-187

Mathur R, Ruiz J, Titley S, Liermann L, Buss H, Brantley S (2005) Cu isotopic fractionation in the supergene environment with and without bacteria. Geochim Cosmochim Acta 69:5233-5246Mathur R, Titley S, Barra F, Brantley S, Wilson M, Phillips

A, Munizaga F, Maksaev V, Vervoort J, Hart G (2009) Exploration potential of Cu isotope fractionation in porphyry copper deposits. J Geochem exp 102:1-6
Mathur R, Dendas M, Titley S, Phillips A (2010) Patterns in the copper isotope composition of minerals in porphyry copper deposits in southwestern United States. Econ Geol 105:1457-1467
Mathur R, Jin L, Prush V, Paul J, Ebersole C, Fornadel A, Williams JZ, Brantley S (2012) Cu isotopes and concentrations during weathering of black shale of the Marcellus Formation, Huntingdon County, Pennsylvania (USA). Chem Geol 304:175-184
Mattielli N, Petit JC, Deboudt K, Flament P, Perdrix E, Taillez A, Rimetz-Planchon J, Weis D (2009) Zn isotope study of atmospheric emissions and dry depositions within a 5 km radius of a Pb-Zn refinery. Atmos Environ 43:1265-1272
McBride MB (1981) Forms and distribution of copper in solid and solution phases of soil. In: Copper in soils and plants. *In*: Copper in soils and plants. Loneragan J, Robson AD, Graham RD, (ed) Academic Press, NY, p 25-45
McDonough WF (2003) Compositional Model for the Earth's Core. *In*: Treatise on Geochemistry. Vol 2. Holland HD, Turekian KK, (eds). p 547-568
Meyer BS, Krishan TD, Clayton DD (1998) Theory of Quasi-Equilibrium Nucleosynthesis and Applications to Matter Expanding from High Temperature and Density. Astrophys J 498:808-830
Mhin BJ, Lee S, Cho SJ, Lee K, Kim KS (1992) $Zn(H2O)_6^{2+}$ is very stable among aqua-Zn (II ) ions. Chem Phys Lett 197:77-80
Moffett JW, Brand LE (1996) The production of strong, extracellular Cu chelators by marine cyanobacteria in response to Cu stress. Limnol Oceanogr 41:288-293
Mott lMJ, Wheat CG, Fryer P, Gharib J, Martin JB (2004) Chemistry of springs across the Mariana forearc shows progressive devolatilization of the subducting plate. Geochim Cosmochim Acta 68:4915-4933
Mountain BW, Seward TM (1999) The hydrosulphide/sulphide complexes of copper(I): experimental determination of stoichiometry and stability at 22c and reassessment of high temperature data. Geochim Cosmochim Acta 63:11-29
Moynier F, Le Borgne M (2015) High precision zinc isotopic measurements applied to mouse organs. Journal of visualized experiments:JoVE:e52479-e52479, doi:10.3791/52479
Moynier F, Fegley B (2015) The Earth's building blocks. *In*: The Early Earth: Accretion and Differentiation. Vol 212. Badro J, Walter MJ, (eds). Wiley, New York, p 27-48
Moynier F, Albarède F, Herzog G (2006) Isotopic composition of zinc, copper, and iron in lunar samples. Geochim Cosmochim Acta 70:6103-6117
Moynier F, Dauphas N, Podosek FA (2009a) A Search for $^{70}Zn$ Anomalies in Meteorites. Astrophys J 700:L92-L95
Moynier F, Pichat S, Pons ML, Fike D, Balter V, Albarède F (2009b) Isotopic fractionation and transport mechanisms of Zn in plants. Chem Geol 267:125-130, doi:DOI 10.1016/j.chemgeo.2008.09.017
Moynier F, Beck P, Jourdan F, Yin Q-Z, Reimold U, Koeberl C (2009c) Isotopic fractionation of zinc in tektites. Earth Planet Sci Lett 277:482-489
Moynier F, Koeberl C, Beck P, Jourdan F, Telouk P (2010a) Isotopic fractionation of Cu in tektites. Geochim Cosmochim Acta 74:799-807, doi:DOI 10.1016/j.gca.2009.10.012

2214 Moynier F, Beck P, Yin Q, Ferroir T, Barrat JA, Paniello RC, Telouk P, Gillet P (2010b)
2215 Volatilization induced by impacts recorded in Zn isotope composition of ureilites. Chem
2216 Geol 276:374-379
2217 Moynier F, Paniello RC, Gounelle M, Albarède F, Beck P, Podosek F, Zanda B (2011)
2218 Nature of volatile depletion and genetic relationships in enstatite chondrites and aubrites
2219 inferred from Zn isotopes. Geochim Cosmochim Acta 75:297-307, doi:Doi
2220 10.1016/J.Gca.2010.09.022
2221 Moynier F, Fujii T, Shaw A, Le Borgne M (2013a) Heterogeneous distribution of natural
2222 zinc isotopes in mice. Metallomics 5:693-699
2223 Moynier F, Fujii T, Wang K, Foriel J (2013b) Ab initio calculations of the Fe(II) and Fe(III)
2224 isotopic effects in citrates, nicotianamine, and phytosiderophore, and new Fe isotopic
2225 measurements in higher plants. Comptes Rendus Geoscience 345:230-240,
2226 doi:10.1016/j.crte.2013.05.003
2227 Nägler TF, Anbar AD, Archer C, Goldberg G, Gordon GW, Greber ND, Siebert C, Sohrin
2228 Y, Vance, D (2014) Proposal for an international molybdenum isotope measurement
2229 standard and data representation. Geostandards and Geoanalytical Research 38, 149-151
2230 Navarette JU, Borrok DM, Viveros M, Ellzey JT (2011) Copper isotope fractionation
2231 during surface adsorption and intracellular incorporation by bacteria. Geochim Cosmochim
2232 Acta 75:784-799
2233 Ochoa Gonzalez, R, Weiss, D (2015) Zinc isotope variability in three coal-fired power
2234 plants: a predictive model for determining isotopic fractionation during combustion.
2235 Environ Sci Technol 49: 12560-12567
2236 O'Neill H (1991) The origin of the Moon and the earlyhistory of the Earth-A chemical
2237 model. Part 2: The Earth. Geochim Cosmochim Acta 55:1159-1172
2238 Pacyna JM, Pacyna EG (2001) An assessment of global and regional emissions of trace
2239 metals to the atmosphere from anthropogenic sources worldwide. Environ Rev 9:269-288
2240 Palme H, O'Neill H (2003) Comochemical Estimates of Mantle Composition. *In*: Treatise
2241 on Geochemistry. Vol 2. Holland HD, Turekian KK, (eds). p 1-38
2242 Paniello RC, Day JM, Moynier F (2012a) Zinc isotopic evidence for the origin of the
2243 Moon. Nature 490:376-379, doi:10.1038/nature11507
2244 Paniello RC, Moynier F, Beck P, Barrat JA, Podosek FA, Pichat S (2012b) Zinc isotopes
2245 in HEDs: Clues to the formation of 4-Vesta, and the unique composition of Pecora
2246 Escarpment 82502. Geochim Cosmochim Acta 86:76-87, doi:Doi
2247 10.1016/J.Gca.2012.01.045
2248 Pasquarello A, Petri I, Salmon PS, Parisel O, Car R, Toth E, Powell DH, Fischer HE, Helm
2249 L, Merbach AE (2001) First solvation shell of the Cu(II) aqua ion: evidence for fivefold
2250 coordination. Science 291:856-859
2251 Peacock CL, Sherman DM (2004) Copper (II) sorption onto goethite, hematite and
2252 lepidocrocite: a surface complexation model based on ab initio molecular geometries and
2253 EXAFS spectroscopy. Geochim Cosmochim Acta 68:2623-2637
2254 Peel K, Weiss D, Sigg L (2009) Zinc isotope composition of settling particles as a proxy
2255 for biogeochemical processes in lakes: insights from the eutrophic Lake Greifen,
2256 Switzerland. Limnol Oceanogr Methods 54:1699-1708
2257 Peel K, Weiss D, Chapman J, Arnold T, Coles B (2008) A simple combined sample-
2258 standard bracketing and inter-element correction procedure for accurate mass bias

2259 correction and precise Zn and Cu isotope ratio measurements. J Anal At Spectrom 23:103-
2260 110, doi:10.1039/b710977f
2261 Peers G, Price NM (2006) Copper-containing plastocyanin used for electron transport by
2262 an oceanic diatom. Nature 441:341-344
2263 Petit JC, Schäfer J, Coynel A, Blanc G, Deycard VN, Derriennic H, Lanceleur L, Dutruch
2264 L, Cossy C, Mattielli N (2013) Anthropogenic sources and biogeochemical reactivity of
2265 particulate and dissolved Cu isotopes in the turbidity gradient of the Garonne River
2266 (France). Chem Geol 359:125-135
2267 Pichat S, Douchet C, Albarède F (2003) Zinc isotope variations in deep-sea carbonates
2268 from the eastern equatorial Pacific over the last 175 ka. Earth Planet Sci Lett 210:167-178
2269 Pogge von Strandmann PAE, Forshaw J, Schmidt DN (2014) Modern and Cenozoic
2270 records of seawater magnesium from foraminiferal Mg isotopes. Biogeosciences 11:5155-
2271 5168
2272 Pokrovsky OS, Viers J, Freydier R (2005) Zinc stable isotope fractionation during
2273 adsorption on oxides and hydroxides. J Colloid Interface Sci 291:192-200
2274 Pokrovsky OS, Viers J, Emnova EE, Kompantseva EI, Freydier R (2008) Copper isotope
2275 fractionation during its interaction with soil and aquatic microorganisms and metal
2276 oxy(hyd)oxides: Possible structural control. Geochim Cosmochim Acta 72:1742-1757
2277 Pons ML, Quitte G, Fujii T, Rosing MT, Reynard B, Moynier F, Douchet C, Albarède F
2278 (2011) Early Archean serpentine mud volcanoes at Isua, Greenland, as a niche for early
2279 life. Proc. Natl. Acad. Sci. USA 108:17639-17643, doi:Doi 10.1073/Pnas.1108061108
2280 Pons M-L, Fujii T, Rosing M, Quitté G, Télouk P, Albarède F (2013) A Zn isotope
2281 perspective on the rise of continents. Geobiology 11:201-214
2282 Ponzevera E, Quetel CR, Berglund M, Taylor PDP, Evans P, Loss RD, Fortunato G (2006)
2283 Mass discrimination during MC-ICPMS isotopic ratio measurements: Investigation by
2284 means of synthetic isotopic mixtures (IRMM-007 series) and application to the calibration
2285 of natural-like zinc materials (including IRMM-3702 and IRMM-651). Journal of the
2286 American Society for Mass Spectrometry 17:1412-1427, doi:10.1016/j.jasms.2006.06.001
2287 Powell KJ, Brown PL, Byrne RH, Gajda T, Hefter G, Sjoberg S, Wanner H (2007)
2288 Chemical speciation of environmentally significant metals with inorganic ligands - Part 2:
2289 The $Cu^{2+}$-$OH^-$, $Cl^-$, $CO_3^{2-}$, $SO_4^{2-}$, and $PO_4^{3-}$ systems. Pure Appl Chem 79:895-950
2290 Rauch, JN, Pacyna, JM (2009) Earth's global Ag, Al, Cr, Cu, Fe, Ni, Pb, and Zn cycles.
2291 Glob Biogeochem Cycles 23: GB2001, 10.1029/2008GB003376
2292 Resing JA, Sedwick PN, German CR, Jenkins WJ, Moffett JW, Sohst BM, Tagliabue A
2293 (2015) Basin scale transport of hydrothermal dissolved metals across the South Pacific
2294 Ocean. Nature 523:200-203
2295 Rodovka Z, Magna T, Zak K, Kato C, Savage P, Moynier F, Skala R (In review) Zinc and
2296 copper isotope systematics in sediments from the Ries Impact Structure and central
2297 European tektites – implications for material sources and loss of volatiles. Geochim
2298 Cosmochim Acta
2299 Rosman KJR (1972) A survey of the isotopic and elemental abundances of zinc. Geochim
2300 Cosmochim Acta 36:801-819
2301 Rudge JF, Reynolds BC, Bourdon B (2009) The double spike toolbox. Chem Geol
2302 265:420-431

Russel SS, Zhu X, Guo Y, Belshaw N, Gounelle M, Mullane E (2003) Copper isotope systematics in CR, CH-like, and CB meteorites: a preliminary study (abstr.). Meteorit Planet Sci 38
Ryan BM, Kirby JK, Degryse F, Scheiderich K, McLaughlin MJ (2014) Copper isotope fractionation during equilibration with natural and synthetic ligands. Environ Sci Tech 48:862-866
Ryan BM, Kirby JK, Degryse F, Harris H, McLaughlin MJ, Scheiderich K (2013) Copper speciation and isotopic fractionation in plants: uptake and translocation mechanisms. New Phytologist 199:367-378
Sancenon V, Puig S, Mateu-Andrés I, Dorcey E, Thiele D, Penarrubia L (2004) The Arabidopsis copper transporter COPT1 functions in root elongation and pollen development. J Biol Chem 269:15348-15355
Savage P, Boyet M, Moynier F (2014) Zinc Isotope Anomalies in bulk Chondrites. 77th Meteoritical Society Meeting, Casablanca, Morocco, p 5246
Savage P, Moynier F, Harvey J, Burton K (2015a) The behavior of copper isotopes during igneous processes. AGU conference, San Francisco
Savage P, Moynier F, Chen H, Shofner G, Siebert J, Badro J, Puchtel IS (2015b) Copper isotope evidence for large-scale sulphide fractionation during Earth's differentiation. Geochemical Perspective Letters 1:53-64
Schauble EA (2004) Applying stable isotope fractionation theory to new systems. Rev Mineral Geochem 55:65-111
Schiller M, Paton C, Bizzarro M (2015) Evidence for nucleosynthetic enrichment of the protosolar molecular cloud core by multiple supernova events. Geochim Cosmochim Acta 149:88-102, doi:10.1016/j.gca.2014.11.005
Schonbachler M, Carlson RW, Horan MF, Mock TD, Hauri EH (2010) Heterogeneous Accretion and the Moderately Volatile Element Budget of Earth. Science 328:884-887, doi:DOI 10.1126/science.1186239
Schulz MS, Bullen TD, White AF, Fitzpatrick JF (2010) Evidence of iron isotope fractionation due to biologic lifting in a soil chronosequence. Geochim Cosmochim Acta 74:A927
Seo JH, Lee SK, Lee I (2007) Quantum chemical calculations of equilibrium copper(I) isotope fractionations in ore-forming fluids. Chem Geol 243:225-237
Shank CG, Ckrabal SA, Whitehead RF, G. BA, Keiber RJ (2004) River discharge of strong Cu-binding ligands to South Atlantic Bight Waters. Mar Chem 88:41-51
Sherman DM (2001) Quantum chemistry and classical simulations of metal complexes in aqueous solutions. *In*: Rev Mineral Geochem. Vol 42. p 273-317
Sherman DM (2013) Equilibrium isotopic fractionation of copper during oxidation/reduction, aqueous complexation and ore-forming processes: predictions from hybrid density functional theory. Geochim Cosmochim Acta 118:85-97
Sherman DM, Little SH, Vance D (2015) Reply to comment on "Molecular controls on Cu and Zn isotopic fractionatin in Fe-Mn crusts". Earth Planet Sci Lett 411:313-315
Shields WR, Murphy TJ, Garner EL (1964) Absolute isotopic abundance ratio and the atomic weight of a reference sample of copper. J Res NBS 68A:589-592
Shields WR, Goldich SS, Garner EL, Murphy TJ (1965) Natural variations in the abundance ratio and the atomic weight of copper. J Geophys Res:479-491
Shiller AM, Boyle EA (1985) Dissolved zinc in rivers. Nature 317:49-52

Siebert J, Corgne A, Ryerson FJ (2011) Systematics of metal–silicate partitioning for many siderophile elements applied to Earth's core formation. Geochim Cosmochim Acta 75:1451-1489

Singha Deb AK, Ali SkM, Shenoy KT, and Ghosh SK (2014) Nano cavity induced isotope separation of zinc: density functional theoretical modeling. J Chem Eng Data, 59:2472-2484

Sinoir M, Butler ECV, Bowie AR, Mongin M, Nesterenko PN, Hassler CS (2012) Zinc marine biogeochemistry in seawater: a review. Mar Freshwater Res 63:644-657

Sivry Y, Riotte J, Sonke JE, Audry S, Schäfer J, Vuers J, Blanc G, Freydier R, Dupré B (2008) Zn isotopes as tracers of anthropogenic pollution from Zn ore-smelters. The Riou Mort-Lot River system. Chem Geol 255:295-304

Sold D, Behra R (2000) Long-term effects of copper on the structure of freshwater periphyton communities and their tolerance to copper, zinc, nickel and silver. Aquatic Toxicol 47:181-189

Sonke JE, Sivry Y, Viers J, Fréydier R, Dejonghe L, André L, Aggarwal JK, Fontan F, Dupré B (2008) Historical variations in the isotopic composition of atmospheric zinc deposition from a zinc smelter. Chem Geol 252:145-157

Sossi PA, Halverson GP, Nebel O, Eggins SM (2015) Combined Separation of Cu, Fe and Zn from Rock Matrices and Improved Analytical Protocols for Stable Isotope Determination. Geostandards and Geoanalytical Research 39:129-149, doi:10.1111/j.1751-908X.2014.00298.x

Sossi PA, Nebel O, O'Neil HST, Moynier F (In review) Progressive accretion of Earth's moderately volatile elements revealed by Zn isotopes. Geochemical Perspective Letters.

Steele RCJ, Coath CD, Regelous M, Russell S, Elliott T (2012) Neutron-poor nickel isotope anomalies in meteorites. Astrophys J 758(59) doi:10.1088/0004-637X/758/1/59

Sunda WG, Huntsman SA (1992) Feedback interactions between zinc and phytoplankton in seawater. Limnol Oceanogr Methods 37: 25-40

Szynkiewicz A, Borrok DB (2016) Isotope variations of dissolved Zn in the Rio Grande watershed, USA: The role of adsorption on Zn isotope composition. Earth Planet Sci Lett 433: 293-302

Takano S, Tanimizu M, Hirata T, Sohrin Y, 10.1038/ncomms6663. IcobcocitoNCd (2014) Isotopic constraints on biogeochemical cycling of copper in the ocean. Nature communications doi: 10.1038/ncomms6663.

Tang Y-T, Cloquet C, Sterckman T, Echevarria G, Carignan J, Qiu R-L, Morel J-L (2012) Fractionation of stable zinc isotopes in the field-grown zinc hyperaccumulator Noccaea caerulescens and the zinc-tolerant plant Silene vulgaris. Environ Sci Technol 46:9972-9979

Tanimizu M, Asada Y, Hirata T (2002) Absolute isotopic composition and atomic weight of commercial zinc using inductively coupled plasma mass spectrometry. Anal Chem 74:5814-5819

Telouk P, Puisieux A, Fujii T, Balter V, Bondanese VP, Morel A-P, G. C, Lamboux A, Albarède F (2015) Copper isotope effect in serum of cancer patients. A pilot study. Metallomics 7:299-308.

Telus M, Dauphas N, Moynier F, Tissot F, Teng FZ, Nebelek PI, Craddock PR, Groat LR (2012) Iron, zinc, magnesium, and uranium isotopic fractionation during continental crust

differentiation : The tale from migmatites, granitoids and pegmatites. Geochim. Cosmochim. Acta 97:247-265.
Thapalia A, Borrok DM, van Metre PC, Musgrove M, Landa ER (2010) Zn and Cu isotopes as tracers of anthropogenic contamination in a sediment core from an urban lake. Environ Sci Technol 44:1544-1550
Thomson CM, Ellwood MJ (2014) Dissolved copper isotope geochemistry in the Tasman Sea, SW Pacific Ocean. Mar Chem 165:1-9
Trinquier A, Elliott T, Ulfbeck D, Coath C, Krot AN, Bizzarro M (2009) Origin of Nucleosynthetic Isotope Heterogeneity in the Solar Protoplanetary Disk. Science 324:374-376
Twining BS, Baines SB (2013) The trace metal composition of marine phytoplankton. Ann Rev Earth Planet Sci 5:191-215
Vance D, Archer C, Bermin J, Perkins J, Statham PJ, Lohan MC, Ellwood MJ, Mills RA (2008) The copper isotope geochemistry of rivers and the oceans. Earth Planet Sci Lett 274:204-213, doi:10.1016/j.epsl.2008.07.026
Vance D, Teagle DAH, Foster GL (2009) Variable Quaternary chemical weathering fluxes and imbalances in marine geochemical budgets. Nature 458:493-496
Vance D, Matthews A, Keech A, Archer C, Hudson G, Pett-Ridge J, Chadwick OA (2016) The behaviour of Cu and Zn isotopes during soil development: controls on the dissolved load of rivers. Chem Geol: accepted
Vance D, Little SH, Archer C, Rijkenberg M (In review) Transition metal isotopes as tracers of oceanic metal budgets and cycling. Phil Trans R Soc A
Viers J, Oliva P, Nonelle A, Gelabert A, Sonke J, Freydier R, Gainville R, Dupre B (2007) Evidence of Zn isotopic frationation in a soil-plant system of a pristine tropical watershed (Nsimi, Cameroon). Chem Geol 239:124-137
Viers, J, Prokushkin, AS, Pokrovsky, OS, Kirdyanov, AV, Zouiten, C, Chmeleff, J, Meheut, M, Chabaux, F, Oliva, P, Dupré, B (2015) Zn isotope fractionation in a pristine larch forest on permafrost-dominated soils in Central Siberia. Geochem Trans 16: 10.1186/s12932-015-0018-0
Völkening J, Papanastassiou DA (1990) Zinc isotope anomalies. Astrophys J 358:L29-L32
Wallerstein G, Iben Jr I, Parker P, Boesgaard AM, Hale GM, Champagne AE, Barnes CA, Kaeppeler F, Smith VV, Hoffman RD, Timmes FX, Sneden C, Boyd RN, Meyer BS, Lambert DL (1997) Synthesis of the elements in stars: forty years of progress. Reviews of Modern Physics, 69: 995-1084
Wang P, Zhou DM, Luo XS, Li LZ (2009) Effects of Zn-complexes on zinc uptake by wheat (Triticum aestivum) roots: a comprehensive consideration of physical, chemical and biological processes on biouptake. Plant Soil 316:177-192
Wanty, RB, Ballistrieri, LS, Wesner, JS, Walsters, DM, Schmidt, TS, Podda, F, De Giudici, G, Stricker, CA, Kraus, J, Lattanzi, P, Wolf, RE, Cidu, R (2015) Isotopic insights into biological regulation of zinc in contaminated systems. Proc Earth Planet Sci 13: 60-63
Wanty, RB, Podda, F, De Giudici, G, Cidu, R, Lattanzi, P (2013) Zinc isotope and transition-element dynamics accompanying hydrozincite biomineralization in the Rio Naracauli, Sardinia, Italy. Chem Geol 337-338: 1-10
Wasson JT, Wang JM (1986) A non magmatic origin of group-IIE iron-meteorites. Geochim Cosmochim Acta 50:725-732

2439 Wasylenki LE, Weeks CL, Bargar JR, Spiro TG, Hein JR, Anbar AD (2011) The molecular
2440 mechanism of Mo isotope fractionation during adsorption to birnessite. Geochim
2441 Cosmochim Acta 75:5019-5031
2442 Weinstein C, Moynier, F., Wang, K., Paniello, R., Foriel, J., Catalano, J., and Foriel, J.
2443 (2011) Cu isotopic fractionation in plants. Chem Geol 286:266-271
2444 Weiss DJ, Mason TFD, Zhao FJ, Kirk GJD, Coles BJ, Horstwood MSA (2005) Isotopic
2445 discrimination of zinc in higher plants. New Phytologist 165:703-710
2446 Weiss DJ, Rausch N, Mason TFD, Coles BJ, Wilkinson JJ, Ukonmaanaho L, Arnold T,
2447 Nieminen TM (2007) Atmospheric deposition and isotope biogeochemistry of zinc in
2448 ombrotrophic peat. Geochim Cosmochim Acta 71:3498-3517
2449 Weiss DJ, Boye K, Caldelas C, Fendorf S (2014) Zinc isotope fractionation during early
2450 dissolution of biotite granite. Soil Sci Amer 78:171-189
2451 Wells ML, Kozelka PB, Bruland KW (1998) The complexation of "dissolved" Cu, Zn, Cd
2452 and Pb by soluble and colloidal organic matter in Narragansett Bay, RI. Mar Chem 62:203-
2453 217
2454 Wiederhold JG, Teutsch N, Kraemer SM, Halliday AN, Kretzschmar R (2007) Iron isotope
2455 fractionation in oxic soils by mineral weathering and podzolization. Geochim Cosmochim
2456 Acta 71:5821-5833, doi:Doi 10.1016/J.Gca.2007.07.023
2457 Wiederhold J (2015) Metal stable isotope signatures as tracers in environmental
2458 geochemistry. . Environmental Science & Technology 49:2606-2624
2459 Wilkinson JJ, Weiss DJ, Mason TFD, Coles BJ (2005) Zinc isotope variation in
2460 hydrothermal systems: preliminary evidence from the Irish Midlands ore field. Econ Geol
2461 110:583-590
2462 Williams HM, Archer C (2011) Copper stable isotopes as tracers of metal-sulphide
2463 segregation and fractional crystallisation processes on iron meteorite parent bodies.
2464 Geochim Cosmochim Acta 75:3166-3178
2465 Yin, N-H, Sivry, Y, Benedetti, MF, Lens, PNL, van Hullebusch, ED (2016) Application of
2466 Zn isotopes in environmental impact assessment of Zn-Pb metallurgical industries: a mini
2467 review. App Geochem 64: 128-135
2468 Yruela I (2009) Copper in plants: acquisition, transport and interactions. Funct Plant Biol
2469 26:409-430
2470 Zhao Y, Vance D, Abouchami W, de Baar HJW (2014) Biogeochemical cycling of zinc
2471 and its isotopes in the Southern Ocean. Geochim Cosmochim Acta 125:653-672,
2472 doi:10.1016/j.gca.2013.07.045
2473 Zhu XK, O'Nions RK, Guo Y, Belshaw NS, Rickard D (2000) Determination of Cu-isotope
2474 variation by plasma souce mass spectrometry: implications for use as geochemical tracers.
2475 Chem Geol 163:139-149
2476 Zhu XK, Guo Y, Williams RJP*, et al.* (2002) Mass fractionation processes of transition
2477 metal isotopes. Earth Planet Sci Lett 200:47-62
2478 Zirino A, Yamamoto S (1972) A pH-dependent model for the chemical speciation of
2479 copper zinc cadmium, and lead in seawater. Limnol Oceanogr 17:661-671
2480

## Figure captions

**Figure 1:** Temperature dependence of lnβ. The lnβ values of hydrated Cu2+ and Cu(II) chlorides, sulphides, phosphates, carbonates and sulfates (see Table 1) are shown as linear functions of $T^2$.

**Figure 2:** Temperature dependence of lnβ. The lnβ values of hydrated Zn2+ and Zn(II) sulphides, phosphates, carbonates and sulfates (see Table 1) are shown as linear functions of $T^2$.

**Figure 3:** $\delta^{65}Cu$ vs $\Delta^{17}O$ for the bulk silicate Earth and the different major groups of chondrites. Meteorite group averages are calculated using data from Luck et al. (2003), Barrat et al (2012) and Savage et al. (2015b). The estimate of the Bulk Silicate Earth is from Savage et al. (2015b). All error bars are 2SD of the mean. The trend implies the presence of at least two, and potentially three, distinct Cu isotope reservoirs which then mixed to create the distinct chondritic bodies, as a result of nebula processing.

**Figure 4:** A) Box-and-whisker plot of $\delta^{66}Zn$ of the different chondrites groups (UOC=Un-equilibrated ordinary chondrites); whiskers denote the maximum and minimum value of the data, box denotes the first and third quartiles and the band denotes the median. Data are taken from Luck et al. (2005), Moynier et al. (2011) and Barrat et al. (2012). Enstatite chondrites, carbonaceous chondrites, and unequilibrated ordinary chondrites have Zn isotopic composition close to the current estimates of BSE. B) Identical plot as 4A but with increased x-axis range. The EL enstatite chondrites of high thermal metamorphic grades (EL6), which are depleted in volatile elements compared to low thermal metamorphic grades (EL3), are highly enriched in the heavier isotopes. This suggests that the origin of the volatile element depletion between EL3 and EL6 chondrites is due to volatilization during the thermal metamorphism.

**Figure 5**: $\delta^{66}Zn$ vs Mg/Zn ratio for different chondrites groups. The negative correlation between $\delta^{66}Zn$ and Mg/Zn (refractory element/moderately volatile element) suggests that the origin of the Zn depletion in carbonaceous chondrites is not due to evaporation and is of nebular origin. Data from Luck et al. (2005) and Barrat et al. (2012)

**Figure 6**: Histogram of the $\delta^{65}Cu$ of the various ultramafic and mafic samples analyzed to date (data from Savage et al. 2015b, Liu et al. 2015, Ben Othman et al. 2006 and Ikehata and Hirata 2013). The grey box represents the estimate of the BSE composition from Savage et al. 2015b. Komatiites , fertile orogenic lherzolites as well as a representative selection of both mid-ocean ridge and ocean island basalts have identical Cu isotope compositions suggesting that mantle melting produces a limited Cu isotope fractionation.

**Figure 7**: $\delta^{66}Zn$ and Zn concentration versus degree of differentiation as represented by MgO content for basalts and their differentiates, komatiites and ultramafic samples (data from Herzog et al., 2011, Chen et al. 2013b and Sossi et al. In review). The most evolved samples are enriched in the heavier isotopes. This trend is interpreted as the result of

crystallization of isotopically light olivines or Ti-oxides (Chen et al. 2013b) and led Sossi et al (in review) to propose a BSE $\delta^{66}$Zn composition of 0.15 ± 0.05 ‰. N.B. the abyssal peridotites underwent metasomatism, most likely affecting their Zn isotope composition.

**Figure 8:** Summary of currently available data for "natural" surface Earth materials. Materials significantly impacted by human activity represent a distinct topic and are treated separately later in this chapter. The range of isotopic compositions found in ore minerals is shown by the black bars at the bottom. Note that Cu isotopes are extremely heterogeneous in Cu-bearing ore minerals, extending well beyond the limits of other Earth surface samples, from $\delta^{65}$Cu -16.5 to +9.98. In the top two panels the thinner lines show the total range of values measured in each type of sample. For the oceanic dissolved pool, the thicker lines show the average and 1SD for all analyses in the homogeneous deep ocean (beneath 600-800m). For the river data the square shows the discharge- and [Cu]- or [Zn]-weighted average for the dissolved flux to the oceans as calculated from the large rivers measured to date. For all the other sample types the thicker line shows the average of all the data ±1SD. In the bottom two panels the red histograms show the range of variability in all igneous rocks, as relative frequencies, including basalts, andesites, dacites, rhyolites, granites, granodiorites, komatiites and peridotites. Clastic sediments (diagonal pattern), including atmospheric aerosols, show close overlap with the igneous samples. In contrast, surface Earth samples whose genesis involves the partitioning of Cu and Zn between solid and aqueous phases (top two panels) exhibit substantial variability. Note the agreement between the values for igneous rocks and clastic sediments with those for the Bulk Silicate Earth in earlier diagrams.

Data from:
Seawater: Bermin et al. (2006), Vance et al. (2008), Boyle et al. (2012), Zhao et al. (2014), Conway and John (2014, 2015), Thomson and Ellwood (2014), Takano et al. (2014). Rivers: Vance et al. (2008), Ilina et al. (2013), Little et al. (2014a), and including two Zn data for the relatively unpolluted Seine system headwaters from Chen et al. (2008). Dust/aerosol: Marechal et al. (2000), Li et al. (2009), Bigalke et al. (2010a), Dong et al. (2013), Little et al. (2014a), and including data for rain (wet deposition?) in Takano et al. (2014). Fe-Mn deposits: Marechal et al. (2000), Little et al. (2014a). Carbonates: Pichat et al. (2003). Siliceous sediments: Andersen et al. (2011), Hendry and Andersen (2013). Organic-rich sediments: Little et al. (2016) Deep, sulphidic Black Sea (dissolved phase):Vance et al. (2016a). Soils and plants: Viers et al. (2007); Bigalke et al. (2010a, 2011), Mathur et al. (2012), Liu et al. (2014), Vance et al. (2016b). Ombrotrophic peat: Weiss et al. (2007, pre-Anthropocene analyses only). Igneous rocks: Marechal et al. (2000), Archer and Vance (2004), Chapman et al. (2006), Cloquet et al. (2006), Bentahila et al. (2008), Toutain et al. (2008), Sonke et al. (2008), Li et al. (2009), Herzog et al. (2008), Chen et al. (2009), Moynier et al. (2010a,b), Bigalke et al. (2010), Weinstein et al. (2011), Moeller et al. (2012), Telus et al. (2012), Chen et al. (2013), Liu et al. (2015), Savage et al. (2015, including data tabulated here from Ben Othman et al., 2006 and Ikehata and Hirata, 2012). Clastic sediments (including dust/aersols in refs above): Marechal et al. (1999, 2000), Asael et al. (2007), Bentahila et al. (2008), Sonke et al. (2008, pre-Anthropocene analyses only), Chen et al. (2009, only relatively unpolluted river sediments from the Seine system, with Zn enrichment factors <2), Bigalke et al. (2010a), Mathur et al. (2012),

Gagnevin et al. (2012), Vance et al. (2016b). Ore minerals: Marechal et al. (1999), Larson et al. (2003), Mason et al. (2005), Wilkinson et al. (2005) Mathur et al. (2005, 2009, 2010), Markl et al. (2006), Asael et al. (2007), Sonke et al. (2008), Gagnevin et al. (2012).

**Figure 9:** Summary of experimental constraints on the isotopic fractionation of Cu and Zn during important Earth surface processes.

Data from:
Redox (Cu only): Zhu et al. (2002), Ehrlich et al. (2004), Mathur et al. (2005). Organic complexation: Ban et al. (2002), Jouvin et al. (2009), Bigalke et al. (2010b), Ryan et al. (2014). Sorption to oxide, clay and microbial surfaces: Pokrovsky et al. (2005, 2008), Gélabert et al. (2006), Ballistrieri et al. (2008), Juillot et al. (2008), Navarette et al. (2011), Kafantaris and Borrok (2014), Bryan et al. (2014), Coutaud et al. (2014), Guinoiseau et al. (2016). Biological uptake: Zhu et al. (2002), Weiss et al. (2005), John et al. (2007), Pokrovsky et al. (2008), Arnold et al. (2009), Moynier et al. (2009), Weinstein et al. (2011), Caldelas et al. (2011), Navarette et al. (2011), Jouvin et al. (2012), Tang et al. (2012), Ryan et al. (2013), Conway and John (2014).

**Figure 10:** Cu-Zn isotope and tau data from relatively unpolluted soils in Hawaii (basaltic) and Scotland (granitic) to illustrate important soil processes as discussed in the text (from Vance et al. 2016b). Panels a,b: data from a sequence of soils, all 400kyr in age but having seen different annual rainfall, on the island of Maui (Hawaiian Islands). Grey shading represents mean annual precipitation (MAP) from 2500mm (white), through 3350mm (grey) to 5050mm (black). Horizontal dashed lines show the isotopic composition of the parent basalt. At the 2500mm site Fe is retained in the soil as Fe oxyhydroxides. Cu is depleted with preferential loss of the heavy isotope to aqueous organic complexes and retention of a sorbed isotopically light pool (solid arrow). At higher rainfall these oxyhydroxides are lost by reduction, leading to loss of almost all this residual light Cu and the retention of a very small pool of Cu that is close to the parent material in isotopic composition (dashed arrow). Panel b shows the Zn data, which has a similar pattern though the move towards light isotopic compositions at the low rainfall site is barely analytically resolvable and the move back to heavy isotopic compositions overshoots to values 0.3‰ heavier than the original rock. Panels c,d: data for soils on the island of Hawaii, all having seen 2500mm MAP with colour shading showing different aged soils from 0.3 kyr (white), through 20 kyr (grey), to 150 kyr (black). The solid arrow shows the trajectory for retention of residual light isotopes during chemical weathering in well-drained conditions as in a,b. The dashed arrows in c show the trajectories that would be followed given addition of Asian dust to move the soils away from this trend. In d the dashed arrows are illustrative only because their exact slope depends on how much Cu and Zn the oils has lost when dust is added. Panels e,f: tau data for Zn and phosphate in the upper organic-matter-rich horizons of granitic Scottish soils, as well as Zn isotopic data for parent material (bar at left), plants (bar at right) and soils (open circles), to illustrate correlated behaviour between Zn and a major plant nutrient.

**Figure 11:** Summary data for soils studied in Viers et al. (2007), Mathur et al. (2012), Liu et al. (2014) and Vance et al. (2016b), in the form of taus and isotopic compositions

integrated over the entire soil profile studied, and in order to assess the overall impact of depletion by chemical weathering on Cu and Zn isotopes. The numbers in brackets in the key, and the intensity of shading, indicate the timescale over which soils have developed, where known. All basaltic soils are shown as diamonds, granitic as circles, and soils developed on black shales as triangles. Preferential loss of the heavy Cu isotope during chemical weathering is clearly significant. The Zn data are plotted on the same scale to illustrate the subtlety of isotope fractionation during weathering by comparison with Cu.

**Figure 12:** All the Zn isotopic data currently available for the dissolved pool in the oceans (right) with Zn concentrations measured in the same samples as the isotopes (left), plotted versus depth. The middle of the grey bar on the isotope plot marks the average $\delta^{66}$Zn for the deep ocean (beneath 800m) while its width shows a typical analytical uncertainty (±0.06‰). This deep ocean inventory is generally very homogeneous and has an average $\delta^{66}$Zn ~ +0.47‰. In the deep ocean, the data depart from this ratio locally, such as near hydrothermal vent systems at 3-4 km in the Atlantic (Conway and John 2014). In the surface ocean isotope compositions are also very close to this deep ocean average in the Southern Ocean (Zhao et al. 2014), but the upper ocean in the North Atlantic and North Pacific depart significantly from it (Boyle et al. 2012; Conway and John 2014, 2015; Zhao and Vance, unpublished data). Relative to this average deep ocean value, the estimates input is slightly isotopically light, at about +0.33‰ (arrow at top: Little et al. 2014a), while the dominant outputs in the oxic open ocean are much heavier (arrow at bottom: +0.90‰ in Fe-Mn oxides, carbonates and siliceous sediments; Little et al. 2014a).

**Figure 13:** All the Cu isotopic data currently available for the dissolved pool in the oceans (right) with Cu concentrations measured in the same samples as the isotopes (left), plotted versus depth. Open symbols on this plot are for data in the pioneering work of Bermin et al. (2006) and Vance et al. (2008). These data were obtained pre-GEOTRACES, on samples that had been stored for times on the order of 10 years. Though acidified, they stand out as having significantly heavier isotopic compositions than more recent work on new, cleanly-collected, GEOTRACES samples, including new (as yet unpublished) data from the same group, and in Takano et al. (2014) and Thompson and Ellwood (2014). It seems likely that these early measurements are compromised in some way by the long storage. The middle of the grey bar on the isotope plot marks the average $\delta^{65}$Cu for the deep ocean (beneath 800m, and excluding these older data plotted as open symbols) while its width shows a typical analytical uncertainty (±0.08‰). As with Zn, this deep ocean inventory is generally very homogeneous and has an average $\delta^{65}$Cu ~ +0.66‰. The estimated input is close to this deep ocean average, at about +0.63‰ (arrow at top: Vance et al. 2008; Little et al. 2014a). The only output yet characterised for Cu, though it is probably the most important, is scavenging to Fe-Mn oxide particulates and transfer to sediment (arrow at bottom, +0.31‰: Little et al. 2014a), is significantly lighter than both the input flux and the deep ocean average.

**Figure 14:** Schematic summary of our current understanding of processes relevant to the overall marine budgets of Cu and Zn isotopes. The inputs are shown as arrows on the left, with the Cu input shown as thick because of the uncertainty over the size of the dust input (Little et al. 2014a; Takano et al. 2014). Within the oceans this input is split into two pools

(schematic isotopic compositions shown as horizontal dashed lines): a dominant ligand-bound pool (ZnL or CuL) and a minor free metal ion pool ($Zn^{2+}$ or $Cu^{2+}$). In both cases the ligand-bound pool is shown as heavy relative to the free metal ion (Jouvin et al. 2009; Ryan et al. 2014). If the oceans are in steady state the isotopic compositions of the outputs (arrows on right) must balance the input. For Zn the outputs to oxic sediments have $\delta^{66}Zn \sim +0.9‰$ (Little et al. 2014a), consistent with a positive $\Delta_{sorbed\text{-}Zn2+}$ (Bryan et al 2015). This is balanced by a light output to organic-rich sediments (Little et al. 2016) whose isotopic composition is probably controlled by partial sequestration of organic-associated Zn to sulphide in pore waters (Vance et al. 2016a). For Cu the only characterised output is via sorption to Fe-Mn particulates, with $\delta^{65}Cu \sim +0.3‰$ (Little et al. 2014a), shown as being consistent with a positive $\Delta_{sorbed\text{-}Cu2+}$ (e.g. Balistrieri et al. 2008; Pokrovsky et al. 2008). This must balanced by an output that is heavy relative to the input (question marks on right), possibly quantitative removal of seawater Cu in euxinic settings as speculated by Thompson and Ellwood (2014).

2685 Table 1 : $\delta^{66}Zn_{JMC\ Lyon}$ and $\delta^{65}Cu_{SRM\ 976}$ of commonly used geological standards and isotopically certified
2686 materials.

| | $\delta^{66}Zn_{JMC\ Lyon}$ | 2se | ref | $\delta^{65}Cu_{SRM\ 976}$ | 2se | ref |
|---|---|---|---|---|---|---|
| IRMM-3702 | 0.38 | 0.10 | 1 | | | |
| IRMM-3702 | 0.25 | 0.09 | 1 | | | |
| IRMM-3702 | 0.30 | 0.02 | 2 | | | |
| IRMM-3702 | 0.29 | 0.05 | 3 | | | |
| IRMM-3702 | | | | | | |
| **IRMM-3702 recommended value** | **0.30** | **0.01** | | | | |
| **ERM-AE633** | | | | -0.01 | 0.05 | 3 |
| **ERM-AE647** | | | | 0.21 | 0.05 | 3 |
| BHVO-2 | 0.33 | 0.04 | 4 | 0.10 | 0.08 | 5 |
| | 0.21 | 0.09 | 6 | 0.10 | 0.04 | 3 |
| | 0.27 | 0.06 | 2 | 0.10 | 0.07 | 4 |
| | 0.31 | 0.03 | 15 | 0.15 | 0.05 | 9 |
| | 0.29 | 0.09 | 16 | 0.13 | 0.03 | 8 |
| **BHVO-2 recommended value** | **0.28** | **0.04** | | **0.12** | **0.02** | |
| BCR-1/2 | 0.20 | 0.04 | | 0.19 | 0.07 | 5 |
| | 0.29 | 0.12 | 10 | 0.14 | 0.05 | 3 |
| | 0.32 | 0.13 | 1 | 0.07 | 0.08 | 11 |
| | 0.23 | 0.08 | 12 | 0.19 | 0.08 | 12 |
| | 0.25 | 0.01 | 2 | 0.22 | 0.04 | 8 |
| | 0.20 | 0.09 | 11 | 0.21 | 0.04 | 8 |
| | 0.26 | 0.05 | 13 | | | |
| | 0.26 | 0.09 | 17 | | | |
| **BCR-1/2 recommended value** | **0.25** | **0.03** | | **0.17** | **0.05** | |
| BIR-1 | 0.31 | 0.04 | 4 | 0.00 | 0.03 | 2 |
| | 0.26 | 0.09 | 7 | 0.08 | 0.07 | 3 |
| | 0.20 | 0.04 | 2 | -0.02 | 0.10 | 14 |
| **BIR-1 recommended value** | **0.26** | **0.06** | | **0.02** | **0.06** | |
| AGV1/2 | 0.32 | 0.04 | 4 | -0.01 | 0.03 | 5 |
| | 0.25 | 0.09 | 6 | -0.01 | 0.09 | 5 |

| | | | | | | |
|---|---|---|---|---|---|---|
| | 0.29 | 0.03 | 15 | 0.01 | 0.11 | 5 |
| | 0.28 | 0.05 | 15 | 0.11 | 0.04 | 3 |
| | | | | 0.1 | 0.11 | 3 |
| | | | | 0.05 | 0.04 | 8 |
| **AGV1/2 recommended value** | **0.29** | **0.03** | | **0.04** | **0.04** | |
| | | | | | | |
| G2 | 0.34 | 0.04 | 15 | | | |
| | 0.30 | 0.09 | 18 | | | |
| | 0.32 | 0.09 | 17 | | | |
| **G2 recommended value** | **0.32** | **0.02** | | | | |

Ref: 1=Cloquet et al. 2006; 2=Sossi et al. 2014, 3=Moeller et al. 2012; 4=Chen et al. 2013; 5=Savage et al. 2015; 6=Moynier et al. 2010; 7=Herzog et al. 2009; 8=Liu et al. 2015; 9=Liu et al. 2014; 10=Chapman et al. 2006; 11=Archer and Vance 2004; 12=Bigalke et al. 2010; 13=Viers et al. 2007; 14=Li et al. 2009 ; 15=S. Chen et al. 2016 ; 16=Telus et al. 2012 ; 17=Paniello et al. 2012a, 18=Paniello et al. 2012b.

Table 2 Logarithm of the reduced partition function, ln β, for the pair $^{65}Cu$-$^{63}Cu$. Cu(II) species. Method/Basis set used: B3LYP/TZP for Sherman (2013) and , B3LYP/6-311+G(d,p) for Fujii et al. (2013, 2014).

| | Species | Coordination number | Temperature (K) | | | | | | | Ref[b] |
|---|---|---|---|---|---|---|---|---|---|---|
| | | | 273 | 298 | 310 | 323 | 373 | 473 | 573 | |
| Solid | CuO (Tenorite) | - | 6.63 | 5.62 | - | 4.81 | 3.65 | 2.29 | 1.57 | 1 |
| Aquo-ion | $Cu(H_2O)_5^{2+}$ | 5 | 5.355 | 4.546 | - | 3.905 | 2.968 | 1.876 | 1.290 | 2 |
| | | | 5.36 | 4.55 | - | 3.91 | 2.97 | 1.88 | 1.29 | 1 |
| | $Cu(H_2O)_6^{2+}$ | 6 | 5.053 | 4.288 | - | 3.682 | 2.798 | 1.767 | 1.215 | 2 |
| Chloride | $CuCl(H_2O)_4^{+}$ | 5 | 4.906 | 4.161 | - | 3.572 | 2.712 | 1.711 | 1.176 | 2 |
| | $CuCl(H_2O)_5^{+}$ | 6 | 4.67 | 3.96 | - | 3.40 | 2.58 | 1.63 | 1.12 | 1 |
| | $CuCl_2(H_2O)_3$ | 5 | 4.709 | 3.988 | - | 3.420 | 2.592 | 1.633 | 1.120 | 2 |
| | $CuCl_2(H_2O)_4$ | 6 | 4.397 | 3.724 | - | 3.193 | 2.421 | 1.525 | 1.046 | 2 |
| | $CuCl_3H_2O^{-}$ | 4 | 3.530 | 2.985 | - | 2.556 | 1.933 | 1.214 | 0.832 | 2 |
| Hydroxide | $CuOH(H_2O)_4^{+}$ | 5 | 5.307 | 4.517 | - | 3.889 | 2.967 | 1.883 | 1.298 | 2 |
| | | | 5.30 | 4.52 | - | 3.89 | 2.97 | 1.89 | 1.30 | 1 |
| | $Cu(OH)_2(H_2O)_3$ | 5 | 5.814 | 4.966 | - | 4.288 | 3.286 | 2.098 | 1.451 | 2 |
| Carbonate | $CuCO_3(H_2O)_2$ | 4 | 5.091 | 4.323 | - | 3.715 | 2.825 | 1.787 | 1.230 | 2 |
| | $Cu(CO_3)_2^{2-}$ | 4 | 6.176 | 5.239 | - | 4.498 | 3.416 | 2.158 | 1.483 | 2 |
| | | | 6.38 | 5.41 | - | 4.65 | 3.53 | 2.23 | 1.53 | 1 |
| | $CuHCO_3(OH)_2^{-}$ | 4 | 5.951 | 5.075 | - | 4.376 | 3.346 | 2.130 | 1.471 | 2 |
| Sulfate | $CuSO_4(H_2O)_4$ | 5 | 6.041 | 5.144 | - | 4.430 | 3.381 | 2.148 | 1.481 | 2 |
| Sulfide | $CuHS(H_2O)_4^{+}$ | 5 | 4.002 | 3.386 | - | 2.900 | 2.194 | 1.377 | 0.942 | 2 |
| | $Cu(HS)_2(H_2O)_3$ | 5 | 3.855 | 3.264 | - | 2.797 | 2.119 | 1.333 | 0.914 | 2 |
| Phosphate | $CuH_2PO_4(H_2O)_4^{+}$ | 5 | 5.515 | 4.684 | - | 4.026 | 3.063 | 1.939 | 1.334 | 3 |
| | $CuH_4(PO_4)_2(H_2O)_3$ | 5 | 5.553 | 4.714 | - | 4.050 | 3.079 | 1.947 | 1.339 | 3 |
| | $CuH_3(PO_4)_2(H_2O)_3^{-}$ | 5 | 5.290 | 4.492 | - | 3.861 | 2.937 | 1.860 | 1.280 | 3 |
| | $CuH_2(PO_4)_2(H_2O)_2^{2-}$ | 4 | 6.360 | 5.403 | - | 4.645 | 3.535 | 2.238 | 1.540 | 3 |
| Citrate | $CuH_2(cit)(H_2O)_2^{+}$ | 5 | 5.286 | 4.486 | - | 3.852 | 2.927 | 1.850 | 1.272 | 2 |
| | $CuH(cit)(H_2O)_2$ | 5 | 5.622 | 4.772 | - | 4.099 | 3.117 | 1.972 | 1.357 | 2 |
| | $Cu(cit)(H_2O)_2^{-}$ | 5 | 6.092 | 5.177 | - | 4.451 | 3.389 | 2.147 | 1.479 | 2 |
| | $Cu(cit)_2^{4-}$ | 4 | 4.998 | 4.231 | - | 3.626 | 2.748 | 1.730 | 1.188 | 2 |
| Oxalate | $CuC_2O_4(H_2O)_2$ | 4 | 6.236 | 5.302 | - | 4.561 | 3.474 | 2.202 | 1.516 | 2 |
| Ascorbate | $CuH(L\text{-ascorbate})(H_2O)_4^{+}$ | 5 | 3.924 | 3.324 | - | 2.850 | 2.161 | 1.362 | 0.935 | 2 |
| | $CuH(D\text{-ascorbate})(H_2O)_4^{+}$ | 5 | 3.989 | 3.380 | - | 2.899 | 2.199 | 1.386 | 0.951 | 2 |
| Malonate | $Cu(H_2C_3O_4)_2(H_2O)_2^{2-}$ | 6 | 7.00 | 5.94 | - | 5.10 | 3.88 | 2.45 | 1.68 | 1 |
| Amino acid | $Cu(Glu)(H_2O)_3^{2+}$ | 5 | 5.230 | 4.436 | 4.117 | 3.808 | 2.891 | - | - | 3 |
| complex | $Cu(Thr)(H_2O)_4^{2+}$ | 5 | 5.220 | 4.429 | 4.110 | 3.803 | 2.889 | - | - | 3 |
| | $Cu(His)(H_2O)_3^{2+}$ | 5 | 5.274 | 4.470 | 4.148 | 3.836 | 2.911 | - | - | 3 |
| | $Cu(His)(H_2O)_4^{2+}$ | 5 | 5.299 | 4.492 | 4.168 | 3.855 | 2.926 | - | - | 3 |
| | $Cu(Cys)(H_2O)_4^{2+}$ | 5 | 3.981 | 3.369 | 3.124 | 2.888 | 2.187 | - | - | 3 |
| | $Cu(Met)(H_2O)_4^{2+}$ | 5 | 4.632 | 3.932 | 3.650 | 3.378 | 2.568 | - | - | 3 |
| | $Cu(GS)H^{0}$ | 4 | 4.945 | 4.194 | 3.892 | 3.600 | 2.734 | - | - | 3 |
| Lactate | $Cu(L\text{-lact})(H_2O)_3^{+}$ | 5 | 5.530 | 4.695 | 4.359 | 4.034 | 3.068 | - | - | 3 |
| | $Cu(L\text{-lact})_2$ | 4 | 7.110 | 6.045 | 5.616 | 5.199 | 3.961 | - | - | 4 |
| | Cu(L-lact)(D-lact) [a] | 4 | 7.125 | 6.057 | 5.627 | 5.210 | 3.969 | - | - | 4 |

[a] Reproduced from Telouk et al. (2015).

[b]1=Sherman (2013), 2=Fujii et al. (2013), 3=Fujii et al. (2014), 4=This study.

Table 3 Logarithm of the reduced partition function, ln β, for the pair $^{65}Cu$-$^{63}Cu$. Cu(I) species. Method/Basis set used: B3LYP/TZP for Sherman (2013) and , B3LYP/6-311+G(d,p) for Fujii et al. (2013, 2014), Seo et al. (2007) and the present study.

| | Species | Coordination number | Temperature (K) | | | | | | | Ref[b] |
|---|---|---|---|---|---|---|---|---|---|---|
| | | | 273 | 298 | 310 | 323 | 373 | 473 | 573 | |
| Solid | $Cu_2O$ (Cuprite) | - | 3.99 | 3.40 | - | 2.92 | 2.23 | 1.41 | 0.97 | 1 |
| | $CuFeS_2$ (Chalcopyrite) | - | 1.80 | 1.51 | - | 1.29 | 0.97 | 0.61 | 0.41 | 1 |
| Aquo-ion | $Cu(H_2O)_2^+$ | 2 | 3.368 | 2.867 | - | 2.468 | 1.882 | 1.193 | 0.822 | 2 |
| Chloride | $CuCl(H_2O)$ | 2 | 3.401 | 2.887 | - | 2.480 | 1.885 | 1.191 | 0.818 | 3 |
| | | | 3.40 | 2.89 | - | 2.48 | 1.89 | 1.19 | 0.82 | 4 |
| | $CuCl_2^-$ | 2 | 2.775 | 2.350 | - | 2.014 | 1.526 | 0.960 | 0.659 | 3 |
| | | | 2.71 | 2.29 | - | 1.97 | 1.49 | 0.94 | 0.64 | 4 |
| | | | 2.87 | 2.42 | - | 2.08 | 1.57 | 0.99 | 0.68 | 1 |
| | $CuCl_3^{2-}$ | 3 | 1.012 | 0.851 | - | 0.725 | 0.545 | 0.339 | 0.231 | 3 |
| | | | 1.02 | 0.85 | - | 0.73 | 0.55 | 0.34 | 0.23 | 4 |
| | | | 1.41 | 1.19 | - | 1.02 | 0.76 | 0.48 | 0.33 | 1 |
| Sulfide | $CuHS(H_2O)$ | 2 | 3.208 | 2.722 | - | 2.337 | 1.775 | 1.121 | 0.770 | 3 |
| | | | 2.89 | 2.45 | - | 2.10 | 1.59 | 1.00 | 0.69 | 1 |
| | $Cu(HS)_2^-$ | 2 | 2.940 | 2.489 | - | 2.133 | 1.616 | 1.017 | 0.697 | 3 |
| | | | 2.90 | 2.46 | - | 2.11 | 1.60 | 1.00 | 0.69 | 4 |
| | | | 2.69 | 2.28 | - | 1.95 | 1.48 | 0.93 | 0.64 | 1 |
| | $Cu_2S(HS)_2^{2-}$ | 2 | 2.648 | 2.239 | - | 1.917 | 1.450 | 0.911 | 0.624 | 3 |
| Lactate | Cu(L-lact) [a] | 2 | 2.195 | 1.859 | 1.725 | 1.595 | 1.209 | - | - | 5 |
| | Cu(D-lact) [b] | 2 | 2.202 | 1.866 | 1.731 | 1.600 | 1.214 | - | - | 5 |

[a] Reproduced from Telouk et al. (2015).

[b] 1=Sherman (2013), 2=Fujii et al. (2013), 3=Fujii et al. (2014), 4=Seo et al. (2007), 5=This study.

Table 4 Logarithm of the reduced partition function, ln β, for the pair $^{66}Zn$-$^{64}Zn$. Zn(II) species. Method/Basis set used:, B3LYP/6-311+G(d,p) for Fujii et al. (2013, 2014), Fujii and Albarede (2013), Moynier et al. (2013a), BP86/SVP for Singha Deb et al. (2014), and B3LYP/aug-cc-pVDZ for Black et al. (2012).

| | Species | Coordination number | Temperature (K) | | | | | | | Ref[a] |
|---|---|---|---|---|---|---|---|---|---|---|
| | | | 273 | 298 | 310 | 323 | 373 | 473 | 573 | |
| Aquo-ion | $Zn(H_2O)_4^{2+}$ | 4 | 4.539 | 3.853 | 3.577 | 3.310 | 2.516 | - | - | 1 |
| | | | - | 5.0 | - | - | - | - | - | 2 |
| | $Zn(H_2O)_6^{2+}$ | 6 | 3.854 | 3.263 | - | 2.797 | 2.119 | 1.334 | 0.915 | 1 |
| | | | 3.61 | 3.05 | - | 2.61 | 1.98 | 1.25 | 0.85 | 3 |
| | | | - | 3.9 | - | - | - | - | - | 2 |
| | $Zn(H_2O)_{18}^{2+}$ | 6 | - | 3.576 | - | - | - | - | 1.004 | 4 |
| | | | 3.67 | 3.11 | - | 2.66 | 2.02 | 1.27 | 0.87 | 3 |
| | | | - | 4.3 | - | - | - | - | - | 2 |
| Chloride | $ZnCl(H_2O)_5^{+}$ | 6 | 3.702 | 3.136 | - | 2.689 | 2.039 | 1.285 | 0.882 | 1 |
| | $ZnCl_2(H_2O)_4$ | 6 | 3.486 | 2.950 | - | 2.528 | 1.915 | 1.205 | 0.826 | 1 |
| | $ZnCl_3(H_2O)^{-}$ | 4 | 3.490 | 2.952 | - | 2.528 | 1.913 | 1.202 | 0.824 | 1 |
| | $ZnCl_4^{2-}$ | 4 | 2.722 | 2.293 | - | 1.957 | 1.474 | 0.921 | 0.629 | 1 |
| | | | 2.77 | 2.33 | - | 1.99 | 1.50 | 0.94 | 0.64 | 3 |
| Hydroxide | $Zn(OH)_2(H_2O)_4$ | 6 | 4.185 | 3.567 | - | 3.075 | 2.350 | 1.495 | 1.032 | 1 |
| Carbonate | $ZnHCO_3(H_2O)_3^{+}$ | 5 | 4.573 | 3.877 | - | 3.326 | 2.525 | 1.593 | 1.095 | 1 |
| | $ZnHCO_3(H_2O)_4^{+}$ [a] | 5 | 4.579 | 3.885 | - | 3.335 | 2.534 | 1.602 | 1.102 | 5 |
| | $ZnHCO_3(H_2O)_5^{+}$ [a] | 6 | 4.109 | 3.482 | - | 2.988 | 2.267 | 1.431 | 0.983 | 5 |
| | $ZnCO_3(H_2O)_3$ | 5 | 4.940 | 4.199 | - | 3.612 | 2.752 | 1.745 | 1.202 | 1 |
| | $ZnCO_3(H_2O)_4$ [a] | 5 | 4.789 | 4.076 | - | 3.509 | 2.677 | 1.700 | 1.172 | 1 |
| | $ZnCO_3(H_2O)_5$ [a] | 6 | 4.356 | 3.704 | - | 3.187 | 2.429 | 1.541 | 1.062 | 5 |
| Sulfate | $ZnSO_4(H_2O)_6$ | 5 | 4.31 | 3.65 | | 3.13 | 2.38 | 1.50 | 1.03 | 3 |
| | $ZnSO_4(H_2O)_5$ | 6 | 4.154 | 3.527 | - | 3.031 | 2.306 | 1.460 | 1.006 | 5 |
| Sulfide | $Zn(HS)_2(H_2O)_4$ | 6 | 3.207[b] | 2.717 | - | 2.330[b] | 1.766[b] | 1.113[b] | 0.764 | 4 |
| | $Zn(HS)_3(H_2O)_2$□ | 5 | 3.580[b] | 3.028 | - | 2.593[b] | 1.962[b] | 1.233[b] | 0.845 | 4 |
| | $Zn(HS)_4^{2}$□ | 4 | 2.598[b] | 2.190 | - | 1.871[b] | 1.411[b] | 0.883[b] | 0.604 | 4 |
| | $ZnS(HS)H_2O$□ | 5 | 3.112[b] | 2.628 | - | 2.247[b] | 1.697[b] | 1.064[b] | 0.728 | 4 |
| Phosphate | $ZnH_2PO_4(H_2O)_5^{+}$ | 6 | 4.092 | 3.468 | - | 2.975 | 2.257 | 1.424 | 0.978 | 6 |
| | $ZnH_4(PO_4)_2(H_2O)_4$ | 6 | 4.047 | 3.428 | - | 2.940 | 2.229 | 1.405 | 0.965 | 6 |
| | $ZnH_3(PO_4)_2(H_2O)_4^{-}$ | 6 | 5.027 | 4.268 | - | 3.667 | 2.789 | 1.764 | 1.214 | 6 |
| | $ZnHPO_4(H_2O)_5$ | 6 | 4.188 | 3.559 | - | 3.060 | 2.330 | 1.476 | 1.017 | 6 |
| | $Zn_2H_2(PO_4)_2(H_2O)_4$ | 6 | 5.156 | 4.380 | - | 3.765 | 2.865 | 1.814 | 1.249 | 6 |
| Citrate | $ZnH(cit)(H_2O)_4$ | 6 | 4.033 | 3.419 | - | 2.934 | 2.227 | 1.406 | 0.967 | 6 |
| | $Zn(cit)(H_2O)_3^{-}$ | 6 | 4.154 | 3.523 | - | 3.024 | 2.297 | 1.452 | 0.999 | 6 |
| | | | 4.39 | 3.72 | - | 3.20 | 2.43 | 1.54 | 1.06 | 3 |
| | $Zn(cit)_2^{4-}$ | 6 | 2.889 | 2.437 | - | 2.083 | 1.572 | 0.986 | 0.675 | 6 |
| | $Zn_2H_{-2}(cit)_2(H_2O)_4^{4-}$ | 4 | 5.330 | 4.523 | - | 3.884 | 2.953 | 1.867 | 1.284 | 6 |
| Malate | $ZnH_2(mal)(H_2O)_4^{2+}$ | 6 | 3.842 | 3.250 | - | 2.784 | 2.107 | 1.325 | 0.909 | 6 |
| | $ZnH(mal)(H_2O)_4^{+}$ | 6 | 3.984 | 3.376 | - | 2.896 | 2.197 | 1.386 | 0.952 | 6 |
| | $Zn(mal)(H_2O)_4$ | 6 | 4.103 | 3.479 | - | 2.987 | 2.268 | 1.433 | 0.986 | 6 |
| | $Zn(mal)_2(H_2O)_2^{2-}$ | 6 | 3.274 | 2.771 | - | 2.376 | 1.801 | 1.135 | 0.780 | 6 |
| Oxalate | $ZnC_2O_4(H_2O)_2$ | 4 | 5.500 | 4.678 | - | 4.025 | 3.068 | 1.946 | 1.341 | 5 |
| | $Zn(C_2O_4)_2^{2-}$ | 4 | 5.215 | 4.421 | - | 3.794 | 2.880 | 1.818 | 1.250 | 5 |
| Amino acid | $Zn(Glu\text{-}H_{-1})^{+}$ [c] | 2 | 1.923 | 1.633 | 1.517 | 1.404 | 1.070 | - | - | 7 |
| complex | $Zn(Glu)(H_2O)_2^{2+}$ | 4 | 4.473 | 3.796 | 3.524 | 3.260 | 2.478 | - | - | 1 |
| | $Zn(Glu)(H_2O)_4^{2+}$ | 6 | 3.888 | 3.292 | 3.053 | 2.822 | 2.139 | - | - | 1 |
| | $Zn(Thr)(H_2O)_3^{2+}$ | 4 | 4.774 | 4.056 | 3.767 | 3.487 | 2.654 | - | - | 1 |
| | $Zn(Thr)(H_2O)_5^{2+}$ | 6 | 3.916 | 3.315 | 3.075 | 2.842 | 2.154 | - | - | 1 |
| | $Zn(His\text{-}H_{-1})+$ [c] | 2 | 4.381 | 3.728 | 3.465 | 3.210 | 2.448 | - | - | 7 |
| | $Zn(His)^{2}+$ [c] | 2 | 4.223 | 3.591 | 3.336 | 3.090 | 2.355 | - | - | 7 |
| | $Zn(His)(H_2O)_2^{2+}$ | 4 | 4.670 | 3.959 | 3.673 | 3.397 | 2.578 | - | - | 1 |
| | $Zn(His)(H_2O)_4^{2+}$ | 6 | 3.541 | 2.996 | 2.777 | 2.566 | 1.943 | - | - | 1 |
| | $Zn(His)(H_2O)_3^{2+}$ | 4 | 4.635 | 3.930 | 3.647 | 3.373 | 2.561 | - | - | 1 |
| | $Zn(His)(H_2O)_5^{2+}$ | 6 | 3.724 | 3.150 | 2.921 | 2.699 | 2.043 | - | - | 1 |
| | $Zn(Cys\text{-}H_{-1})^{+}$ [c] | 1 | 1.417 | 1.196 | 1.108 | 1.023 | 0.771 | - | - | 7 |
| | $Zn(Cys)^{2+}$ [c] | 1 | 1.545 | 1.307 | 1.211 | 1.119 | 0.847 | - | - | 7 |
| | $Zn(Cys)(H_2O)_3^{2+}$ | 4 | 3.912 | 3.313 | 3.072 | 2.840 | 2.152 | - | - | 1 |

| | | | | | | | | | |
|---|---|---|---|---|---|---|---|---|---|
| $Zn(Cys)(H_2O)_5^{2+}$ | 6 | 3.196 | 2.702 | 2.504 | 2.313 | 1.750 | - | - | 1 |
| $Zn(Met)(H_2O)_3^{2+}$ | 4 | 4.397 | 3.733 | 3.466 | 3.207 | 2.438 | - | - | 1 |
| $Zn(Met)(H_2O)_5^{2+}$ | 6 | 3.478 | 2.947 | 2.734 | 2.528 | 1.918 | - | - | 1 |
| $Zn(GS)^-$ | 4 | 4.311 | 3.655 | 3.392 | 3.137 | 2.381 | - | - | 1 |

[a] $HCO_3^-$ and $CO_3^{2-}$ were treated as monovalent ligands.
[b] Reproduced from Fujii et al. (2011).
[c] Hydration water molecules were not arranged (anhydrous).
[d] 1=Fujii et al. (2014), 2=Singha Deb et al. (2014), 3=Black et al. (2011), 4=Fujii et al. (2011), 5=This Study, 6=Fujii and Albarède (2012), 7=Moynier et al. (2013a).

2735

2736 **Moynier et al. RIMG Cu-Zn Figure 1**

2737

2738

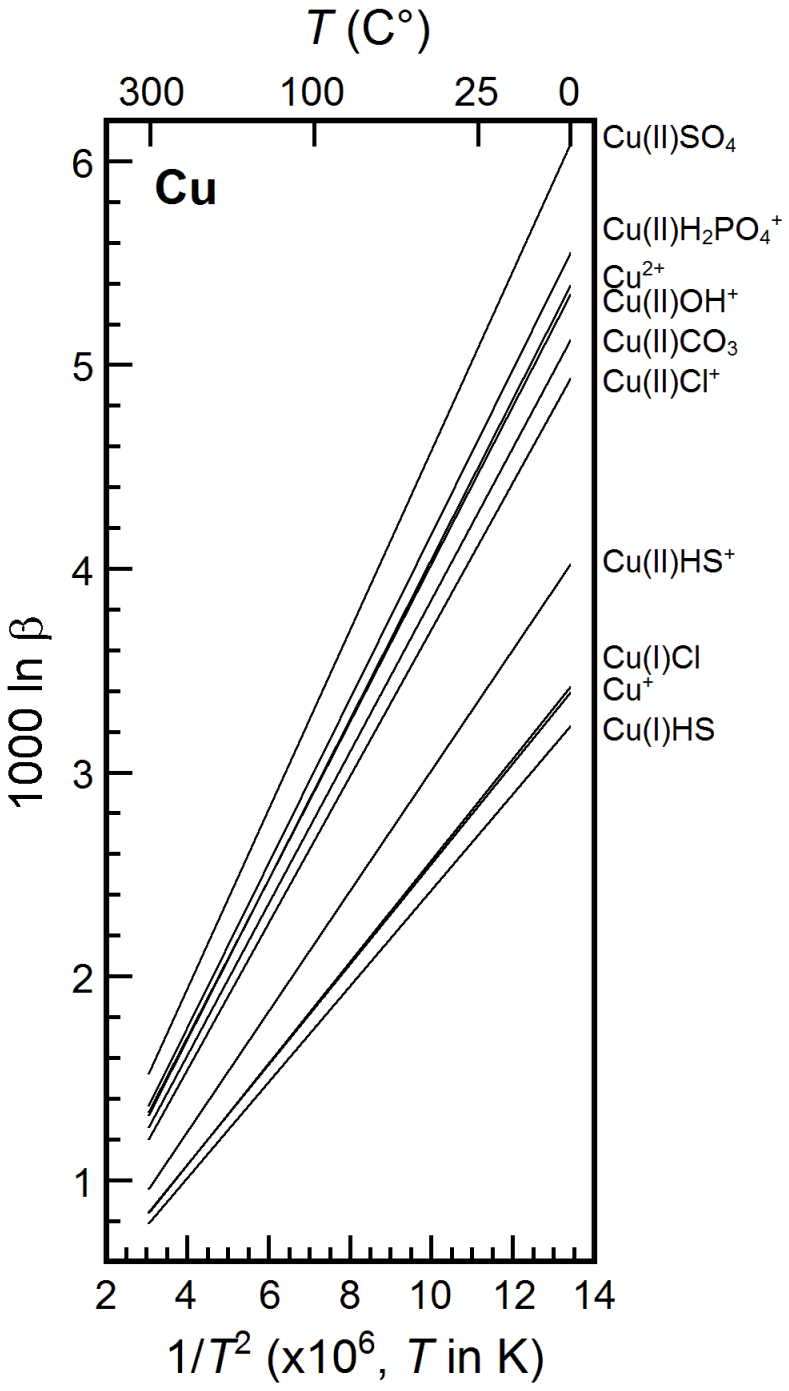


2739

2740

2741 **Moynier et al. RIMG Cu-Zn Figure 2**

2742

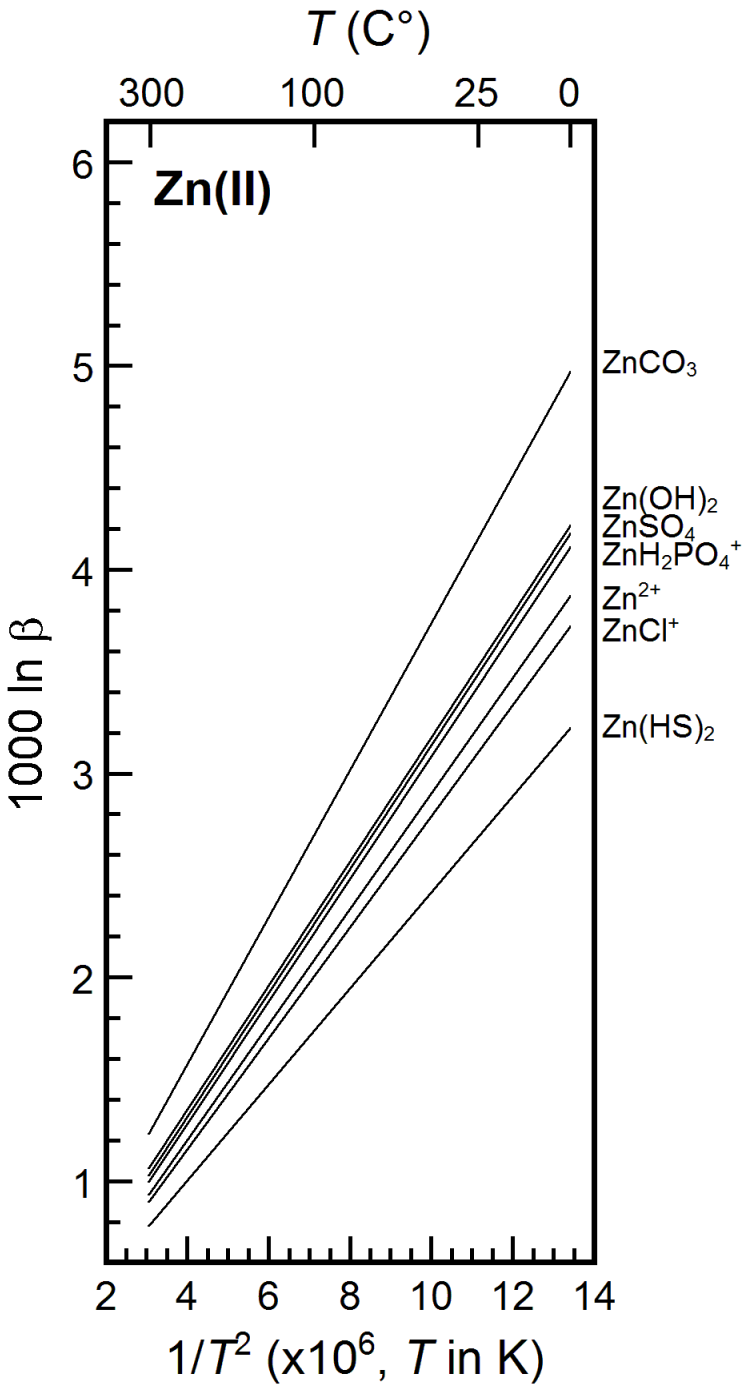


2743

2744

**Moynier et al. RIMG Cu-Zn Figure 3**

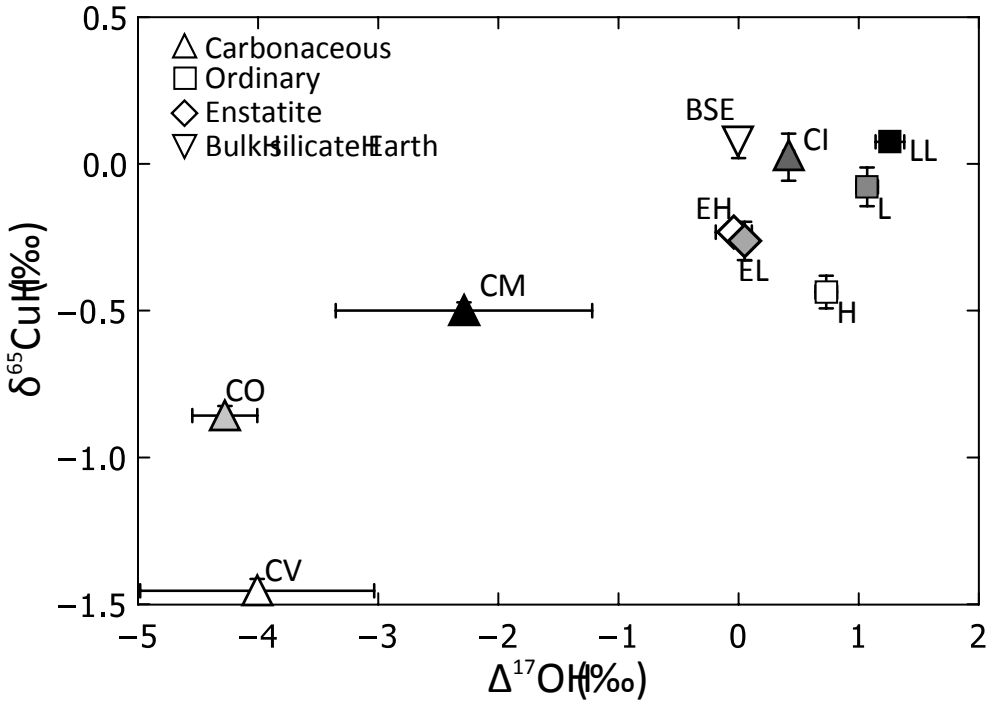

**Moynier et al. RIMG Cu-Zn Figure 4**

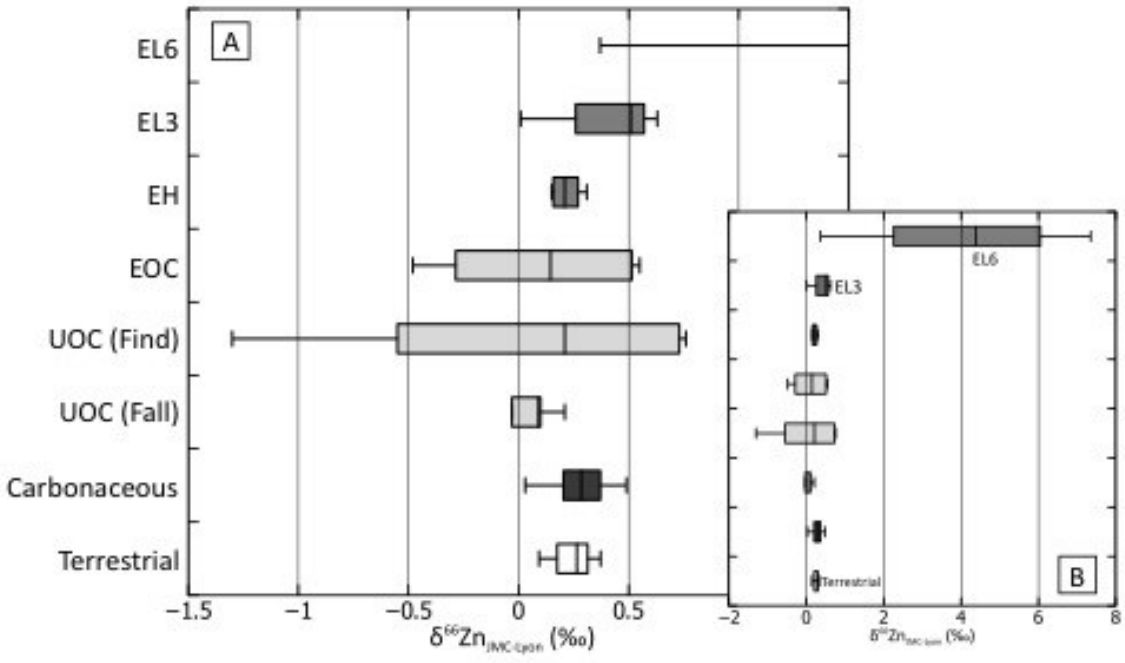

**Moynier et al. RIMG Cu-Zn Figure 5**

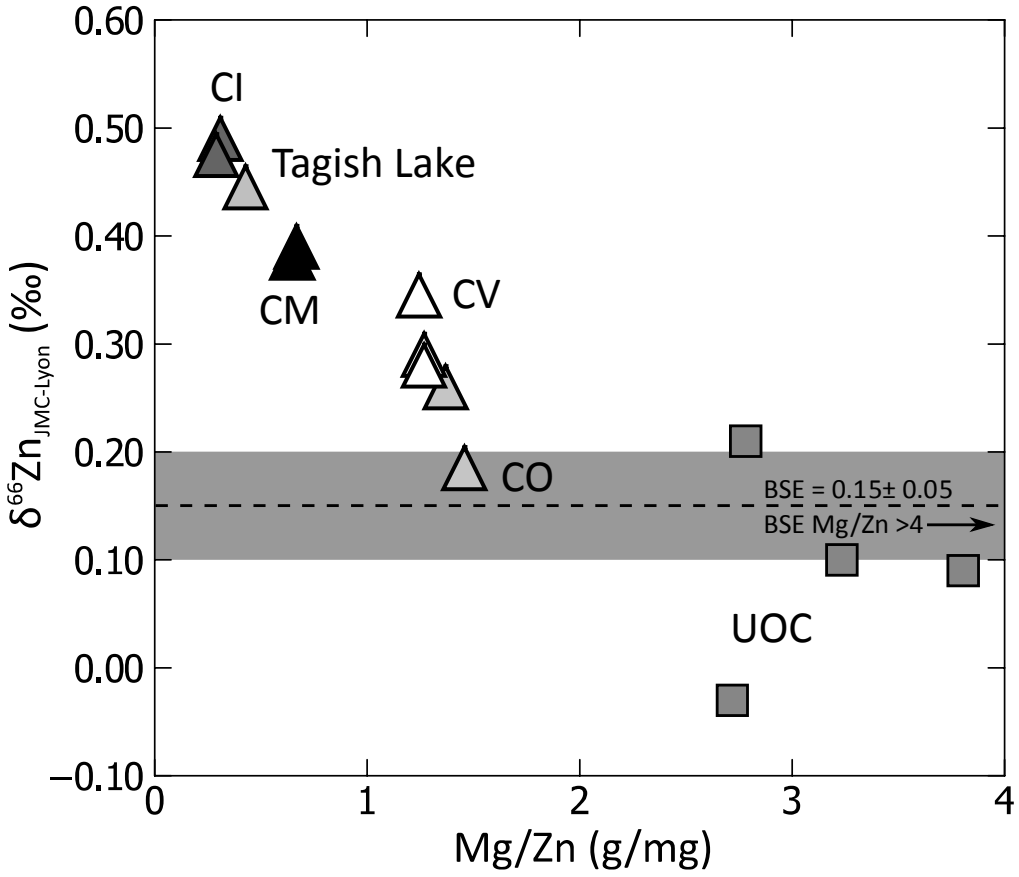

**Moynier et al. RIMG Cu-Zn Figure 6**

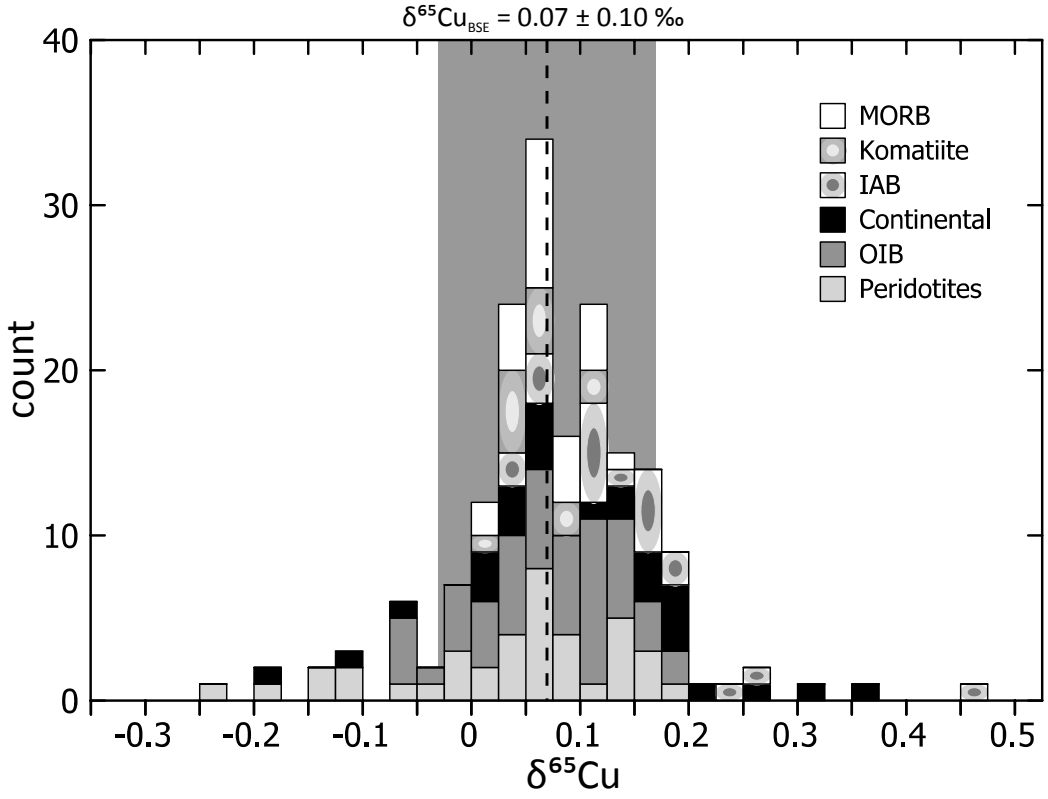

**Moynier et al. RIMG Cu-Zn Figure 7**

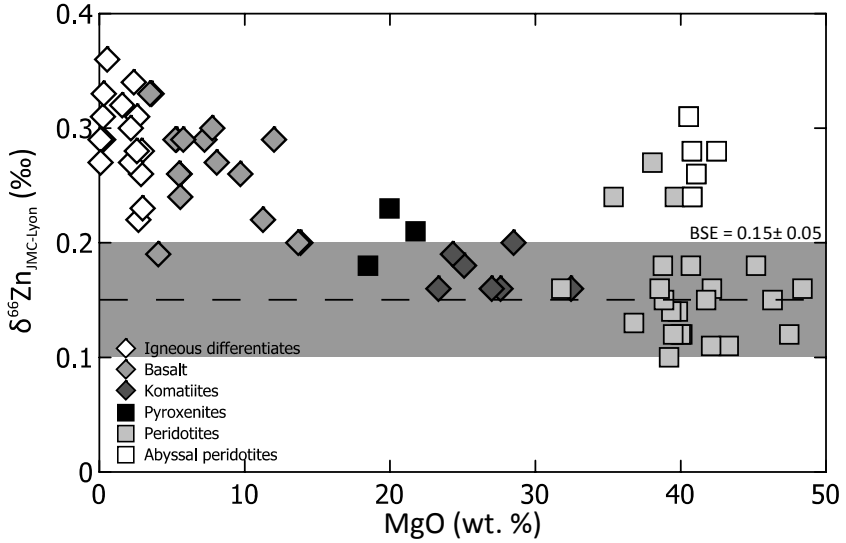

2841 **Moynier et al. RIMG Cu-Zn Figure 8**
2842

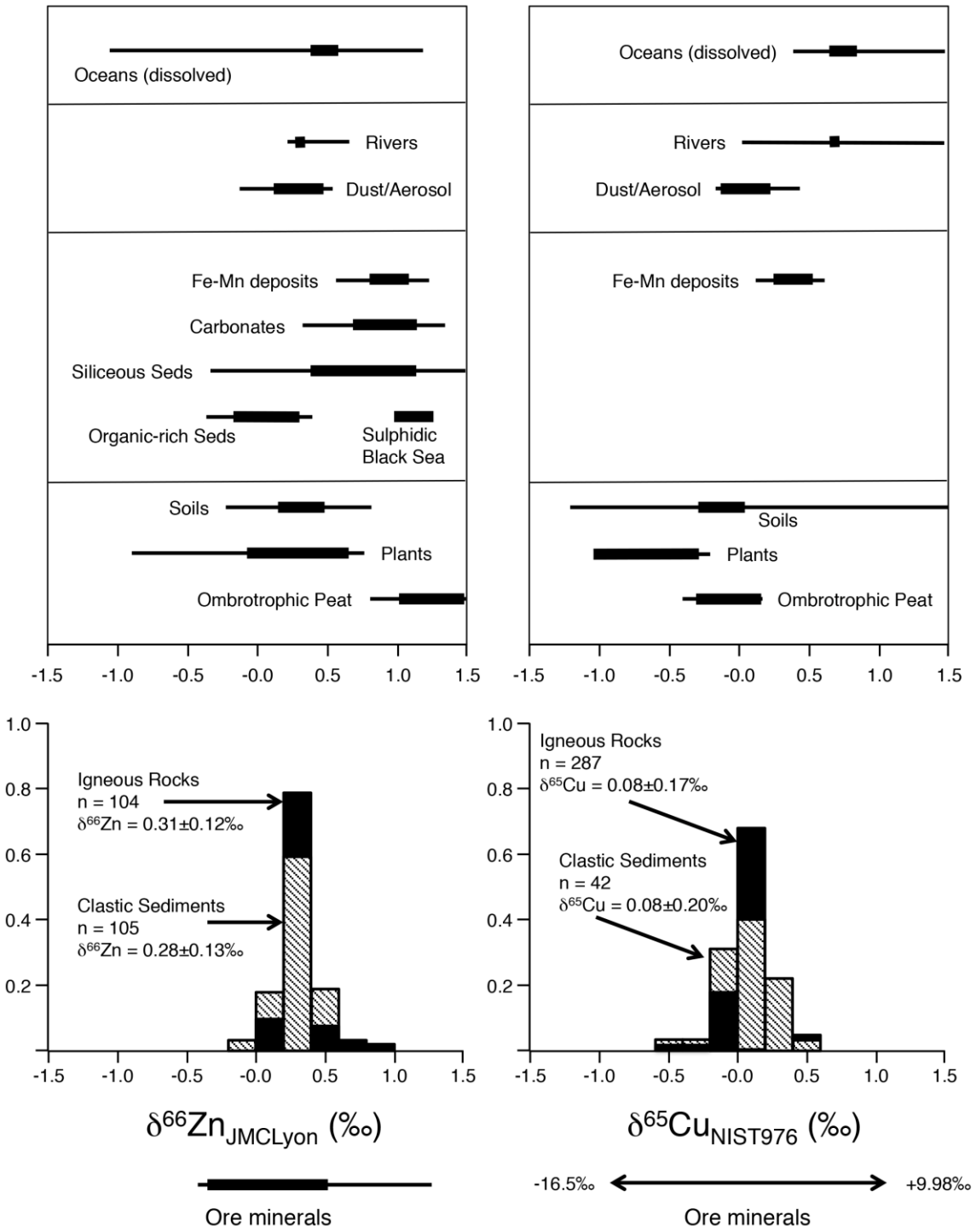


2843
2844
2845

**Moynier et al. RIMG Cu-Zn Figure 9**

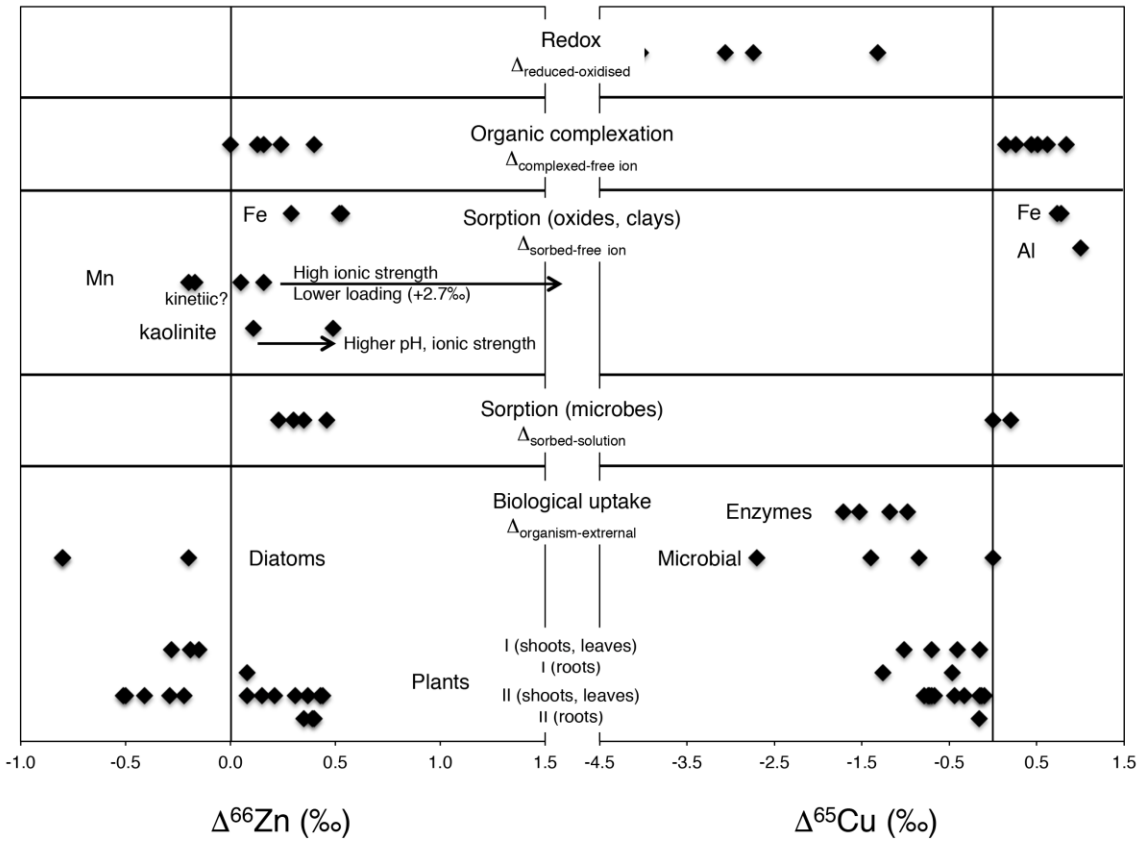

2852 **Moynier et al. RIMG Cu-Zn Figure 10**
2853

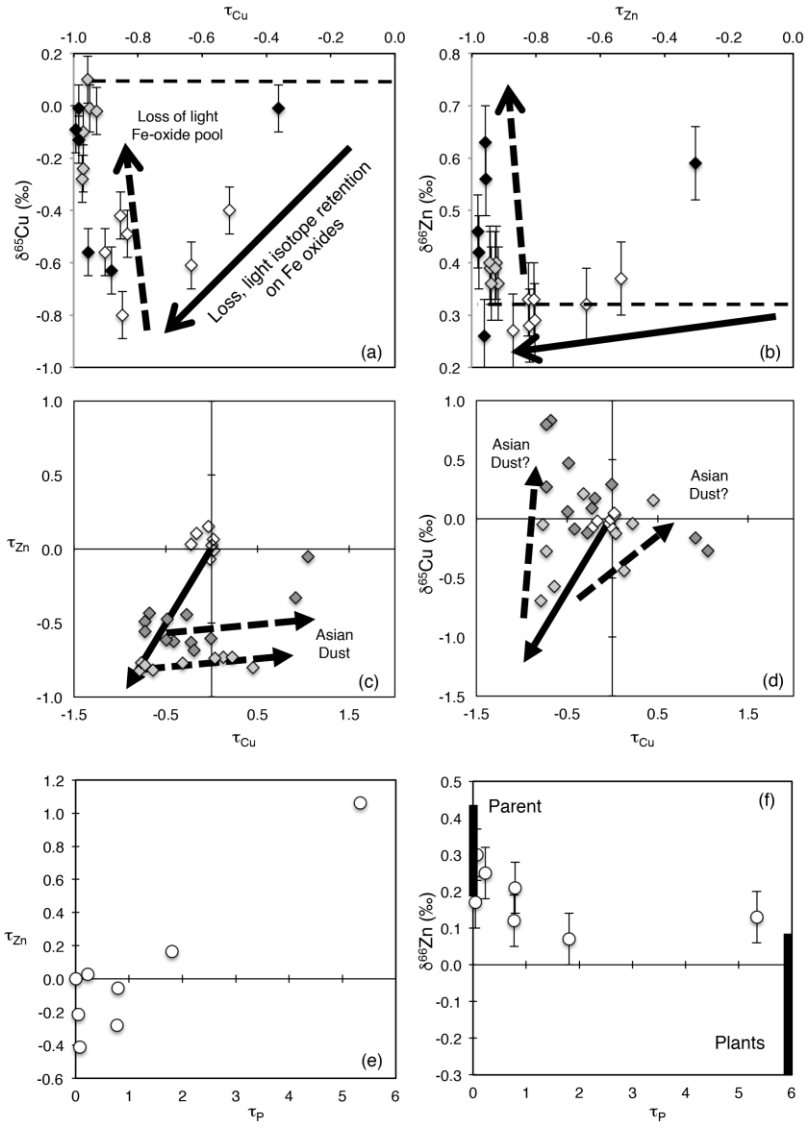


2854
2855

**Moynier et al. RIMG Cu-Zn Figure 11**

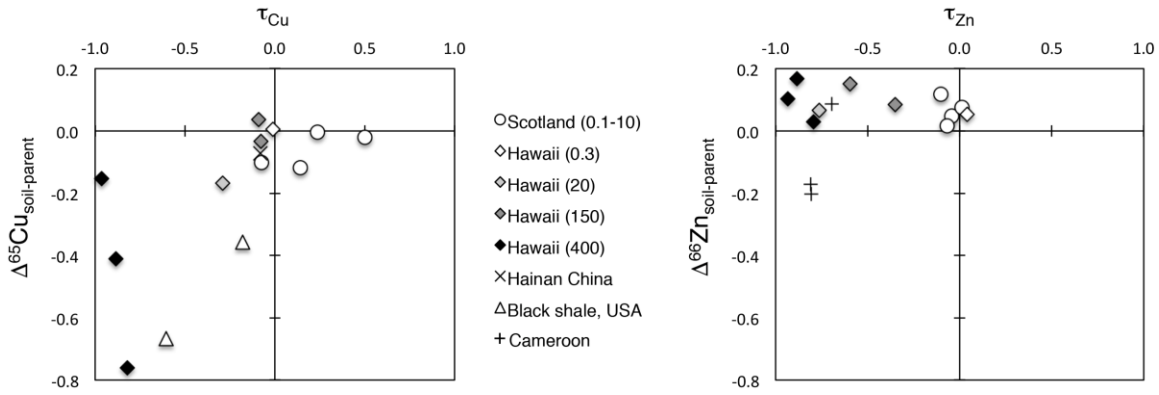

**Moynier et al. RIMG Cu-Zn Figure 12**

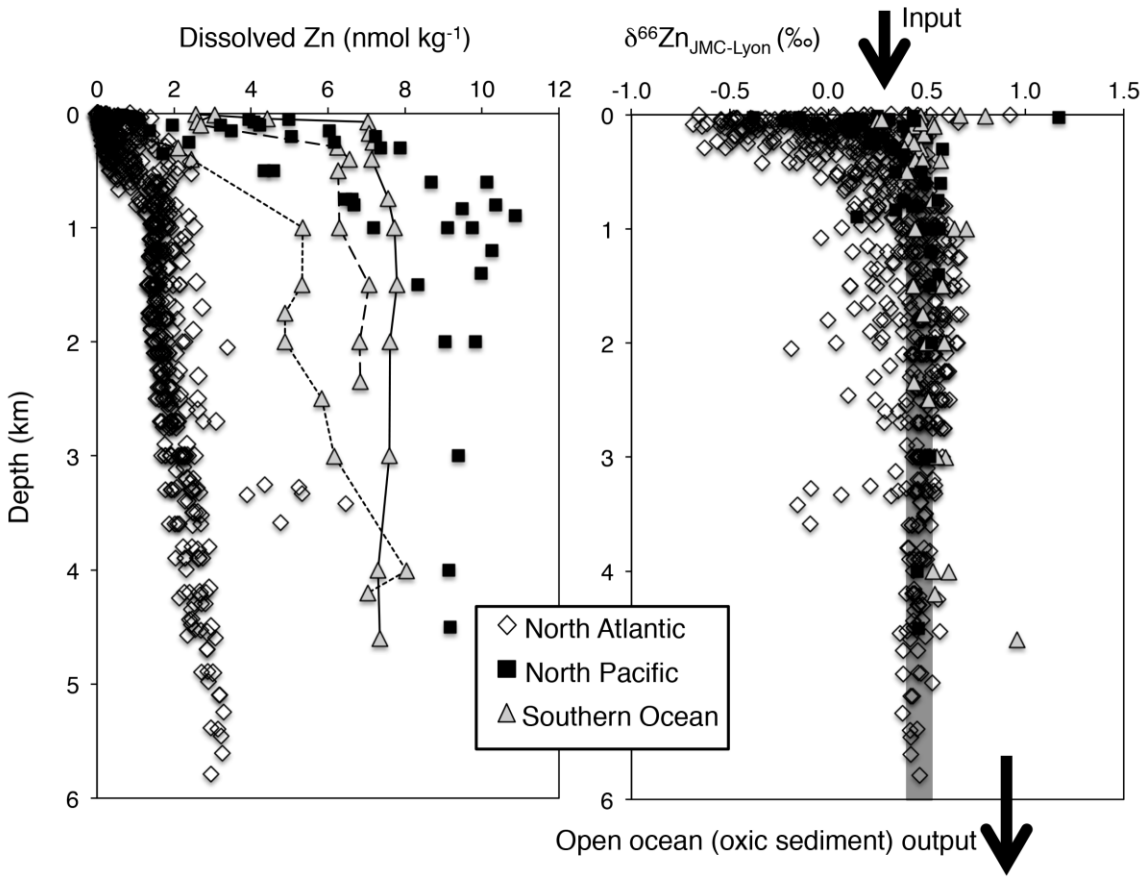

2866 **Moynier et al. RIMG Cu-Zn Figure 13**
2867

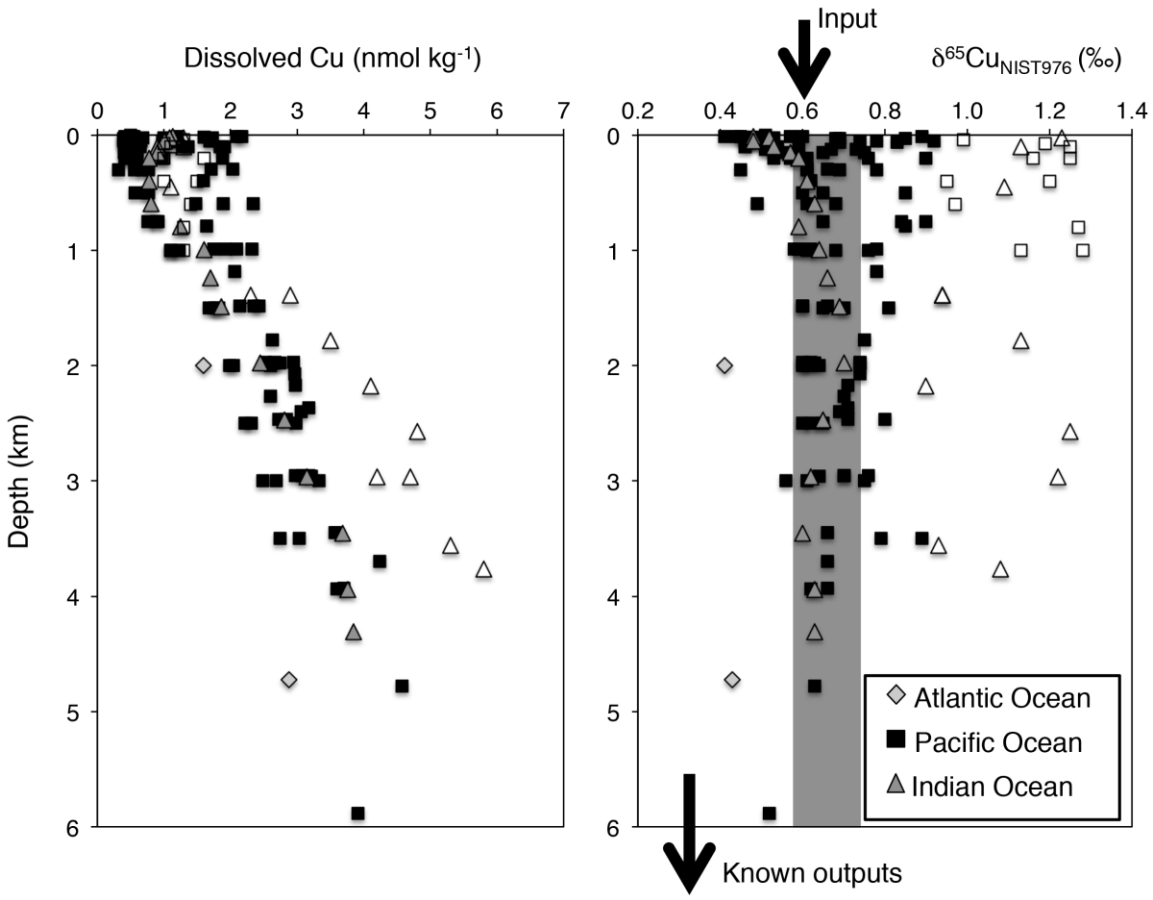


2868
2869
2870

**Moynier et al. RIMG Cu-Zn Figure 14**